

2020

Understanding phenyloxenium ions: Spectroscopic properties, spin configurations and reactivities

Yunfan Qiu
Iowa State University

Follow this and additional works at: <https://lib.dr.iastate.edu/etd>

Recommended Citation

Qiu, Yunfan, "Understanding phenyloxenium ions: Spectroscopic properties, spin configurations and reactivities" (2020). *Graduate Theses and Dissertations*. 17967.
<https://lib.dr.iastate.edu/etd/17967>

This Thesis is brought to you for free and open access by the Iowa State University Capstones, Theses and Dissertations at Iowa State University Digital Repository. It has been accepted for inclusion in Graduate Theses and Dissertations by an authorized administrator of Iowa State University Digital Repository. For more information, please contact digirep@iastate.edu.

Understanding phenyloxenium ions: Spectroscopic properties, spin configurations and reactivities

by

Yunfan Qiu

A dissertation submitted to the graduate faculty
in partial fulfillment of the requirements for the degree of

DOCTOR OF PHILOSOPHY

Major: Organic Chemistry

Program of Study Committee:
Arthur H. Winter, Major Professor
Yan Zhao
Brett VanVeller
Emily A. Smith
Theresa Windus

The student author, whose presentation of the scholarship herein was approved by the program of study committee, is solely responsible for the content of this dissertation. The Graduate College will ensure this dissertation is globally accessible and will not permit alterations after a degree is conferred.

Iowa State University

Ames, Iowa

2020

Copyright © Yunfan Qiu, 2020. All rights reserved.

DEDICATION

to

My beloved parents and my darling wife

Thanks for being supportive and creating a lovely life I have been enjoying. I hope this little achievement would make you proud of me.

TABLE OF CONTENTS

	Page
ACKNOWLEDGMENTS	v
ABSTRACT.....	vi
CHAPTER 1. INTRODUCTION	1
1.1 A Brief Overview of Oxenium Ions and Their Significance	1
1.2 Laser Flash Photolysis Permits Direct Detection of Reactive Intermediates.....	7
1.3 Previous Experimental Discoveries of Phenyloxenium Ions	8
1.4 Computations as Theoretical Approaches to Studying Phenyloxenium Ions	13
1.5 Organization of the Dissertation	15
1.6 References.....	17
CHAPTER 2. DIRECT DETECTION OF THE OPEN-SHELL SINGLET PHENYLOXENIUM ION: AN ATOM-CENTERED DIRADICAL REACTS AS AN ELECTROPHILE	20
2.1 Abstract	20
2.2 Introduction.....	21
2.3 Experimental Section	25
2.4 Results and Discussion.....	27
2.5 Conclusions.....	38
2.6 Acknowledgments.....	39
2.7 References.....	39
CHAPTER 3. DIRECT DETECTION OF THE n,π^* EXCITED TRIPLET PHENYLOXENIUM ION: EXPLOITING EL-SAYED'S RULE	41
3.1 Abstract	41
3.2 Introduction.....	42
3.3 Experimental Section	46
3.4 Results and Discussion.....	49
3.5 Conclusions.....	54
3.6 References.....	55
CHAPTER 4. ARYL OXENIUM IONS WITH UNUSUAL HIGH-SPIN π, π^* GROUND STATES: EXPLOITING (ANTI)AROMATICITY.....	57
4.1 Abstract	57
4.2 Introduction.....	58
4.3 Experimental Section	60
4.4 Results and Discussion.....	61
4.5 Conclusions.....	73
4.6 Acknowledgments.....	74
4.7 References.....	74

CHAPTER 5.	ANOMALOUS ELECTRONIC PROPERTIES OF IODOUS MATERIALS: APPLICATION TO HIGH-SPIN PHENYLOXENIUM IONS	78
5.1	Abstract	78
5.2	Introduction	79
5.3	Experimental Section	83
5.4	Results and Discussion.....	84
5.5	Conclusions.....	88
5.6	Acknowledgments.....	89
5.7	References	90
CHAPTER 6.	GENERAL CONCLUSIONS.....	94
APPENDIX A.	SUPPLEMENTAL INFORMATION ACCOMPANYING CHAPTER 2.....	96
APPENDIX B.	SUPPLEMENTAL INFORMATION ACCOMPANYING CHAPTER 3	111
APPENDIX C.	SUPPLEMENTAL INFORMATION ACCOMPANYING CHAPTER 4	113
APPENDIX D.	SUPPLEMENTAL INFORMATION ACCOMPANYING CHAPTER 5.....	116

ACKNOWLEDGMENTS

I would like to express my greatest appreciation to my doctoral advisor, Prof. Arthur H. Winter for his thoughtful guidance during the course of my graduate career. I consider myself extremely lucky to have pursued my Ph.D. under Prof. Winter's supervision. I am pleased to sincerely thank him for offering me the opportunity to work in his research group and training me to become a qualified chemist as well as a good person. His dedication to scientific research has always inspired me and encouraged me.

I would like to acknowledge the tremendous help from my graduate committee members, Drs. Yan Zhao, Brett VanVeller, Emily A. Smith, Theresa Windus for their valuable advice and support. I would like to thank my previous and current group members for their suggestions and being wonderful friends and colleagues.

I would like to thank Prof. David Lee Phillips and Dr. Lili Du from the University of Hong Kong for being wonderful collaborators and providing immense experimental support in regards to the ultrafast spectroscopies. I also feel fortunate to have the chance to visit their research laboratory and operate their advanced ultrafast systems.

Last not least, I would like to thank all my friends, colleagues, faculties, and staff for making my time at Iowa State University a fabulous journey. With all of you, Ames has become my second hometown in my life. Most importantly, I want to thank my family members for granting me love and encouragement, lifting me to carry on and look forward.

ABSTRACT

It is believed that understanding the reactive intermediates is essential to unveil mechanisms of synthetic chemistry and biological processes. In the library of reactive intermediates, oxenium ions are highly reactive with the formula $R-O^+$. These reactive intermediates possess lone pairs of electrons on their central oxygen atoms, permitting different energetically accessible electronic configurations. More importantly, reactive intermediates with diverse electronic structures would very likely bear distinct reactivities, and thus various reaction pathways may occur. In general, intermediates with closed-shell singlet states usually react as electrophiles, while ions with triplet states show typical radical reaction pattern, such as hydrogen atom abstractions. Moreover, the chemical formula of oxenium ions suggest that these species are isoelectronic to the better understood nitrene intermediates but bear a formally positive charge on a hypovalent oxygen atom, which is substantially interesting considering the high electronegativity value of oxygen element. Although oxenium ions have been proposed as intermediates in numerous processes, relative studies about these ions themselves are surprisingly rare, largely because the isolation of oxenium ions is utterly difficult due to the extremely short lifetimes.

To probe these exceedingly short-lived intermediates, a combination of theoretical calculation and experimental laser flash photolysis (LFP) has been applied. On one hand, LFP technology has allowed us to directly observe these reactive intermediates within femtosecond time scale in the aspects of the absorption spectroscopy, Raman spectroscopy, etc. On the other, owing to the advanced theoretical models, computational investigation helps us to validate and interpret the experimental spectroscopic data. Moreover, the theoretical approach also provides a close insight to the spin configurations of these reactive intermediates, guiding us to design

oxenium ions with desired electronic configurations. In this manner, appropriate photo-precursors are strongly demanded for generating corresponding oxenium ions photochemically.

My research focuses on synthetically developing new photoprecursors which can potentially produce corresponding oxenium ions possessing intriguing electronic structures. LFP studies perform direct observation of these transient species. By comparison to the theoretical predictions, each transient species collected by LFP shall be attributed correctly. Photo product studies are conducted to determine the reactivities of these reactive intermediate. I have also carried out my investigation in searching for anomalous electronic configurations of oxenium ions using computational methods. Oxenium ions with different electronic configurations exhibit distinct reactivities, which are potentially useful for future synthetic applications. More importantly, reactive intermediates bearing triplet states, if well stabilized, are capable of acting as practical magnetic materials.

CHAPTER 1. INTRODUCTION

1.1 A Brief Overview of Oxenium Ions and Their Significance

Oxenium ions are highly reactive intermediates with the formula $R-O^+$. These species are isoelectronic to another more well-known intermediate nitrenes whose formula is $R-N$. Similar to nitrenes, oxenium ions, both alkyl and aryl oxenium ions, possess one lone pair of electrons that can be distributed into two orbitals with nearly degenerate orbital energies, resulting in multiple energetically accessible electronic configurations (see Figure 1.1). [1] If the orbital mixing with the R functional group in Figure 1.1 is negligible, oxenium ions have three prevailing electronic configurations: closed-shell singlet, open-shell singlet and triplet. In contrast to nitrenes, oxenium ions bear a formally positive charge on the hypovalent oxygen atom, which is substantially interesting considering the high electronegativity value of oxygen element. The existence of the positive charge on oxygen atom brings about many questions regarding the reactivities of oxenium ions, driving me to investigate this poorly studied intermediate.

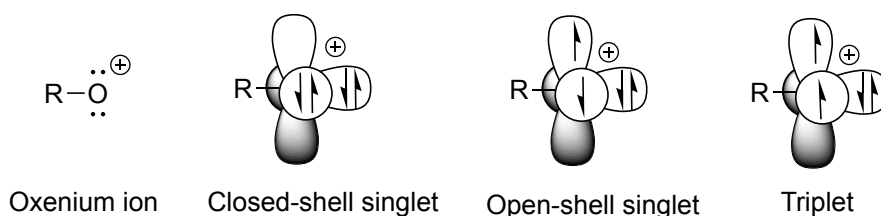


Figure 1.1 Commonly considered electronic configurations of oxenium ions. R stands for substituents.

It is worth noting that reactive intermediates with diverse electronic structures would exhibit distinct reactivities, and thus various reaction types may occur. In general, for most

reactive intermediates such as carbenes, nitrenes, etc., the closed-shell singlet state usually reacts as electrophiles, while triplet states show typical radical reaction pattern, such as hydrogen atom abstractions. It is commonly acknowledged that the electronic configuration a certain reactive intermediate adopts dominates the reactivity of this species. [1] Take carbenes as examples [2], their reactivities largely rely on the electronic configurations, which lead to spin-selective products. Figure 1.2 depicts the details of such selectivities. For a singlet carbene, it normally acts as a typical two-electron nucleophile and adds to alkenes in a concerted way. In the case of

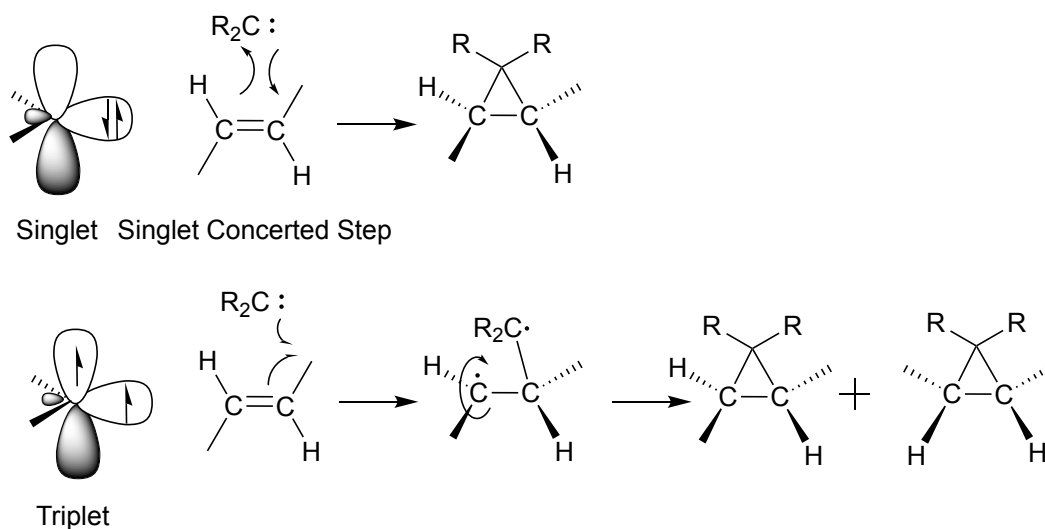


Figure 1.2 Distinct reactivities of singlet and triplet carbenes. Briefly, singlet carbene reacts as a typical two-electron nucleophile while triplet carbene shows radical reaction pattern. (See context for a more detailed explanation.)

the triplet carbene, the addition reaction is stepwise due to the diradical character of triplets. After the initial radical recombination reaction, the newly generated radical center is able to rotate freely along the bond direction before the second step of the radical recombination, which leads to a mixture of stereoisomers as the final products. Thus, it is substantially important to

study the electronic configuration of oxenium ions, especially those of the ground states. By comprehending the spin states, the reactivity would be predicted and it can provide us synthetic guidance when encountering these reactive intermediates in realistic experiments.

As described earlier, knowing the electronic configuration of the ground state gives an overall estimation of the reactivity of a certain reactive intermediate because most of the chemical reactions occur thermally, that is, on the ground state unless under special conditions (e.g. photochemistry). Like the majority of the reactive intermediates, the singlet–triplet energy gap (ΔE_{ST}) is picked to be an important factor for determining the ground state of oxenium ions and elucidating their corresponding spin configurations. It is calculated by subtracting the lowest triplet energy from the lowest singlet energy, shown in eq. 1.

$$\Delta E_{ST} = E_{\text{singlet}} - E_{\text{triplet}} \quad (1)$$

Notably, the simplest oxenium ion, OH^+ , has $\Delta E_{ST} = 54$ kcal/mol and favors the triplet ground state. [3] Conceptually, the preference of the triplet state of this parent oxenium ion results from a degeneracy in the p orbitals on the oxygen atom of OH^+ , which leads to the lowest-energy spin unpaired electronic configuration complying with a molecular orbital (MO) extension of Hund's rule. The ground states of parent phenyloxenium ions, however, are predicted to have closed-shell singlet ground due to the broken degeneracy of the p orbitals. Indeed, experimental studies reveal that the parent phenyloxenium ions adopt closed-shell singlet ground states, [4] because the filled p orbitals on the benzene ring mix with the out-of-plane p orbital on the centered atom (oxygen atom), raising its energy, and both stabilizing the singlet state and destabilizing the triplet state. The parent phenyloxenium ion is calculated to have $\Delta E_{ST} = -22$ kcal/mol at the level of CASPT2(8,8)/pVTZ, which agrees well with the previous quantitative interpretation. [5] With most of the aryl oxenium ion computed to have singlet ground states,

only few aryl oxenium ions, such as heteroaryl and substituted aromatic, may exhibit triplet ground states (see Figure 1.3) based on both experimental and theoretical investigations. [6-8] These triplet aryl oxenium ions are expected to switch the reactivity behavior from reacting as electrophilic species (singlet states) to acting as diradicals (triplet states). All the singlet states discussed so far, however, are considered to be closed-shell singlet states by default. Open-shell singlet states are higher in energy than closed-shell singlet states due to the loss of paired electrons. Rapid internal conversion from open-shell to closed-shell singlet is to happen even though the reactive intermediate is produced at the higher singlet state, preventing the direct observation of the reactivity and other properties of open-shell singlet species. Open-shell singlet phenyloxenium ion has been awaiting for scientific discoveries.

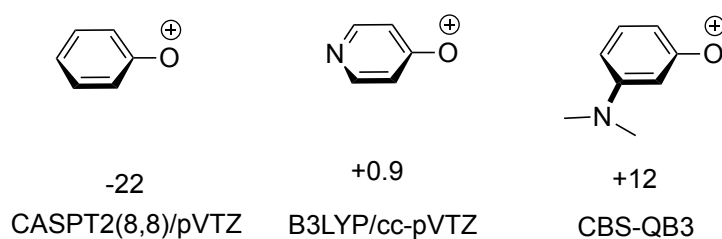
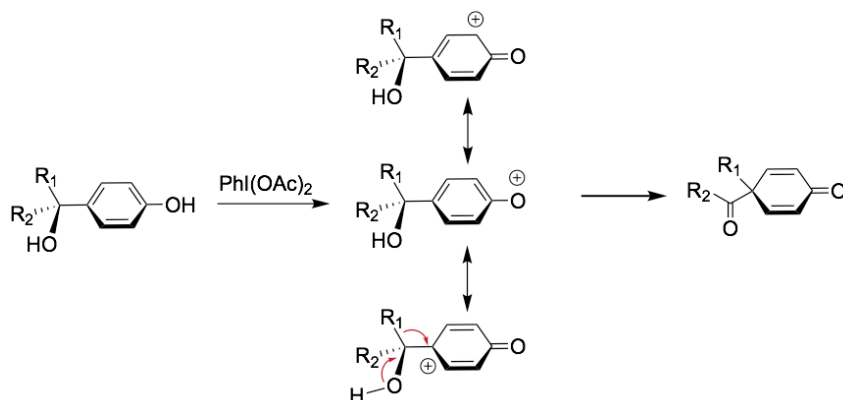


Figure 1.3 Computed singlet-triplet gaps in kcal/mol of selected aryl oxenium ions. Parent phenyloxenium ion has the singlet ground state. Aryl oxenium ions can have computed triplet ground states by modifying the core aromatic structure or substituting specific functional groups.

Apart from the intriguing electronic configurations of oxenium ions, the reactions of these intermediates play indispensable roles in numerous alkane and phenol oxidations, [9-11] including the oxidative Wagner–Meerwein transposition, the oxidative Hosomi–Sakurai reaction, and a number of other phenolic oxidations and tautomerization reactions. [12-15] Figure 1.4.a displays the oxidative Wagner–Meerwein transposition involving a phenyloxenium ion

a.)



b.)

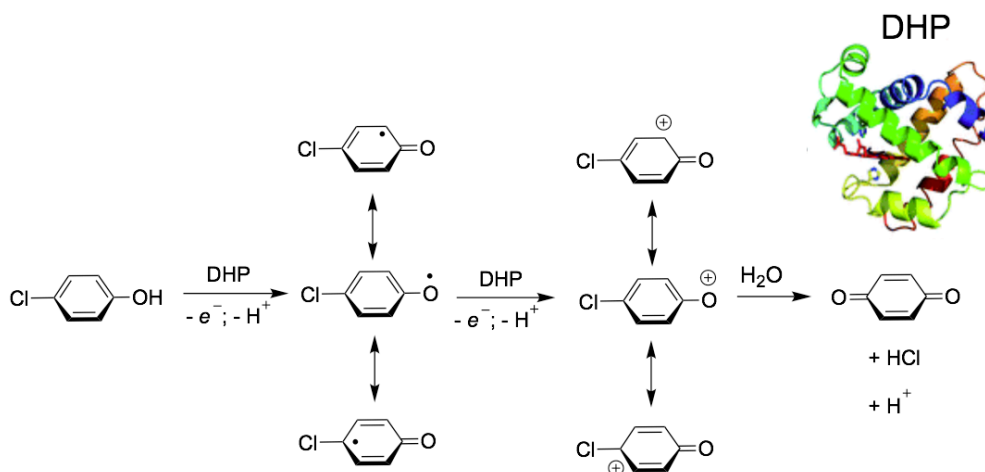


Figure 1.4 a.) An oxidative Wagner–Meerwein transposition involving an oxenium ion intermediate; b.) Two consecutive one-electron oxidation reaction by *Amphitrite ornata* dehaloperoxidase (DHP) involving oxenium ions.

intermediate. As shown, phenol is oxidized to produce an oxenium ion intermediate with three subsequent resonance structures, followed by an alkyl shift to generate the final quinone compound. Moreover, phenyloxenium ions anticipate in synthetic umpolung reactions as well as

some biological processes such as enzymatic oxidations of phenols into quinone compounds (see Figure 1.4.b). [16] Amphitrite ornata dehaloperoxidase (DHP) is a heme enzyme with a globin structure, which usually performs two consecutive one-electron oxidation reaction involving oxenium ions. As shown in Figure 1.4b, in the presence of DHP, dehalogenation of p-chlorophenol initially goes through the first one-electron oxidation process and form a radical intermediate. The radical species is further catalyzed by DHP to produce another oxenium ion intermediate, which ultimately transfers into quinones via the reaction with water. Simple oxenium ions also have relevance to astrochemistry and have been detected as persistent species in interstellar clouds and planet atmospheres. [17,18] Similar to carbenes and nitrenes, oxenium ions can be stabilized by transition metals as coordination ligands. [19]

Beyond the applications described above, relevant studies of oxenium ions themselves regarding their spectroscopic properties and reactivities are limited because the isolation of oxenium ions is utterly difficult due to the extremely short lifetime. To probe these extremely short-lived intermediates, suitable photo-precursors are desired for laser flash photolysis (LFP), which allows us to directly observe these reactive intermediates within femtosecond time scale in the aspects of the absorption spectroscopy, Raman spectroscopy, etc. It is also worth noting that, though studying OH^+ (or alkyl oxenium ions in general) is of fundamental importance, aryl oxenium ions, however, seemingly involve in more studies as discussed earlier and its narrower singlet-triplet energy gap ($\Delta E_{\text{ST}} = -22$ kcal/mol at CASPT2(8,8)/pVTZ) permits more accessible energy levels, which potentially offers chemists higher chance to unlock more spin configurations. To clarify, this dissertation extensively focuses on the aryl oxenium ions.

1.2 Laser Flash Photolysis Permits Direct Detection of Reactive Intermediates

Reactive intermediate chemistry has been extensively widened since the invention of the technique, laser flash photolysis, which allows the direct observation of these short-lived species in the picosecond (10^{-12} s) or nanosecond (10^{-9} s) time scale with UV-visible and infrared detection frame. Along with the advanced theoretical simulations, LFP has been reported to successfully observe and identify various reactive intermediates, such as nitrenes, carbenes, nitrenium ions, etc. [1] With so many excellent accomplishments of detecting intermediates, it is logical to assume LFP should be capable of detecting phenyloxenium ions as well.

Figure 1.5 shows a simplistic schematic representation of a laser flash photolysis system. A laser pulse is generated and travels through the photo activatable sample, followed by the photo excitation of the sample to the excited states. Once the photo excited state of the sample is formed after the first laser pulse, a conventional light source, such as a xenon lamp, which produces broadband UV-visible or infrared light, is operated to collect subsequent spectra of the photo-excited sample. The absorbance of the initial starting material is the background spectrum. It will be at their maximum at the very beginning right after the excitation by the laser and decays over time. All of the following spectra is subtracted from the initial background spectrum to generate the time resolved transient absorption spectrum.

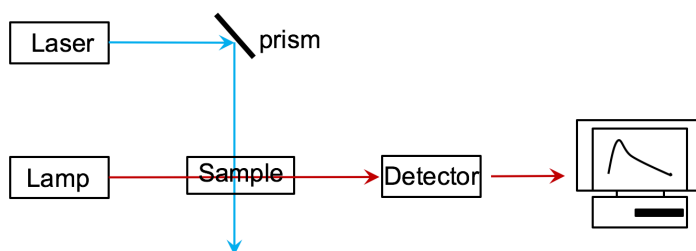


Figure 1.5 Schematic representation of a laser flash photolysis set-up.

By analyzing the series of spectra and the continuous changes, qualitatively and quantitatively, we can accordingly conclude much useful information in regards to the nature of short lived photo generated intermediates. For instance, the decay rates of the species can be determined by fitting experimental data to exponential data models. It is also important to learn the reactivities by reading the trapping rate constants when trapping solvents or other reagents are present in the same system.

LFP has been widely used to investigate photophysical behavior of various molecular systems, where target samples usually do not undergo photo degradation after photo excitation and tend to relax back to their ground states. [19] On the contrary, to study reactive intermediates, such as oxenium ions, suitable photo precursors are required for photo heterolysis occurring through the photo reaction pathway via conical intersection. The lack of appropriate photo precursors inevitably leads to the limited knowledge of oxenium ions at present.

1.3 Previous Experimental Discoveries of Phenyloxenium Ions

As discussed earlier, aryl oxenium ions, in comparison to alkyl oxenium ion, have more energetically accessible electronic configurations due to the broken degeneracy of the p orbitals located on the oxygen atom and closer singlet triplet energy gap. Previous experimental studies of oxenium ions have focused on phenyloxenium ions by thermal generation methods. Studies of their stable end products permitted indirect characterizations of their reactivities. In the 1970s and early 1980s, Abramovitch and Okamoto used thermolytic methods to generate phenyloxenium ions and learn from the thermo products (see Figure 1.6).

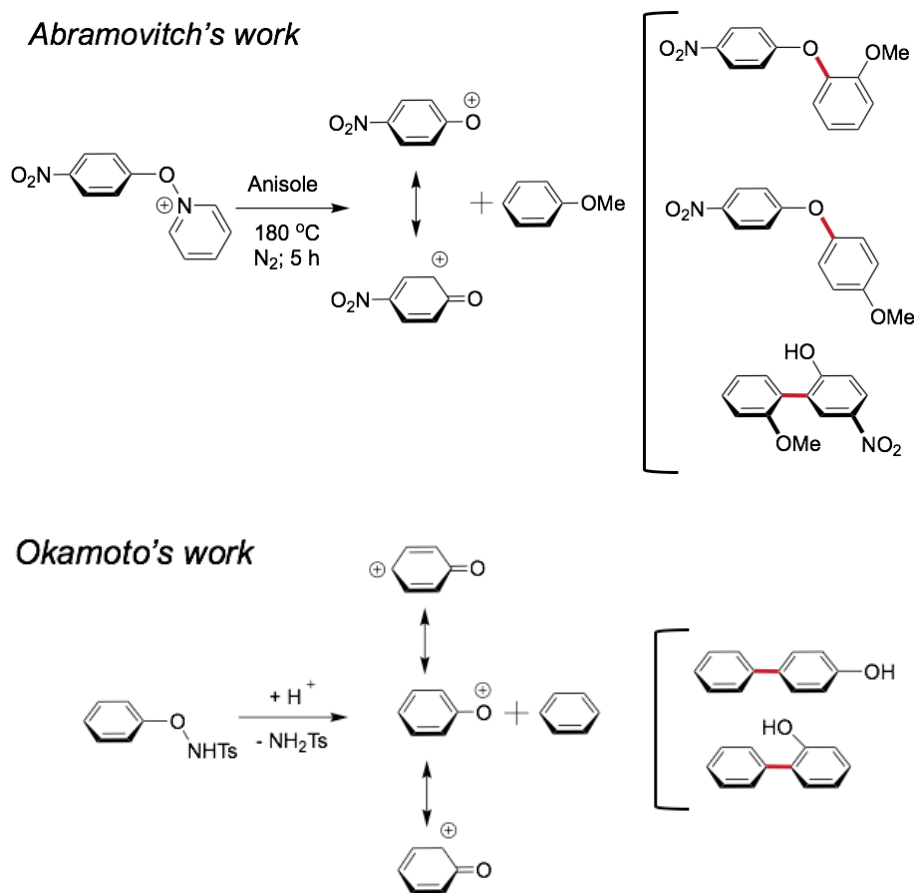


Figure 1.6 Early discoveries of oxenium ions done by Abramovitch and Okamoto. (See context for more details.)

In one of Abramovitch's works shown in Figure 1.6, a pyridinium salt of the corresponding phenyloxonium ion was submitted into high temperature under inert gas condition (N_2 atmosphere) for 5 hours in anisole, and thermolysis in a heterolysis fashion occurred, producing the nitro phenyloxonium ion, which was not directly observed because of the instrumentation restriction but its existence was confirmed by the thermolysis products. The products obtained from the thermolysis elaborates that the generated phenyloxonium ion reacts as an electrophile with the nucleophilic solvent, anisole, on the oxygen atom or the ortho position of the benzene core, which can be explained by the two resonance structures of the oxenium ion displayed in Figure

1.6. The existence and electrophilic nature of phenyloxenium ion was further suggested in the solvolysis studies completed by Okamoto. In one of his research achievements shown in Figure 1.6, the solvolysis precursor released the leaving group, p-Toluenesulfonamide, in the acidic condition, producing the parent phenyloxenium ion, which then reacted with the ambient solvent, benzene, in a nucleophilic addition fashion. The three resonance structures tell that the positive charge can only maintain on the ortho or para sites in the aromatic core, allowing the ortho and para adducts detected from the reaction mixtures.

With the laser flash photolysis invented, only recently have phenyloxenium ions been directly observed by LFP in solutions. In 2007, Novak, Platz, and coworkers published the first direct detection of an aryloxenium ion in solution (a biphenyl oxenium ion) using laser flash photolysis, providing definitive evidence that these reactive ions are actually discrete intermediates. [20] Figure 1.7 exhibits the details of this study, 4-methyl-4-biphenyloxenium ion, along with the biphenyl radical resulted from the photohomolysis reaction pathway, was generated by photolysis of the 4-(4-methylphenyl)-4-acetoxy cyclohexadienonyl derivative. The LFP data obtained at 20 nanosecond showed two transient peaks: one located around 380 nm was attributed to the known biphenoxy radical; the other was assigned to be the corresponding biphenyl oxenium ion. These two species are further differentiated by their distinct lifetimes: the radical moiety had relatively longer lifetime up to micro second time scale in comparison to the much shorter lived biphenyl oxenium ion, which was reported to be approximately 170 ns. Another experimental study also backed the assignments: when sodium azide (NaN_3 , an excellent nucleophile) was added into the solution, the decay rate of the previously assigned radical peak was not affected while the nucleophilic biphenyl oxenium ion peak decayed more rapidly because of the nucleophilic trapping reaction taking place. These studies were of great

importance because they elaborated the first direct observation of a discrete oxenium ion using laser flash photolysis, allowing chemists taking a direct look at the spectroscopic properties and reactivities of oxenium ions for the very first time.

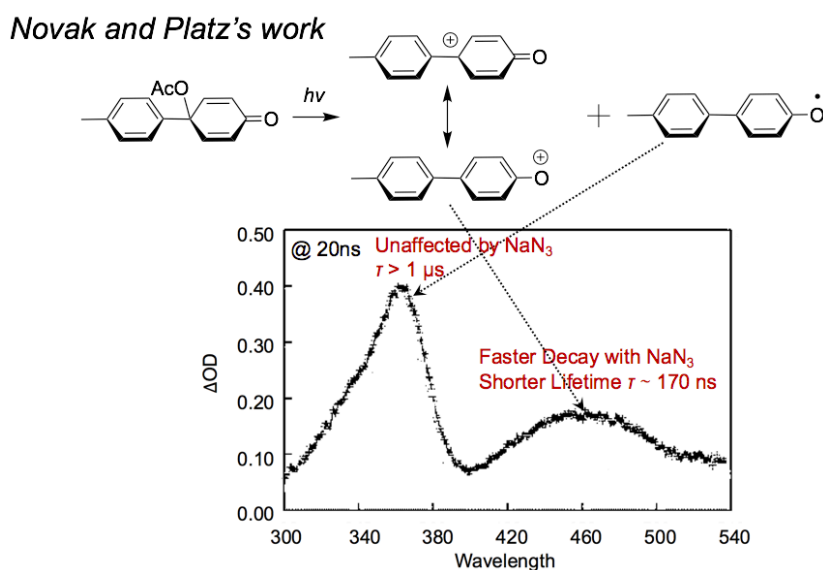


Figure 1.7 First direct detection of an aryl oxenium ion in solution with LFP spectral evidence.

The peak at 380nm was assigned to be biphenoxy radical and the other broad peak with much shorter lifetime was attributed to be the biphenyl oxenium ion, which had faster decay rate with the addition of nucleophiles, such as sodium azide.

It is absolutely exciting and encouraging of the first observation of the oxenium ion. This biphenyl photoprecursor, however, has its intrinsic limitation that it requires a para substituent to prohibit tautomerization, making it not practical for the photogeneration of the parent phenyloxenium ion. Understanding the reactivity of the parent phenyloxenium ion is able to benchmark the reactivity of this class of reactive intermediate among the related phenylnitrene, phenylnitrenium ion, and phenylcarbene.

Following Novak and Platz's detection of a substituted biphenyl oxenium ion, to generate and study the parent phenyloxenium ion, our research lab selected protonated hydroxylamine tetrafluoroborate salts as photoprecursors to generate the parent phenyloxenium ion. [4] In addition to a concomitant homolytic process that generates a radical side product, these hydroxylamine salts undergo heterolytic bond cleavage of the O–N bond to give the products: the closed-shell singlet parent phenyloxenium ion and neutral ammonia. The parent phenyloxenium ion studied in this work demonstrates closed-shell singlet ground state has a lifetime of a few nanoseconds in solution, typically reacting as an electrophile with nucleophiles (e.g., ammonia, chloride, water) at the ortho and para positions to produce phenols as the final stable photo products (see Figure 1.8).

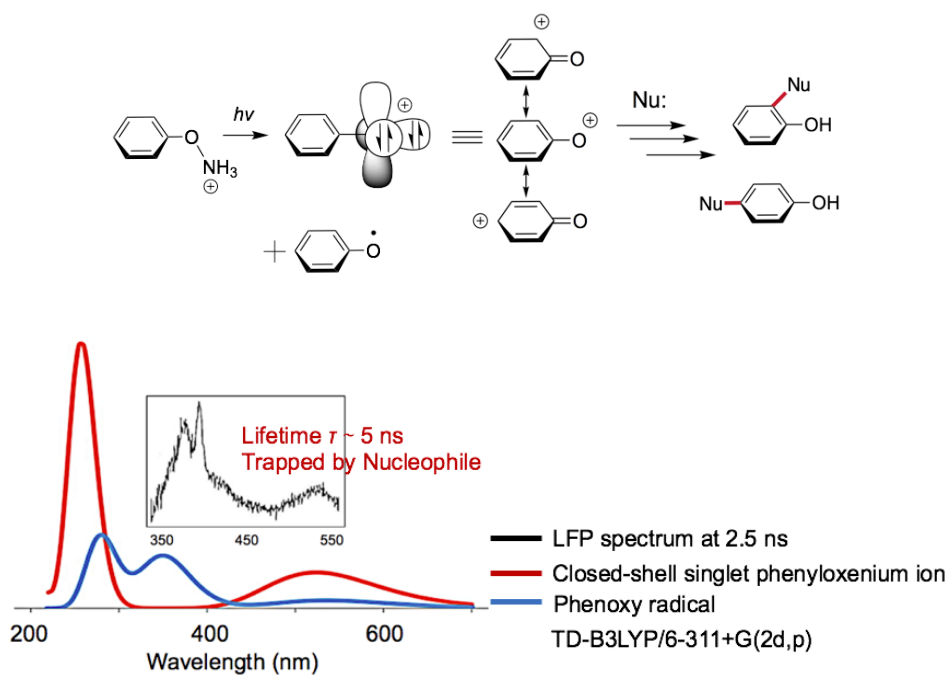


Figure 1.8 First direct detection of parent phenyloxenium ion in solution with LFP spectral evidence. (See context for more details.)

Figure 1.8 also provides the experimental LFP data obtained at 2.5 ns. By comparing to the computed UV-vis spectrum of closed-shell singlet phenyloxenium ion (in red) and phenoxy radical (in blue). Based on the absorbance wavelength, we can clearly tell that the experimental data suggests the phenyloxenium ion was what LFP detected. Moreover, phenoxy radical has known lifetime far longer than that of detected species, which was 5 ns. The additional trapping studies also confirmed the photo generation of the closed-shell singlet phenyloxenium ion and it reacted as typical electrophiles in solution.

The only other electronic configurations of phenyloxenium ion that has been reported is the π,π^* triplet ground state.[6] In this case shown in Figure 1.3, a meta pi donating group, dimethylamino group, has stabilized the triplet state to be its ground state in preference to the singlet state by 12 kcal/mol calculated at CBS-QB3 level of theory. This π,π^* triplet ground state phenyloxenium ion exhibits radical reactivity and undergoes two consecutive hydrogen atom abstractions to form the final reduced phenol product, indicating the triplet reacts as radicals similar to most reactive intermediates adopting triplet states. Other spin configurations of phenyloxenium ions await discoveries and modern computations could provide some profound clues.

1.4 Computations as Theoretical Approaches to Studying Phenyloxenium Ions

Computational analysis has been proven extremely helpful in predicting the ground states and demonstrating the electronic configurations of reactive intermediates. Typically, single-reference methods (such as density functional theory) give good estimates for singlet-triplet energy gaps. When strict broken symmetry systems are required, more sophisticated methods are used, such as high level multireference CASSCF/CASPT2 computations. One supportive

example of modern computation's capabilities for evaluating the ground state is the realization of π,π^* triplet ground state phenyloxenium ion shown in Figure 1.3, which was theoretically predicted years before the experimental detection. [6,21] Another finding that can be drawn from the study of π,π^* triplet ground state is that by changing the substitutions in a proper fashion, the singlet triplet state energies would vary and could reverse the ground states of aryl oxenium ion to be triplet ground states.

The detailed adiabatic and vertical energies of phenyloxneium ion have also been revealed using detailed computational investigations (see Table 1.1). The parent phenyloxenium ion adopts closed-shell singlet ground state and its first singlet excited state is the open-shell singlet state whose adiabatic energy is 30.8 kcal/mol higher in comparison to its ground state. The theoretical evaluation of the ground state can assist chemist to analyze and characterize the reactivities of certain oxenium ions from the photo products. For instance, if the ground state is calculated to be closed-shell singlet state, one can anticipate to see the nucleophilic addition compounds in the final product mixture. Figure 1.9 displays schematic configurations of several singlet and triplet phenyloxenium, which can be used for conceptual understanding of the spin configuration. Computations are also powerful to visualize the selected molecular orbitals, which can further aid the reactivity prediction.

Another important fact shows why computation plays a significant role in reactive intermediates chemistry is that most LFP experiments result in the spectrum of uncharacterized intermediates and need modern computational evidence to support the LFP spectral assignments using UV-vis simulations.

Table 1.1 Adiabatic and vertical energies (kcal/mol) of phenyloxenium ion electronic states (CASPT2(8,8)/pVTZ//CASSCF(8,8)/pVTZ, C_{2v} symmetry)

Irreducible representation (C_{2v})	Principal determinant (s)	Relative energy adiabatic (vertical)
1A_1	$(1b_1^2)(2b_1^2)(1a_2^2)(1b_2^2)$	0(0)
1A_2	$(1b_1^2)(2b_1^2)(1a_2^2)(1b_2^1)(3b_1^1)$	30.8(34.8)
3A_2	$(1b_1^2)(2b_1^2)(1a_2^2)(1b_2^1)(3b_1^1)$	22.1(26.1)
3B_2	$(1b_1^2)(2b_1^2)(1a_2^1)(1b_2^2)(3b_1^1)$	29.9(38.7)

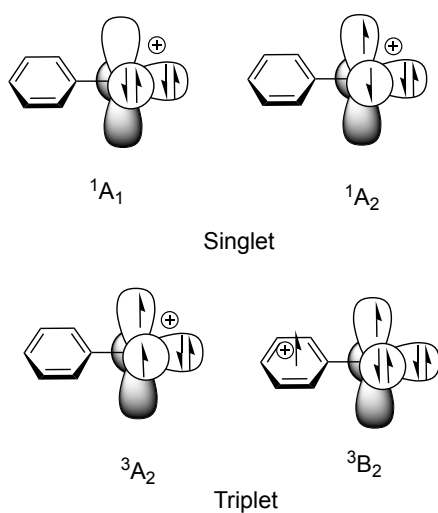


Figure 1.9 Schematic configurations of the singlet and triplet irreducible representations (C_{2v}) of parent phenyloxenium ion.

1.5 Organization of the Dissertation

Chapter 1 overviews the current progress in the phenyloxenium ion research area and points out the significance of studying such reactive intermediates as they have been proposed in numerous reaction mechanisms. In this chapter, general investigation techniques involving laser

flash photolysis and computational approaches are briefly introduced. In general, the parent phenyloxenium ions have closed-shell singlet ground states and react as typical electrophiles. Additionally, computations show powerful capabilities in analyzing the structural effect on the electronic configuration of oxenium ions

Chapter 2 describes the direct detection of an open-shell singlet phenyloxenium ion, which is considered to be an atom-centered diradical but show reactivities as an electrophile. This chapter shows a time-resolved spectroscopic study of the photochemistry of precursor 4-methoxyphenoxy pyridinium tetrafluoroborate. An open-shell singlet phenyloxenium ion (1A_2) was claimed to be observed. An efficient nucleophilic addition reaction between the open-shell singlet phenyloxenium and the solvent, MeCN, was found by laser flash photolysis and photochemical product studies, unveiling the chemical reactivity of open-shell singlet phenyloxenium ions and more broadly giving insight into the reactivity patterns of singlet diradicals. This chapter is thought to complement the field of spin configurations of oxenium ions.

Chapter 3 describes the synthesis of a photoprecursor to the p-acetyl phenyloxenium ion, which is computed to have a n,π^* triplet as its first triplet excited state. Due to the El sayed's rule, carbonyl group facilitates the intersystem crossing because there is a change of molecular orbital type ($S_1 n,\pi^* \rightarrow T_2 \pi,\pi^* \rightarrow T_1 n,\pi^*$), and the phenyloxenium ion will be produced at its n,π^* triplet state. Photolysis of this precursor was studied using product studies as well as by preliminary LFP studies. These results demonstrate evidence that the formation of a n,π^* triplet state phenyloxenium ion and allow the studies of its reactivities and spectroscopic properties.

Chapter 4 describes that azulenyl oxenium ions can have unusual high-spin π,π^* ground states by exploiting (anti)aromaticity, which replenish the knowledge of the ground states of aryl

oxenium ions. Changes in ring aromaticity/antiaromaticity lead to both a destabilized singlet state (Hückel antiaromatic) and a stabilized triplet (Baird aromatic) state and thus switch the ions from ground-state singlet ions to triplet-favored ions. Density functional theory (UB3LYP/6-31+G(d,p)) was used to determine substituent effects on the singlet–triplet energy gaps for azulenyl oxenium ions, and these unusual ground triplet states can be further tuned by deploying electron -donating or -withdrawing groups on the azulene core. By taking advantages of the (anti)aromaticity criteria from a computational perspective, the ground state of oxenium ions can be successfully manipulated and this could possibly lead to future synthetic applications.

Chapter 5 introduces a simple strategy for achieving high-energy in-plane orbitals for aromatics simply by positioning iodine atoms next to each other. The lone pair orbitals on the iodines mix to give a high-energy in-plane σ -antibonding orbital as the highest occupied molecular orbital (HOMO). It shows that this effect can be used to manipulate orbital gaps, the symmetry of the highest occupied orbital, and the adopted electronic state for reactive intermediates. Phenyloxenium ions appear to have triplet ground states using this scheme.

Chapter 6 provides a summary of all research projects and prospects of oxenium ion research area.

1.6 References

- [1] Moss, R. A.; Platz, M. S.; Jones, M., Jr. *Reactive Intermediate Chemistry*; Wiley: Hoboken, NJ, 2004.
- [2] Bourissou, D.; Guerret, O.; Gabbai, F. P.; Bertrand, G. *Chem. Rev.* **2000**, *100*, 39.
- [3] Katsumata, S.; Lloyd, D. R. *Chem. Phys. Lett.* **1977**, *45* (3), 519.

- [4] Hanway, P. J.; Xue, J.; Bhattacharjee, U.; Milot, M. J.; Ruixue, Z.; Phillips, D. L.; Winter, A. H. *J. Am. Chem. Soc.* **2013**, *135* (24), 9078.
- [5] Hanway, P. J.; Winter, A. H. *J. Am. Chem. Soc.* **2011**, *133* (13), 5086.
- [6] Li, M. D.; Albright, T. R.; Hanway, P. J.; Liu, M.; Lan, X.; Li, S.; Peterson, J.; Winter, A. H.; Phillips, D. L. *J. Am. Chem. Soc.* **2015**, *137* (32), 10391.
- [7] Winter, A. H.; Falvey, D. E.; Cramer, C. J. *J. Am. Chem. Soc.* **2004**, *126* (31), 9661.
- [8] P. J. Hanway and A. H. Winter, *J. Phys. Chem. A*, **2012**, *116*, 9398.
- [9] C. Sabot, K. C. Guerard and S. Canesi, *Chem. Commun.*, **2009**, 2941;
- [10] K. C. Guerard, C. Chapelle, M. A. Giroux, C. Sabot, M. A. Beaulieu, N. Achache and S. Canesi, *Org. Lett.*, **2009**, *11*, 4756;
- [11] C. Sabot, B. Commare, M. A. Duceppe, S. Nahi, K. C. Guerard and S. Canesi, *Synlett*, **2008**, 3226.
- [12] T. A. Wenderski, S. Huang and T. R. Pettus, *J. Org. Chem.*, **2009**, *74*, 4104.
- [13] F. Troisi, T. Pierro, C. Gaeta and P. Neri, *Org. Lett.*, **2009**, *11*, 697.
- [14] K. Omura, *J. Org. Chem.*, **1996**, *61*, 7156.
- [15] J. S. Swenton, K. Carpenter, Y. Chen, M. L. Kerns and G. W. Morrow, *J. Org. Chem.*, **1993**, *58*, 3308. *J. Org. Chem.* **2012**, *77*, 2121.
- [16] R. L. Osborne, M. K. Coggins, G. M. Raner, M. Walla and J. H. Dawson, *Biochemistry*, **2009**, *48*, 4231.

- [17] J. Lewis and R. Prinn, *Planets and Their Atmospheres*, Academic Press, New York, 1994.
- [18] D. Smith, *Chem. Rev.*, **1992**, *92*, 1473.
- [19] P. P. Levin, I. V. Khudyakov., *J. Phys. Chem. A* **2011**, *115*, 40, 10996
- [20] Wang, Y.-T.; Jin, K. J.; Leopold, S. H.; Wang, J.; Peng, H.-L.; Platz, M. S.; Xue, J.; Phillips, D. L.; Glover, S. A.; Novak, M. *J. Am. Chem. Soc.* **2008**, *130*, 16021
- [21] Winter, A., Cramer, C., Gherman, B., Falvey, D. *J. Am. Chem. Soc.* **2007**, *129* (33), 10113.

CHAPTER 2. DIRECT DETECTION OF THE OPEN-SHELL SINGLET PHENYLOXENIUM ION: AN ATOM-CENTERED DIRADICAL REACTS AS AN ELECTROPHILE

Modified and reprinted from *J. Am. Chem. Soc.* **2017**, *139*, 42, 15054-15059

Copyright © 2017, American Chemical Society

Yunfan Qiu, Lili Du, Xin Lan, Ruixue Zhu, David Lee Phillips, Ming-De Li, Andrew S. Dutton and Arthur H. Winter.

2.1 Abstract

A new photoprecursor to the parent phenyloxenium ion, 4-methoxyphenoxyppyridinium tetrafluoroborate (**1**), was investigated using trapping studies, product analysis, computational investigations, and laser flash photolysis experiments ranging from the femtosecond to the millisecond time scale. These experiments allowed the completion of the photophysics and photochemistry of this photoprecursor beginning with the initially populated excited states to its sequential formation of transient intermediates and ultimate formation of stable photoproducts. In this chapter, the excited state of this photoprecursor undergoes photoheterolysis to generate the parent phenyloxenium ion in ~2 ps but surprisingly generates the ion in its open-shell singlet diradical configuration (1A_2 , $^{os}2$), permitting an unexpected look at the reactivity of an atom-centered open-shell singlet diradical, which also complements the investigations of phenyloxenium ions since only closed-shell singlet and triplet oxenium ions have been studied thus far. The open-shell phenyloxenium ion (1A_2) has a much shorter lifetime ($\tau \sim 0.2$ ns) in acetonitrile than the previously observed closed-shell singlet (1A_1) phenyloxenium ion ($\tau \sim 5$ ns). Remarkably, despite possessing singly occupied molecular orbitals and no empty valence orbitals, this open-shell singlet phenyloxenium ion behaves as an even more powerful

electrophile than the closed-shell singlet phenyloxenium ion, undergoing solvent trapping by weakly nucleophilic solvents such as water and acetonitrile or externally added nucleophiles rather than engaging in typical diradical chemistry, such as hydrogen atom abstraction, which we have previously observed for a triplet oxenium ion. In acetonitrile, the open-shell singlet oxenium ion is trapped to generate ortho and para Ritter intermediates, one of which (para) is directly observed as a longer-lived species ($\tau \sim 0.1$ ms) in time-resolved resonance Raman experiments. The Ritter intermediates are ultimately trapped by either the 4-methoxypyridine leaving group (in the case of para addition) or trapped internally via an essentially barrierless rearrangement (in the case of ortho addition) to generate a cyclized product. The expectation that singlet diradicals react similarly to triplet or uncoupled diradicals needs to be reconsidered. This chapter provides direct spectroscopic observation of an atom-centered open-shell singlet diradical reacting as a powerful electrophile.

2.2 Introduction

Despite oxenium ions taking part in a variety of important processes, studies of the reactivities and properties of oxenium ions have been limited by the lack of general photoprecursors to these reactive intermediates. In 2007, Novak and co-workers [1,2] reported the first direct detection of an aryl oxenium ion in solution from laser flash photolysis of the 4-(4-methylphenyl)-4-acetoxycyclohexadienonyl derivatives and observed the 4-methyl-4-biphenyloxenium ion directly, which demonstrated that oxenium ions are discrete intermediates as well as the feasibility of studying oxenium ions with time-resolved spectroscopic methods. However, further studies on the design of suitable precursors for the phenyloxenium ion have been difficult due to the limitations on the requirements for the para

substituent of the precursors in efficiently generating the oxenium ion. Following Novak and co-workers' initial reports, we observed the closed-shell ground-state parent phenyloxenium ion ^{CS}**2** from photolysis of a protonated phenylhydroxylamine (see Figure 2.1). [3] The design of positively charged precursors has several advantages, including the ability to (in principle) generate the oxenium ion in any solvent system, rather than requiring ionizing solvents. However, like the photoprecursors in the work of Novak and co-workers, photolysis of the protonated hydroxylamine photoprecursors led to competing generation of phenoxy radicals, complicating the subsequent analysis. Protonated hydroxylamine derivative was also used to photochemically generate a π,π^* triplet ground state phenyloxenium ion (see Figure 2.1). A meta pi donating group, dimethylamino group, has stabilized the triplet state to be its ground state in preference to the singlet state by 12 kcal/mol calculated at CBS-QB3 level of theory. This π,π^* triplet ground state phenyloxenium ion exhibits radical reactivity and undergoes two consecutive hydrogen atom abstractions to form the final reduced phenol product, indicating the triplet oxenium ions reacts as radicals as anticipated. [4,5] Inspired by previous studies [6] for generating aryl nitrenium ions from photolysis of N-pyridinium ions, precursor, 4-methoxyphenoxy pyridinium tetrafluoroborate **1** was synthesized as a potentially improved photoprecursor for the phenyloxenium ion **2** and was anticipated to reduce the concomitant radical generation resulting from competing homolysis. (See APPENDIX A for detailed synthesis scheme and compound characterizations) Indeed, photolysis of this photoprecursor relatively cleanly generates the phenyloxenium but surprisingly generates the oxenium ion in its excited open-shell singlet diradical (¹A₂) electronic configuration, This result is encouraging because it allows us to directly observe an atom-centered open-shell singlet oxenium ions considering only closed-shell single and triplet oxenium ions have been studied thus far.

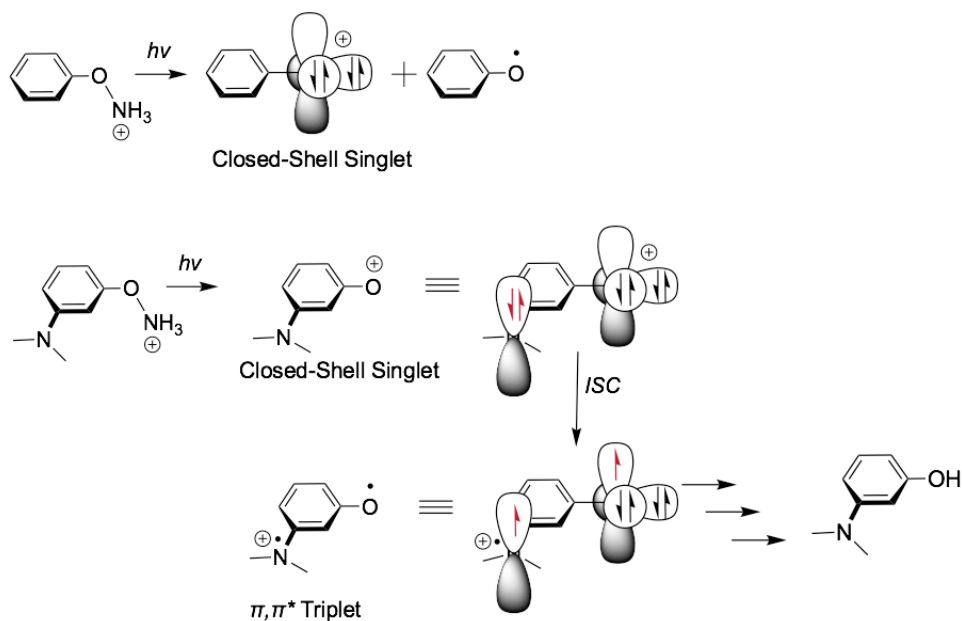


Figure 2.1 Protonated phenylhydroxylamine derivatives have been used to generate a closed-shell singlet phenyloxenium ion and triplet oxenium ions.

In this chapter, a time-resolved spectroscopic study of the photochemistry of precursor **1** and an investigation of the reactivity of phenyloxenium^{os} **2** using femtosecond transient absorption (fs-TA), nanosecond transient absorption (ns-TA), and nanosecond time-resolved resonance Raman (nsTR³) spectroscopy methods. This chapter demonstrates the remarkable effect of the photoleaving group, as a related protonated hydroxylamine photoprecursor [3] generates the closed-shell singlet phenyloxenium ion (¹A₁) in combination with the phenoxy radical, while this new photoprecursor with a pyridine leaving group intriguingly produces the open-shell singlet parent phenyloxenium ion (¹A₂). Figure 2.2 exhibits reaction pathways for the reactions of this open-shell singlet phenyloxenium ion **2** with the solvents and other quenchers, including the leaving group itself (pyridine is also considered to be nucleophilic.). The

quenching study of this open-shell singlet phenyloxenium **2** with weakly nucleophilic solvents such as water, as well as externally added azide, gives evidence of the electrophilic character of this open-shell singlet oxenium ion species.

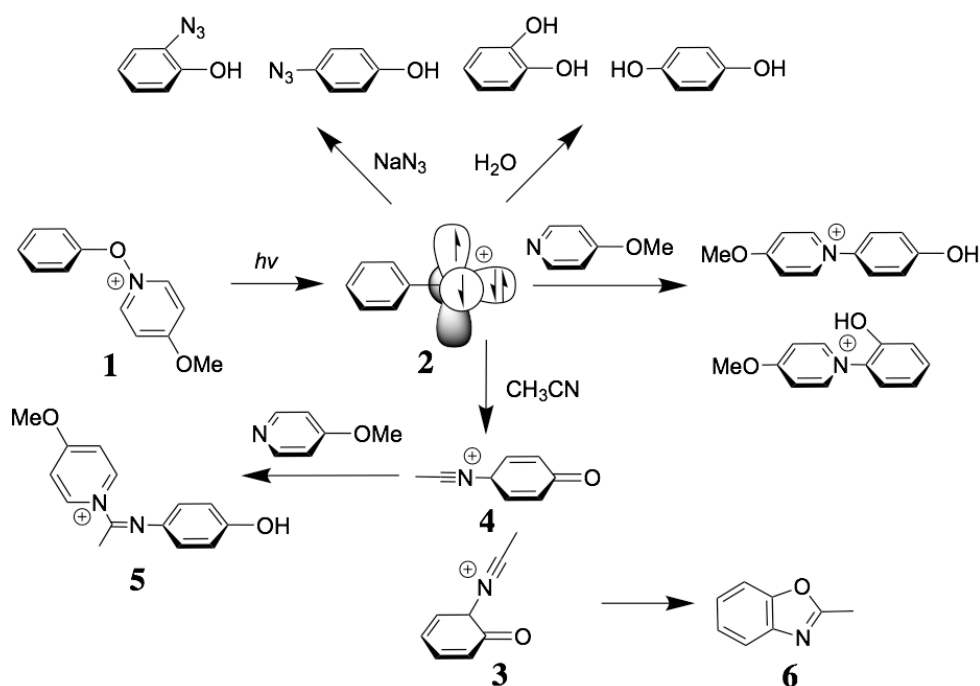


Figure 2.2 Reaction pathways for the reactions of the open-shell singlet phenyloxenium ion **2** with the solvents and other quenchers

Furthermore, in MeCN, an efficient nucleophilic addition reaction is detected between the open-shell singlet phenyloxenium **2** and the solvent by laser flash photolysis and photochemical product studies. The consequent nitrilium ion adducts **3** and **4** are known to be significant intermediates in Ritter reactions. [7] Nucleophilic additions to diradicals or diradicaloids have been proposed by Perrin and Reyes-Rodriguez [8] and Myers et al. [9] for the addition of nucleophiles to p-benzyne and dehydrotoluene. In the latter case, Myers et al.

proposed the zwitterionic character for the intermediate. Squires and co-workers [10] have also shown that benzyne can be formed from collision-induced dissociation (CID) of halo anions, which can be thought of as this process in reverse. Here direct spectroscopic supports that an atom-centered diradical **2** acts as an electrophile. The formation of the Ritter intermediate provides new insight into the structure and chemical reactivity of open-shell singlet oxenium ions and more broadly provide insight into the reactivity patterns of singlet diradicals. To the question of whether a nucleophile can attack a singly occupied molecular orbital, the answer is apparently yes, at least if another partially occupied orbital is available to avoid violation of the rules of valence.

2.3 Experimental Section

fs-TA, ns-TA, and ns-TR³ Experiments. The experimental setups and methods used for these experiments have been previously reported. [11] Briefly, the fs-TA measurements were accomplished using a femtosecond regenerative amplified Ti:sapphire laser system in which the amplifier was seeded with the 120 fs laser pulses from an oscillator laser system. The laser probe pulse was produced by utilizing ~5% of the amplified 800 nm laser pulses to generate a white-light continuum (325–650 nm) in a CaF₂ crystal, and then this probe beam was split into two parts before traversing the sample. The flowing sample was excited by a 267 nm pump laser beam. An absorbance of **1** at 267 nm was used for the sample solutions for the fs-TA experiments in order to maintain the same number of photons being absorbed for the same irradiating conditions for the samples. The nanosecond (ns-TA) experiments were performed using the fourth harmonic output of an Nd:YAG laser that supplied the 266 nm laser pump pulse. The probe light came from a 450 W xenon lamp. The 266 nm pump laser beam photoexcited the

sample, and at a right angle the probe light from the xenon lamp traversed the sample held in a 1 cm flowing quartz cell. The transmitted probe light was then detected by a single detector (for kinetic analysis) or by an array detector (for spectral analysis). The nanosecond time-resolved Resonance Raman (ns-TR³) experiments were performed using the fourth harmonic of an Nd:YAG nanosecond pulsed laser that supplied the 266 nm pump wavelength. The pump pulse photoexcited the sample to start the photochemical processes, and the probe pulse monitored the sample and the intermediate species formed. The laser beams were lightly focused and lined up so that they merged together onto a flowing argon-purged sample solution. A pulse delay generator was utilized to electronically set the time delay between the pump and probe laser pulses. The Raman scattered signal was collected using a backscattering geometry and observed by a liquid-nitrogen-cooled charge coupled device (CCD) detector. The ns-TR³ spectra shown here were found by subtraction of an appropriately scaled probe-before-pump spectrum from the correlated pump-probe resonance Raman spectrum to mostly get rid of nontransient bands. The Raman bands of MeCN were used to calibrate the Raman shifts with an estimated uncertainty of 5 cm⁻¹.

Computational Methods. Density functional theory (DFT) computations were performed using the Gaussian09 software suite. [12] In all cases, optimized geometries were found to have zero imaginary frequencies, and corrections for the zero-point vibrational energy were added unscaled. Geometries of the closed-shell singlet phenyloxenium ion and the phenoxy radical molecular were optimized at the B3LYP/cc-pVTZ level of theory. The computed UV-vis spectrum of Ritter intermediate **4** was calculated at the TD-(U)B3LYP/6-31+G(d,p) level with the optimized geometry at the (U)B3LYP/6-31+(d,p) level employing a SMD (acetonitrile) solvent model. To predict the TR³ spectra of the Ritter intermediate **4**, B3PW91/6-31+G(d,p)

was employed to optimize the structure and predict the Raman spectra. A simulated bandwidth for the spectra was determined using a Lorentzian of 10 cm^{-1} bandwidth for the vibrational band frequencies. A frequency scaling factor of 0.960 was used in the comparison of the calculated results with the experimental spectra. CASPT2(8,8)/ANOL calculation was utilized to optimize the geometry of the open-shell singlet phenyloxenium ion (1A_2) using the Molcas 8.0 software. [13] To predict the UV-vis absorption spectrum, single-point energies at the MS-CASPT2 level were calculated using the final geometry from the previous calculation for five states, and the transition dipole for the transitions between the states was calculated. The band shapes were simulated using the GaussSum method.

Product Studies. Photochemical product studies in deuterated solvents were performed with 2.5 mg of precursor **1** dissolved in 1 mL of CD_3CN and 1 μL of the internal standard decane. The mixture was filtered and an initial ^1H NMR was taken with a 90° angle and a relaxation delay of 60 s in a quartz NMR tube. The sample was then irradiated with 254 nm UV light from a mercury vapor lamp for different desired time durations in a Rayonet photoreactor. Spectra were taken with the previous parameters. After the photolysis and ^1H NMR characterization were completed, the sample was submitted to LC-MS for further product confirmation. Comparison between the ^1H NMR spectra of the sample and the standard chemicals also clarified the peak assignments and the products generated. (See APPENDIX A for ^1H NMR spectra of authentic compounds.)

2.4 Results and Discussion

Transient Absorption Study of 1. Photolysis of **1** by fs-TA was investigated in MeCN solution after excitation by 267 nm, and the resulting transient absorption spectra are shown in

Figure 2.3.a, b. The initial spectrum at 1 ps (Figure 1a) shows a broad band at 510 nm and a band tail from 325 to 350 nm, which can be assigned to the singlet excited state of the precursor **1**.

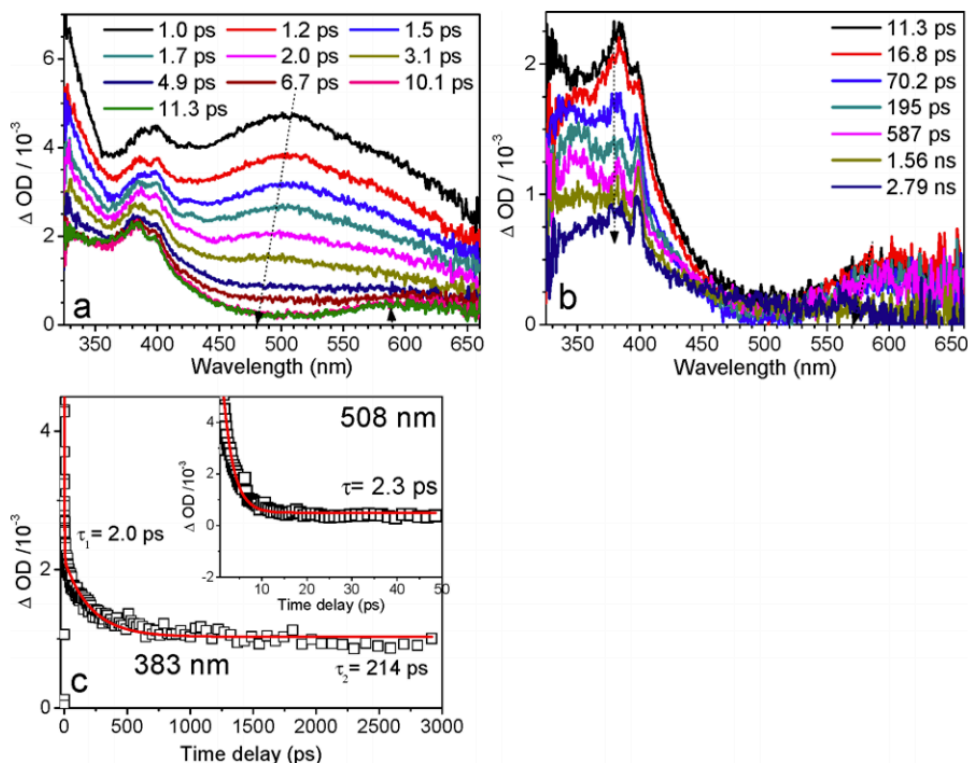


Figure 2.3 fs-TA of the precursor **1** after 267 nm excitation in MeCN (a, b); the kinetics at 383 nm are shown in part c and the kinetics at 508 nm are shown in the inset. The solid red lines indicate the fitting to the experimental data.

Both bands at 510 and 325 nm simultaneously decay over a few picoseconds, giving rise to a new peak having maxima at 383 nm and a small broad tail ~ 600 nm, assignable to a new species after cleavage of the O–N bond. Fitting the kinetics at 383 nm to a biexponential function, two time constants (2 and 214 ps) were determined in Figure 2.3.c. The first (2 ps) is attributed to bond cleavage of the excited state to yield the open-shell oxenium ion, while the second is assigned to the decay of the open-shell oxenium ion into downstream intermediates.

Assignment of the Open-Shell Oxenium Ion. A recent high-level (CASPT2/ANO-L) computational study of the phenyloxenium ion indicated that the phenyloxenium ion possesses a closed-shell singlet ground state (1A_1 , S_0 , C_{2v}) with a singlet–triplet gap of ~ 20 kcal/mol (1A_1 – 3A_2). An open-shell n,π^* singlet state (1A_2) is computed as its first singlet excited state (S_1), with an adiabatic energy gap of ~ 31 kcal/mol. [14] Other π , π^* singlet excited states are higher in energy. Surprisingly, the new species following the excited state of the precursor **1** is not the expected closed-shell singlet oxenium ion, which was previously detected at 524 nm in MeCN following decay of the excited state (the computed closed-shell phenyloxenium ion band has maxima at 520 nm, in good agreement with experiment; Figure 2.4, red line). [3] Instead, it is assigned to the open-shell singlet phenyloxenium ion $^{os}2$ from the following observations.

As shown in Figure 2.4, comparison of the spectrum at 11.3 ps in MeCN solution with the MS-CASPT2 simulated UV–vis spectrum of the 1A_2 singlet open-shell phenyloxenium ion indicates that the bands at 383 and 600 nm are in reasonable agreement (experimentally, the long wavelength shoulder band appears to be solvatochromic, explaining some disagreement with the gas-phase computed value for this peak). In principle, the excited state of the photoprecursor can connect to any electronic state of the product **2**. MS-CASPT2-simulated UV–vis spectra (see APPENDIX A) of the other low-lying singlet excited states of the phenyloxenium ion (e.g., 1B_1 and 1B_2) are in poorer agreement with the experimental spectrum than the 1A_2 state. Furthermore, these alternative states at their optimized geometries are close in energy with the 1A_2 state and would be expected to rapidly undergo internal conversion to the 1A_2 state if they were initially populated upon heterolytic cleavage of **1**. Although in appearance the sharp peaks at 380 and 400 nm resemble the absorption of the phenoxy radical, [3] several experiments show that it is not

mainly because of the radical. First, most of this transient signal is trapped by azide and by water to generate water adducts, and the species has a much shorter lifetime in water than in MeCN (14 ps in H₂O vs 214 ps in MeCN). In pure MeCN, most of this transient signal is followed by solvent-trapping Ritter intermediates, which are clearly characterized by the ns-TR³ experiments described later. These behaviors are indicative of a cationic intermediate, not a radical.

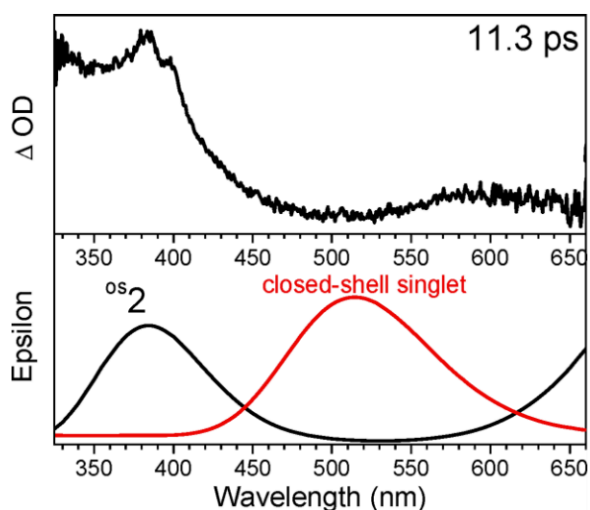


Figure 2.4 fs-TA spectrum of **1** at 11.3 ps in MeCN solution (top). Computed UV-vis spectra of the open-shell phenyloxenium ion **2** (bottom, black) at the CASPT2(8,8)/ANO-L-VTZP level and the closed-shell phenyloxenium (bottom, red) at the TD-B3LYP/6-311G (2d,p) level. The computed 380 nm band of ^{os}2, which has a low computed oscillator strength, is artificially magnified by 100-fold relative to the near-IR shoulder bands to make it observable.

Moreover, the previously observed phenoxy radical has a lifetime of 150 ns in MeCN, [3] while most of this transient signal has a lifetime of ~0.2 ns in MeCN. It suggests that because the open-shell singlet oxenium ion has an identical π orbital occupation as the phenoxy radical, it has a relatively similar absorption profile. While it is possible that a small amount of radical is

generated concomitantly with the oxenium ion, it is present in too small amounts to be seen in the ns-TR³ experiments. This is in contrast to prior studies of the closed-shell singlet states, where the side product radical could be clearly seen in the ns-TR³ experiments. [1-3] The possibility that the transient is the triplet oxenium ion can be ruled out because it is generated too quickly to allow for intersystem crossing, which for π,π^* absorptions typically occurs with rate constants on the order of $10^6 - 10^8 \text{ s}^{-1}$. Furthermore, the previously observed π,π^* triplet ground state phenyloxenium ion underwent H atom abstraction reactions, [4] not nucleophilic additions. Though **2** is generated in the form of the open-shell singlet excited state, the internal conversion to its ground state (^{cs}2) is not detected within a 200 ps lifetime before reaction occurs based on the absence of the closed-shell singlet transient peak (Figure 2.4, red line). Indeed, a prior theoretical investigation that has mentioned earlier has demonstrated that phenyloxenium ion has a closed-shell singlet ground state (¹A₁, S₀, C_{2v}), and its open-shell singlet state (¹A₂) is computed as its first singlet excited state with a 30.8 kcal/ mol adiabatic energy difference. [14] This large energy gap between the ¹A₁ and ¹A₂ is anticipated to cause a slow internal conversion over 200 ps. In addition, the symmetry restriction could also prevent the adequate mixing of the orbitals, preventing the internal conversion from occurring efficiently. This relatively slow internal conversion permits the direct spectroscopic observation of the reactivity of the open-shell singlet phenyloxenium ion.

An intriguing question is why the protonated hydroxylamine affords the closed-shell singlet phenyloxenium upon photolysis (see Figure 2.1) while **1** generates the open-shell singlet state. While this question can really only be addressed by excited-state PES mapping and conical intersection searches, a TD-DFT ground state–excited state difference density plot (Figure 2.5) indicates that the nature of the first singlet excited states between the two photoprecursors is

quite different. The protonated hydroxylamine photoprecursor has a π,π^* singlet excited state necessarily located on the benzene ring. In contrast, **1** has an excited state featuring significant charge redistribution to the pyridine ring. The differing excited state electronic distribution may lead to the unique adiabatic heterolysis for **1**.

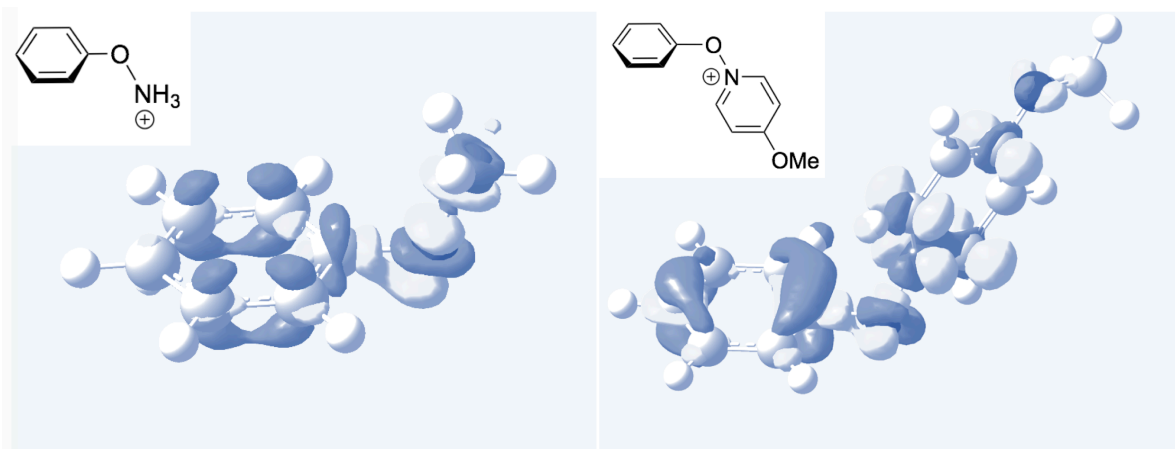


Figure 2.5 Total electron density difference plots of two photochemical precursors of the phenyloxenium ion. The contrasting distribution could result in different photoreaction channels and thus different photo products (1A_1 and 1A_2 phenyloxenium ions).

Azide Trapping Studies. As further confirmation of the existence of the phenyloxenium ion $^{os}2$ and its electrophilic character, a quenching study was performed by adding an azide trap to the solution in Figure 2.6. As shown in Figure 2.6.a, there are two transient absorption bands around 300 and 370 nm just after the pulse in the 1:4 H₂O:MeCN solution. At a later delay time, the 370 nm transient absorption band gradually disappears and the 300 nm transient band shifts down to 280 nm. The band at 370 nm has a lifetime of around 100 μ s in the 1:4 H₂O: MeCN solution. However, in the presence of 12.5 mM NaN₃ (Figure 2.6.b), no band at 370 nm shows up and a more noticeable sharp band at 400 nm is observed. The comparison of the spectra just

after the pulse is also displayed in Figure 2.6.c. In the presence of the quencher, the band at 370 nm is lower than the one without a quencher. The initial band at 370 nm is assigned to Ritter intermediate **4** (after deprotonation), produced from the efficient reaction between the open-shell singlet phenyloxenium ion **2** and MeCN, based on the ns-TR³ spectrum with resonance enhancement of this band, which will be discussed later. These trapping results are consistent with a photogenerated phenyloxenium ion **2** that can undergo the nucleophilic addition reaction with MeCN to form Ritter intermediates **3** or **4** (after deprotonation), while NaN₃ performs as a superior competing trapping agent. Though the open-shell singlet ^{os}**2**, as an atom-centered diradical, would be anticipated to react similarly to triplet or uncoupled diradicals, both the formation of the Ritter intermediates and the quenching study indicate that this phenyloxenium ion **2** reacts as a powerful electrophile.

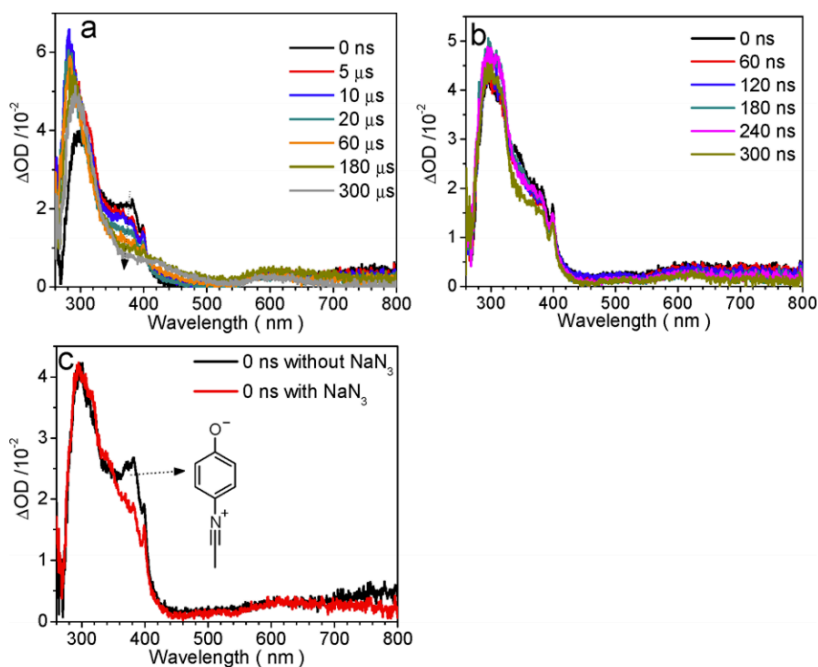


Figure 2.6 ns-TR spectra of the precursor **1** after 266 nm excitation in (a) 1:4 H₂O:MeCN and (b) 1:4 H₂O:MeCN with the presence of 12.5 mM NaN₃. (c) Comparison of spectra immediately after the pulse under both conditions.

ns-TR³ Study of 1. In the ns-TA spectra (Figure 2.6), the long-lived intermediate gives a band ranging from 325 to 380 nm. In order to unveil the nature of this intermediate, ns-TR³ experiments of this photoprecursor **1** were performed by using both 355 and 369 nm as the probe wavelengths in pure MeCN under different time scales, and this data are shown in Figures 2.7.

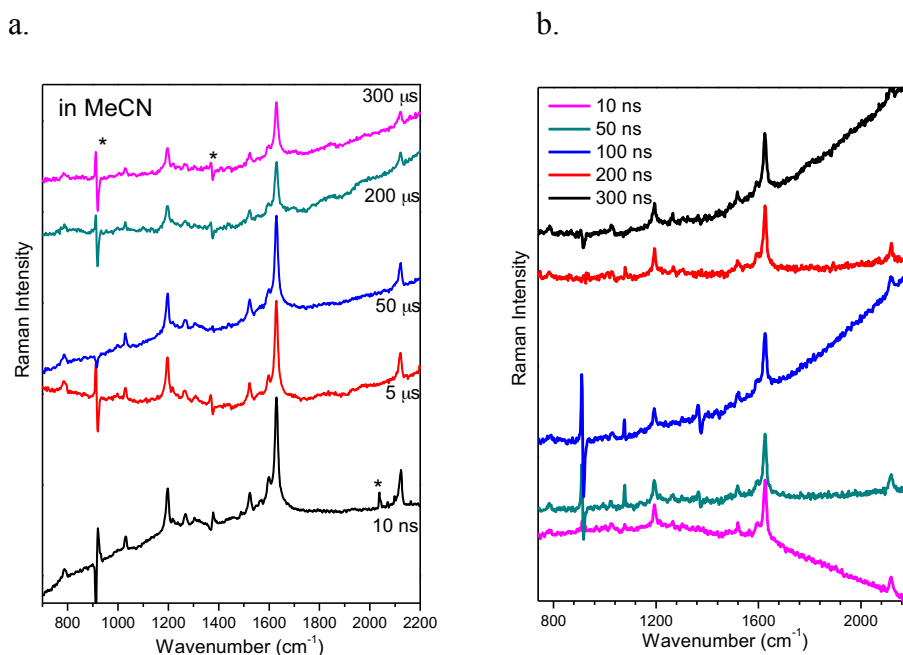


Figure 2.7 Shown are the ns-TR³ spectra of **1** in different solutions by employing a.) 355 nm; b.) 369 nm probe, 266 pump. Asterisks represent solvent subtraction artifacts.

The same Raman spectra obtained in Figure 2.7 indicate that the same species is detected by both of these probe wavelengths within the measuring time frame, which is consistent with the ns-TA results. Therefore, we only discuss the spectra we observed using the 355 nm probe wavelength here. As shown in Figure 2.7, only one species is obtained and it decays from 10 ns to 300 μ s. An unusual band at 2124 cm^{-1} is typical of a triple bond, such as an isonitrile. As discussed above, both Ritter intermediates **3** and **4** are possible reaction intermediates in MeCN.

In an attempt to identify these intermediates, DFT calculations were used to predict the Raman spectra for intermediates **3** and **4** at the B3PW91/6-31+G(d,p) level of theory. However, the deprotonated version of Ritter intermediate **3** was not found to be a minimum and underwent cyclization apparently without a barrier to produce compound **6** (shown in Figure 2.2), a compound isolated in our product studies. Thus, it is perhaps not surprising that we only detect the para Ritter intermediate **4** (after deprotonation), as it does not have access to this internal trapping decay channel. A comparison of the computed normal Raman spectrum of **4** with the experimental ns-TR³ spectrum is displayed in Figure 2.8, which shows that both the Raman vibrational frequencies and relative intensities computed for Ritter intermediate **4** are reasonably consistent with the TR³ spectrum.

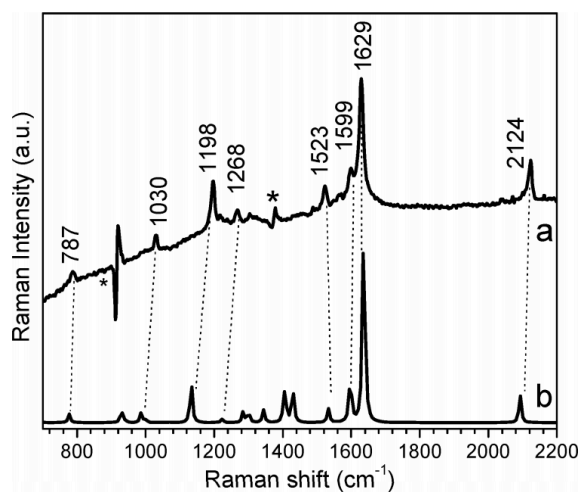


Figure 2.8 (a) ns-TR³ spectrum at 10 ns of the precursor **1** after 266 nm excitation in pure MeCN. (b) Computed Raman spectrum of Ritter intermediate **4** (B3PW91/6-31+G(d,p)). Asterisks represent solvent subtraction artifacts.

The transient species observed by ns-TR³ at an early time can be tentatively assigned to the reaction product of Ritter intermediate **4** that is produced from the reaction of the phenyloxonium ion **2** and MeCN. In Figure 2.8.a, the most intense Raman band is ascribed to the aromatic C=C stretches of the phenyl group near 1629 cm⁻¹. The second most intense Raman band in this region is the 2124 cm⁻¹ band due to the stretching mode of the isonitrilium C–N triple bond. The changes with time for the 1629 cm⁻¹ feature integrated area are shown in Figure 2.9 and the fitted lifetime is 134 μs, which is assigned to the lifetime of the Ritter intermediate **4**, about the same as the longer-lived 380 nm transient observed in the ns-TA experiments, also attributed to this intermediate. Our photo product studies indicate that this long-lived species is ultimately trapped by the p-methoxypyridine leaving group to generate an unusual imino pyridinium salt.

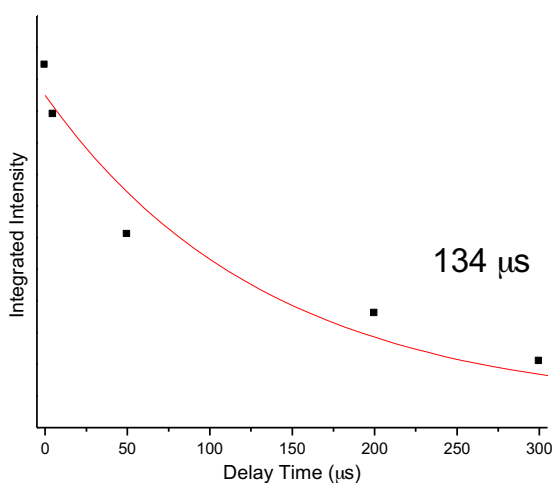


Figure 2.9 The time dependence of the 1629 cm⁻¹ Raman band fit by a one-exponential function with time constant at 134 μs.

Photochemical Product Study of 1. Stable ultimate photo product analysis was performed both in the presence and absence of trapping agents. Upon formation of the open-shell

singlet phenyloxenium ion **2** in pure acetonitrile, both the solvent (acetonitrile) and the leaving group (4-methoxyphenyl) are found to attack either the para or ortho position of the ring to produce the ultimate pyridine adducts and two nitrilium ions, **3** and **4**. These particular types of nitrilium ions are important intermediates in Ritter reactions where a nitrile undergoes nucleophilic addition. Compound **6** is immediately generated after a barrierless cyclization reaction of **3** according to the computational geometry optimization, as discussed above. Another nitrilium ion **4** is detected by fs-TA and ns-TR³ and reacts with 4-methoxyphenyl to generate a pyridine stabilized nitrilium ion. This type of reaction has been investigated recently by van Dijk and co-workers. [15] Notably, the reaction between a closed-shell singlet phenyloxenium ion and the solvent acetonitrile was not observed in our previous study in which close-shell singlet phenyloxenium ion was investigated, [3] while the existence of **3** and **4** demonstrates that the open-shell singlet phenyloxenium ion **2** can react with acetonitrile to produce para and ortho ring adducts. Photochemical products in water also show the electrophilic property of the open-shell singlet phenyloxenium ion, forming the water adducts hydroquinone and catechol (Figure 2.10).

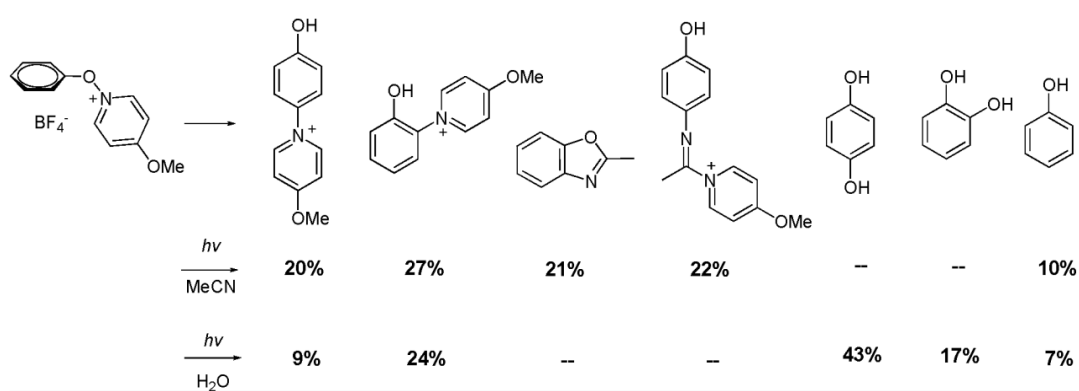


Figure 2.10 Photochemical Product Studies (254 nm) of **1**. Relative percentages were determined by ¹H NMR integration.

2.5 Conclusions

In conclusion, the new photoprecursor for the generation of the phenyloxenium ion, 4-methoxyphenoxy pyridinium tetrafluoroborate salt, was investigated using time-resolved spectroscopic experiments (fs-TA, ns-TA, and ns-TR³) along with the necessary computational calculations and photochemical product studies. These experiments draw several conclusions. First, the pyridinium leaving group appears to provide a better photo generation to oxenium ions than the previously investigated ammonia leaving groups, as we observe only oxenium generation, rather than a mixture of oxenium and radical generation (a small amount of generated radical, undetectable by the ns-TR³ experiments, cannot be ruled out). Second, this study demonstrates the importance of excited state dynamics on photochemical reaction outcomes, as this precursor gives birth to the oxenium ion in its first excited state rather than its ground state. Of more general importance, this study provides direct spectroscopic evidence for a concept proposed by Perrin from deuterium isotope studies on p-benzyne: [8] the unsettling possibility that a nucleophile can attack a singly occupied orbital. Furthermore, not only does the open-shell oxenium ion show surprising electrophilic behavior, but it appears to be a much more powerful electrophile than the closed-shell species, with a much shorter lifetime (0.2 vs 5 ns in MeCN) and its ability to trap recalcitrant nucleophiles such as MeCN to form Ritter intermediates, which is not seen with the closed-shell oxenium ion. A theoretical basis for understanding nucleophilic additions to singlet diradicals is clearly needed and has been well addressed recently: [16] briefly speaking, a nonplanar cyclic allene acts as the transitioning structure between open-shell and closed-shell species for the addition of nucleophiles, with a continuous and smooth changing of the wave function by the evolution of orbital and configuration interaction (CI) coefficients, such that there is no abrupt switch from diradical to closed-shell species along the reaction coordinate.

2.6 Acknowledgments

Financial support from NSF (CHE-1464956) and ACS PRF (PRF55820-ND4) for AHW are gratefully acknowledged. A.H.W. thanks the Iowa State Chemistry Instrumentation Facilities. D.L.P. thanks support from the Hong Kong Research Grants Council (grants HKU 7035/13P, AoE/P-03/08, SEG HKU/07) and The University of Hong Kong Development Fund 2013-2014 project “New Ultrafast Spectroscopy Experiments for Shared Facilities”.

2.7 References

- [1] Wang, Y.-T.; Wang, J.; Platz, M. S.; Novak, M. *J. Am. Chem. Soc.* **2007**, *129*, 14566.
- [2] Wang, Y.-T.; Jin, K. J.; Leopold, S. H.; Wang, J.; Peng, H.-L.; Platz, M. S.; Xue, J.; Phillips, D. L.; Glover, S. A.; Novak, M. *J. Am. Chem. Soc.* **2008**, *130*, 16021.
- [3] Hanway, P. J.; Xue, J. D.; Bhattacharjee, U.; Milot, M. J.; Zhu, R.; Phillips, D. L.; Winter, A. H. *J. Am. Chem. Soc.* **2013**, *135*, 9078.
- [4] Li, M. D.; Albright, T. R.; Hanway, P. J.; Liu, M.; Lan, X.; Li, S.; Peterson, J.; Winter, A. H.; Phillips, D. L. *J. Am. Chem. Soc.* **2015**, *137* (32), 10391.
- [5] Winter, A. H.; Falvey, D. E.; Cramer, C. J. *J. Am. Chem. Soc.* **2004**, *126* (31), 9661.
- [6] Chiapperino, D.; McIlroy, S.; Falvey, D. E. *J. Am. Chem. Soc.* **2002**, *124*, 3567.
- [7] Ritter, J. J.; Kalish, J. *J. Am. Chem. Soc.* **1948**, *70*, 4048.
- [8] Perrin, C. L.; Reyes-Rodríguez, G. J. *J. Am. Chem. Soc.* **2014**, *136*, 15263.
- [9] Myers, A. G.; Dragovich, P. S.; Kuo, E. Y. *J. Am. Chem. Soc.* **1992**, *114*, 9369

- [10] Wenthold, P. G.; Wierschke, S. G.; Nash, J. J.; Squires, R. R. *J. Am. Chem. Soc.* **1994**, *116*, 7378.
- [11] Du, L.; Zhang, X.; Xue, J.; Tang, W.; Li, M.-D.; Lan, X.; Zhu, J.; Zhu, R.; Weng, Y.; Li, Y.; Phillips, D. L. *J. Phys. Chem. B* **2016**, *120*, 11132.
- [12] Frisch, M. J.; Trucks, G. W.; Schlegel, H. B.; Scuseria, G. E.; Robb, M. A.; Cheeseman, J. R.; Scalmani, G.; Barone, V.; Mennucci, B.; Petersson, G. A.; Nakatsuji, H.; Caricato, M.; Li, X.; Hratchian, H. P.; Izmaylov, A. F.; Bloino, J.; Zheng, G.; Sonnenberg, J. L.; Hada, M.; Ehara, M.; Toyota, K.; Fukuda, R.; Hasegawa, J.; Ishida, M.; Nakajima, T.; Honda, Y.; Kitao, O.; Nakai, H.; Vreven, T.; Montgomery, J. A., Jr.; Peralta, J. E.; Ogliaro, F.; Bearpark, M. J.; Heyd, J.; Brothers, E. N.; Kudin, K. N.; Staroverov, V. N.; Kobayashi, R.; Normand, J.; Raghavachari, K.; Rendell, A. P.; Burant, J. C.; Iyengar, S. S.; Tomasi, J.; Cossi, M.; Rega, N.; Millam, N. J.; Klene, M.; Knox, J. E.; Cross, J. B.; Bakken, V.; Adamo, C.; Jaramillo, J.; Gomperts, R.; Stratmann, R. E.; Yazyev, O.; Austin, A. J.; Cammi, R.; Pomelli, C.; Ochterski, J. W.; Martin, R. L.; Morokuma, K.; Zakrzewski, V. G.; Voth, G. A.; Salvador, P.; Dannenberg, J. J.; Dapprich, S.; Daniels, A. D.; Farkas, Ö.; Foresman, J. B.; Ortiz, J. V.; Cioslowski, J.; Fox, D. J. *Gaussian 09*, Gaussian, Inc.: Wallingford, CT, 2009.
- [13] Aquilante, F.; Autschbach, J.; Carlson, R. K.; Chibotaru, L. F.; Delcey, M. G.; De Vico, L.; Fdez. Galvan, I.; Ferre', N.; Frutos, L. M.; Gagliardi, L.; Garavelli, M.; Giussani, A.; Hoyer, C. E.; Li Manni, G.; Lischka, H.; Ma, D.; Malmqvist, P. Å.; Müller, T.; Nenov, A.; Olivucci, M.; Pedersen, T. B.; Peng, D.; Plasser, F.; Pritchard, B.; Reiher, M.; Rivalta, I.; Schapiro, I.; Segarra-Martí, J.; Stenrup, M.; Truhlar, D. G.; Ungur, L.; Valentini, A.; Vancoillie, S.; Veryazov, V.; Vysotskiy, V. P.; Weingart, O.; Zapata, F.; Lindh, R. *J. Comput. Chem.* **2016**, *37*, 506.
- [14] Hanway, P. J.; Winter, A. H. *J. Am. Chem. Soc.* **2011**, *133*, 5086.
- [15] van Dijk, T.; Bakker, M. S.; Holtrop, F.; Nieger, M.; Slootweg, J. C.; Lammertsma, K. *Org. Lett.* **2015**, *17*, 1461
- [16] Wenthold, P., Winter, A.H. *J. Org. Chem.*, **2018**, *83*, 12397.

CHAPTER 3. DIRECT DETECTION OF THE n,π^* EXCITED TRIPLET PHENYLOXENIUM ION: EXPLOITING EL-SAYED'S RULE

Yunfan Qiu, Lili Du, David Lee Phillips, Arthur H. Winter.

3.1 Abstract

Oxenium ions are important reactive intermediates in synthetical chemistry and biological processes. However, little is investigated in aspects of their reactivities, lifetimes, spectroscopic features and electronic configurations. Only recently, with the rapid advancement in laser flash photolysis technique, phenyloxenium ions have been directly detected in the close-shell ground singlet state, open-shell excited singlet state and a π,π^* triplet ground triplet state, allowing the insight of their chemical characteristics. To learn more about and complement the present knowledge of oxenium ions, alternative electronic configurations of phenyloxenium ions are demanded. In this chapter, a new photoprecursor to the acetylphenyloxenium ion, 4-acetylphenoxy pyridinium tetrafluoroborate (**1**), was investigated preliminarily using a combination of time-resolved transient absorption spectroscopy, product analysis and computations. These experiments allowed observation of the photophysics and photochemistry of this photoprecursor beginning with the initially populated singlet excited states to its sequential triplet transient intermediates via rapid intersystem crossing due to El-sayed's rule, followed by photoheterolysis on the triplet energy surface and ultimate formation of stable photoproducts. In this chapter, the combined preliminary studies suggest the generation of a n,π^* triplet oxenium ion (its first triplet excited state), permitting the insight into the reactivity of a triplet oxenium ion with two spins in two distinct symmetries, which also supplements the research of phenyloxenium ions. This n,π^* triplet phenyloxenium ion has a much shorter lifetime

($\tau \sim 0.5$ ns) than the previously observed π,π^* triplet ground state phenyloxenium ion ($\tau \sim 1.7$ μ s), which probably results from its excited state nature. Remarkably, despite possessing different triplet symmetries in comparison to the π,π^* triplet ground state moiety, this n,π^* triplet phenyloxenium ion behaves the same in terms of reactivities, reacting in a typical diradical fashion, such as H atom abstraction, which is confirmed by the major end photo product characterized by ^1H NMR. This chapter provides direct spectroscopic observation of a n,π^* triplet phenyloxenium ion and extends the research of oxenium ions.

3.2 Introduction

In the previous chapters, the closed-shell ground-state parent phenyloxenium ion has been reported from photolysis of a protonated phenylhydroxylamine (see Figure 3.1). [1] Protonated hydroxylamine derivative was also used to photochemically generate a π,π^* triplet ground state phenyloxenium ion (see Figure 3.1). A meta π donating group, dimethylamino group, has stabilized the triplet state to be its ground state in preference to the singlet state by 12 kcal/mol calculated at CBS-QB3 level of theory. This π,π^* triplet ground state phenyloxenium ion exhibits radical reactivity and undergoes two consecutive hydrogen atom abstractions to form the final reduced phenol product, indicating the triplet oxenium ions reacts as radicals as anticipated. [2,3] Upon laser pulse, the photoprecursor produces the singlet oxenium ion at the very beginning but gradually transforms into triplet ground state through intersystem crossing (ISC). It is worth noting that this π,π^* triplet ground state phenyloxenium ion was computationally predicted before the experimental realization. which clearly encourages that computational studies can guide the investigation of the singlet triplet gap for aryl oxenium ions.

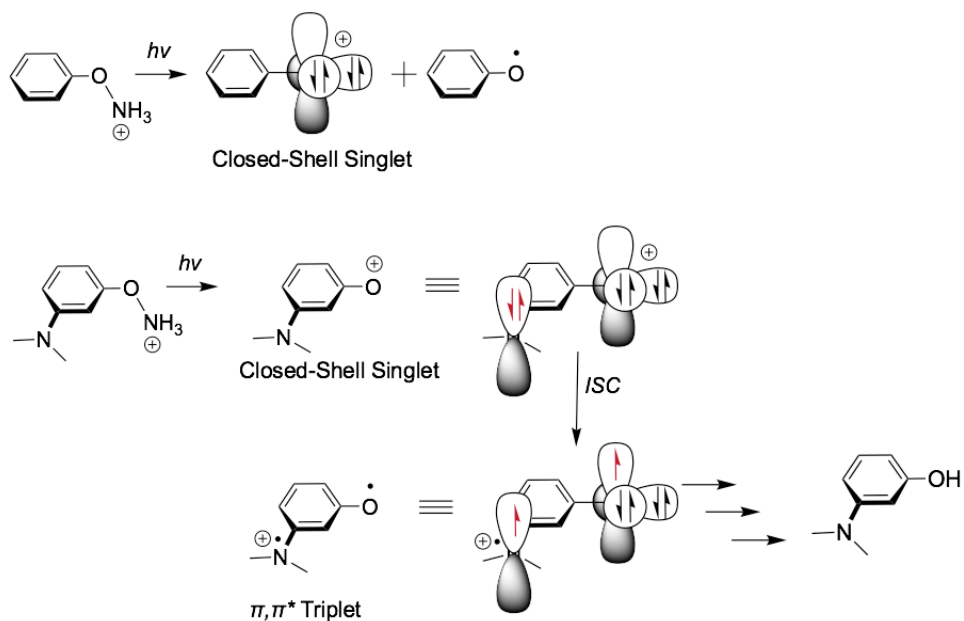
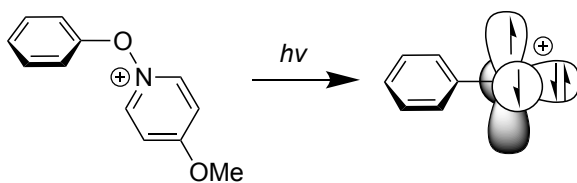


Figure 3.1 Protonated phenylhydroxylamine derivatives have been used to generate a closed-shell singlet phenyloxenium ion and triplet oxenium ions.

Prior work



This work

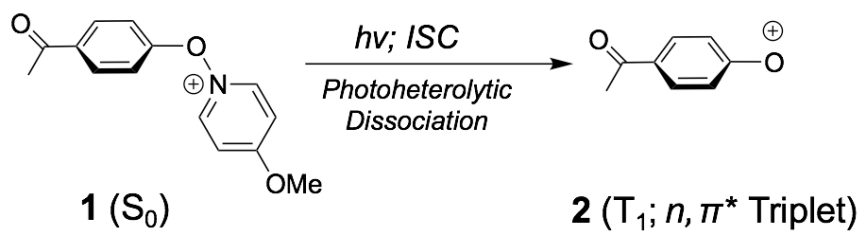


Figure 3.2 Pyridium salts used to generate open-shell singlet phenyloxenium ion and a n, π^* triplet phenyloxenium ion.

Later, a pyridium salt was implemented to generate the phenyloxenium ion with higher oxenium ion yield compared to other side products, typically radical, which is not desired and sometimes would hinder the direct studies of oxenium ion because the absorbance band of phenoxy radical on the TA spectroscopy shares common region with those of oxenium ions. The excited state of this pyridium photoprecursor undergoes photoheterolysis to generate the parent phenyloxenium ion in ~ 2 ps but surprisingly generates the ion in its open-shell singlet diradical configuration (1A_2 , see Figure 3.2), permitting an intriguing insight into the reactivity of open-shell excited singlet phenyloxenium ion, which is also an atom-centered open-shell singlet diradical conceptually. [4] To the best of our knowledge, only three types of electronic configurations have been studied thus far for phenyloxenium ion including closed-shell ground singlet state, open-shell excited singlet state and a π, π^* triplet ground state phenyloxenium ion with a strong meta π donor. It is always interesting and significant to study alternative electronic configurations to explore potentially novel reactivity of oxenium ion. With such hope, the idea of El-Sayed's rule is borrowed, [5,6] which states that ISC will be much more favored when it involves a change of molecular orbital type. 4-acetylphenoxy pyridinium tetrafluoroborate (**1**)

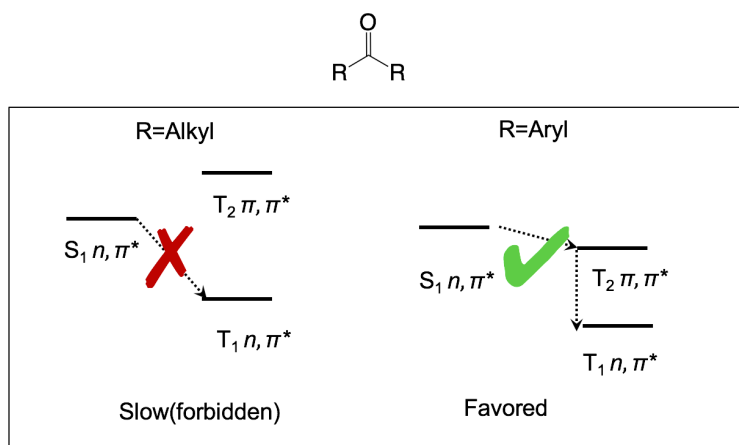


Figure 3.3 The simplistic overview of El-Sayed's rule for the carbonyl group

Kasha's rule suggests a principle that once singlet precursor is photoexcited to its higher level of singlet excited state (S_n), it will immediately undergo rapid internal conversion (IC) to its lowest excited state (S_1) and nearly all the photochemical processes and photo physics occur on the S_1 or T_1 state. [7] Figure 3.3 elaborates the core scheme of El-Sayed's rule for the carbonyl group. For the alkyl substituted carbonyl group, the first singlet excited state is considered to be n,π^* state, whose energy level is lower than the second triplet excited state (π,π^*) but higher than the first n,π^* triplet excited state. After the photo activation, due to Kasha's rule, S_1 state is achieved without any further ISC because both S_1 and T_1 possess the n,π^* orbital type, preventing El-Sayed's rule from taking place and making this ISC process a forbidden reaction channel. In this case, all the sequential phenomenon will merely happen on the S_1 state. On the other hand, T_2 state of the aryl substituted carbonyl group will be greatly stabilized by the conjugation from the aromatic substituents, leading to a lower energy of T_2 compare to the energy of S_1 . In this circumstance, the ISC between S_1 n,π^* and T_2 π,π^* will be facilitated owing to El-Sayed's rule. In addition, once T_2 π,π^* state is arrived, it will quickly decays to T_1 n,π^* eventually because Kasha's rule would emerge again.

Inspired by these established theories, 4-acetylphenoxy pyridinium tetrafluoroborate (**1**) is managed to be synthesized and T_1 n,π^* triplet excited state phenyloxenium ion is thought to be generated after photolysis instead of forming its closed-shell singlet phenyloxenium ion (see Figure 3.2). The existence of this n,π^* triplet excited state phenyloxenium is supported by a preliminary combined study including time-resolved transient absorption spectroscopy, product analysis and computational analysis. This work allows the direct detection of a n,π^* triplet excited state phenyloxenium ion and straight insight into its reactivity. Moreover, this study strongly reiterates the feasibility of using pyridium salts as photo precursors for generating

phenyloxenium ions with cleaner photoheterolytic products. Another concern of not using phenylhydroxylamine derivatives as precursors for this work is the imine condensation reaction between the carbonyl groups with the amine leaving group.

3.3 Experimental Section

Fs-TA Experiments. The experimental setups and methods used for these experiments have been previously described. [8] Briefly, the fs-TA measurements were accomplished using a femtosecond regenerative amplified Ti:sapphire laser system in which the amplifier was seeded with the 120 fs laser pulses from an oscillator laser system. The laser probe pulse was produced by utilizing ~5% of the amplified 800 nm laser pulses to generate a white-light continuum (325–650 nm) in a CaF₂ crystal, and then this probe beam was split into two parts before traversing the sample. The flowing sample was excited by a 267 nm pump laser beam. An absorbance of 1 at 267 nm was used for the sample solutions for the fs-TA experiments in order to maintain the same number of photons being absorbed for the same irradiating conditions for the samples. The global analysis was performed by adopting Evolution Associated Difference Spectra (EADS) data model.

Computational Methods. Density functional theory (DFT) computations were performed using the Gaussian09 software suite. [9] In all cases, optimized geometries were found to have zero imaginary frequencies, and corrections for the zero-point vibrational energy were added unscaled. Geometries of the phenyloxenium ions and the phenoxy radical molecules were optimized at the B3LYP/6-311+G(d,p) level of theory. The computed UV–vis spectrum was calculated at the TD-(U)B3LYP/6-311+G(d,p) level with the previously optimized geometries employing a PCM (acetonitrile) solvent model.

Synthesis of 4-acetylphenoxyiodonium tetrafluoroborate (1).

(Figure 3.4)

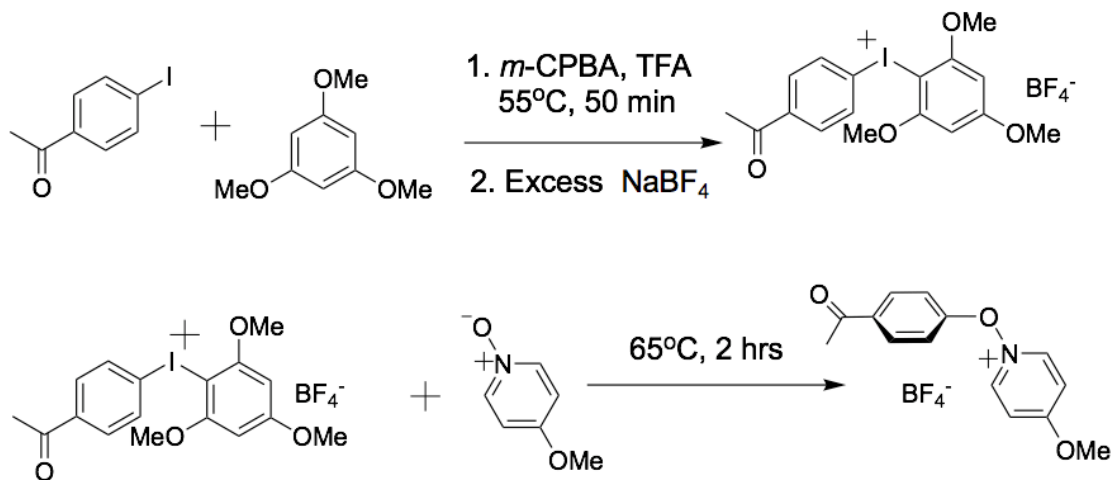


Figure 3.4 Synthesis scheme of 4-acetylphenoxyiodonium tetrafluoroborate (1).

Synthesis of diaryliodonium tetrafluoroborate.

Aryl iodide (1 mmol, 1 equiv) and acetonitrile (1 mL) were added to a 5 mL vial, equipped with a magnetic stir bar. *m*-chloroperoxybenzoic acid (81% active oxidant, 1.2 mmol, 0.208 g, 1.2 equiv) was added in one portion, followed by the dropwise addition of TFA (1 mmol, 76 μ L, 1 equiv). After sealing the tube with a screw cap, the reaction was placed in an oil bath set to 55°C and stirred. After 50 min, 1,3,5-trimethoxybenzene (1 mmol, 0.168 g, 1 equiv) was added in one portion, and the mixture was stirred at 55°C for another 15 min. The postreaction mixture was removed from heat and concentrated under reduced pressure, and the crude residue was triturated with diethyl ether (10 mL). The solid was collected by vacuum filtration and washed by slurry filtration with diethyl ether (3 times 10 mL). After drying under reduced pressure, the diaryliodonium salt was obtained in analytically pure form. The diaryliodonium salt was then added to 50 mL of boiling water. If the salt did not dissolve after

boiling for 1-2 min, then methanol was added portionwisely until the solution had a homogeneous appearance. While the mixture was still hot, a salt containing the target tetrafluoroborate anion was added in excess (10-100 equiv). The resulting solution was left to cool to ambient temperature, before chilling further in an ice-bath. The mixture was suction filtered, and the filter cake was washed by slurry filtration with water (3 times 30 mL). The cake was dried under suction for 10-20 min and then washed by slurry filtration with diethyl ether (3 time 30 mL). The sample was finally dried under high vacuum to remove residual solvent. The solid was used without further purification.

Synthesis of 4-acetylphenoxypyridinium tetrafluoroborate **1**

4-methoxypyridine-1-oxide (230 mg, 1.84 mmol) was dissolved in 5 mL dry acetonitrile and then freshly prepared diaryliodonium tetrafluoroborate salt (1.82 mmol) was added in small portions to the solution. The solution was heated at 65 °C for 2 hours under Argon. Evaporation of the acetonitrile gave a light brown solid and recrystallization from MeOH. The solid was then dried under reduced pressure to yield the desired salt. It was reasonably stable stored in a freezer in the dark under inert atmosphere.

Product Studies. Photochemical product studies in deuterated solvents were performed with 2.5 mg of precursor **1** dissolved in 1 mL of CD₃CN with 5% deionization water in order to keep consistence with the data collected from laser flash photolysis. An initial ¹H NMR was taken in a quartz NMR tube. The sample was then irradiated with 254 nm UV light from a mercury vapor lamp for different desired time durations in a Rayonet photoreactor. Spectra were taken with the previous parameters. Spiking experiments were also conducted to confirm the assignments of the generated photoproducts.

3.4 Results and Discussion

Laser Flash Photolysis (LFP) of 4-acetylphenoxyridinium tetrafluoroborate (**1**).

Photolysis of **1** was performed in a mixture of acetonitrile and 5% of water (water was included due to solubility issues), using 266 nm excitation pulse. The LFP spectra is compiled in Figure 3.4.

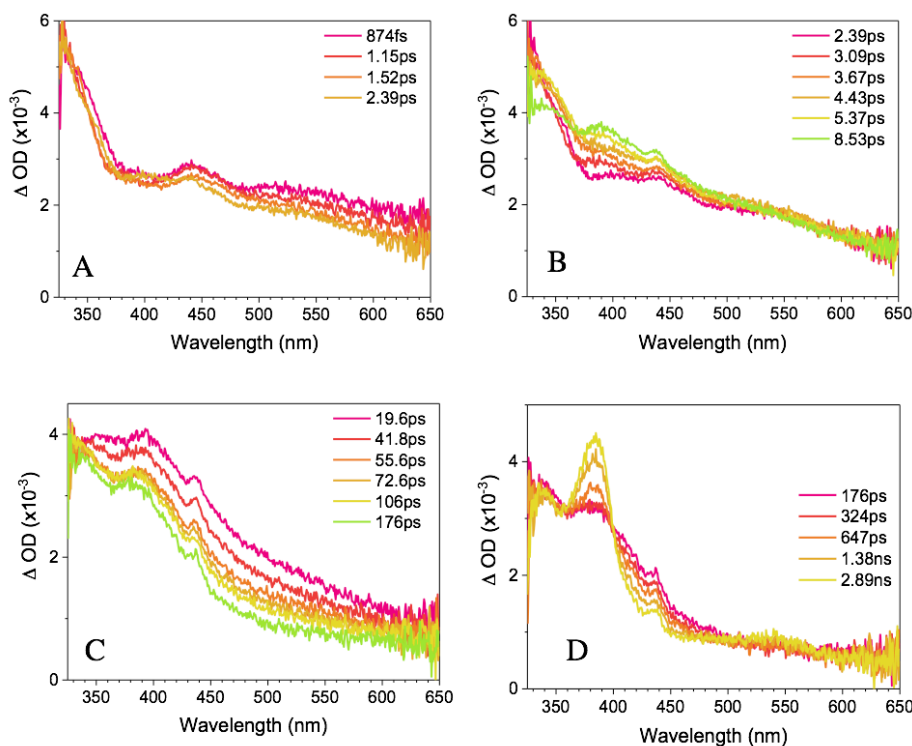


Figure 3.4 Shown are the fs-TA spectra of species produced in a MeCN/H₂O 95:5 solution acquired after 266 nm irradiation of the precursor **1**. (A) LFP from 0.87 to 2.4 ps; (B) from 2.4 to 8.5 ps; (C) from 19 to 176 ps; (D) from 176 to 2890 ps.

Figure 3.4.A shows that after the initial photo activation, the precursor **1** reaches to its singlet excited state S_n . within 1ps and rapidly decay to its first singlet excited state S_1 because of Kasha's rule. Followed by the internal conversion from S_n to S_1 of the precursor, a change of molecular orbital symmetry type leads to swift ISC from S_1 (n,π^*) to T_2 (π,π^*) over nearly 6 ps

due to El-Sayed's rule, which is depicted in Figure 3.4.B. At the same time, Kasha's rule takes place again and brings the precursor from $T_2 (\pi, \pi^*)$ to $T_1 (n, \pi^*)$. Once the $T_1 (n, \pi^*)$ precursor is established, the bond dissociation occurs barrierlessly on the triplet energy surface and the corresponding 4-acetylphenoxy cation is produced at its $T_1 (n, \pi^*)$ triplet excited state, shown in Figure 3.4.C. The slight blue shift and sharpening of the bands is characteristic of vibrational cooling, wherein the vibrationally hot species sheds heat to the surrounding solvent. The last figure suggests that this $T_1 (n, \pi^*)$ triplet excited state phenoxy cation has a lifetime of approximately 0.5 ns before converting into other chemical species, which is identified later as the one-electron reduction mono-radical product. The proposed overall photo reaction pathway is exhibited in Figure 3.5.

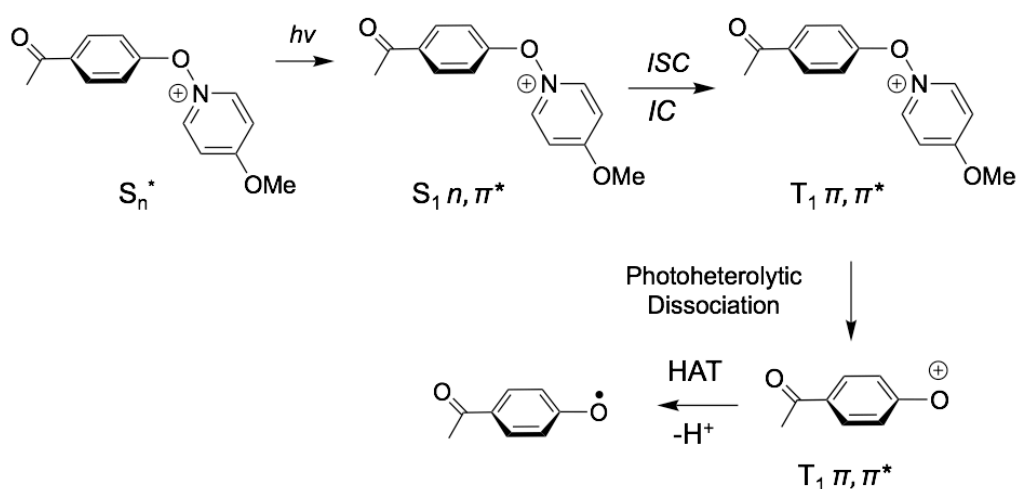


Figure 3.5 Proposed mechanistic pathway of the photochemical process of **1**.

The global analysis of fs-TA spectra performed by adopting Evolution Associated Difference Spectra (EADS) data model (see Figure 3.6) suggests that within the fs-TA detection

time limit, the conversion between each transient species is equivalent (1:1 ratio), indicating a clean photogeneration of oxenium ion and a good agreement with the current proposed pathway.

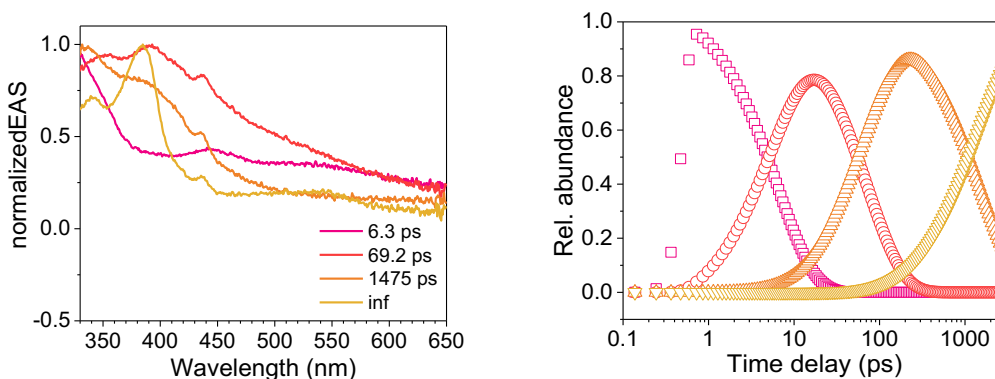


Figure 3.6 The global analysis of fs-TA spectra performed by adopting Evolution Associated Difference Spectra (EADS) model.

Justification of the assignments using computational simulations. The generated species after photo dissociation could be singlet state oxenium ion or phenoxy radical via photohomolysis channel. To justify the current assignments and the proposed pathway, TD-DFT are used to evaluate the experimental fs-TA data. Noticeably, previous studies show that TD-DFT can provide reasonable estimate UV-vis spectra for related reactive intermediates. [10-12] Thus, absorption spectra is computed in Figure 3.7 including the closed-shell singlet 4-acetylphenyloxenium ion, the n,π^* triplet excited state (first triplet excited state) and the 4-acetylphenoxy radical (see APPENDIX B). Indeed, the radical possibility can be easily ruled out due to the inconsistency in terms of the lifetime. Parent phenoxy radical is known to persist up to hundreds of nanosecond, which is far longer than the species discussed here. [13-15]

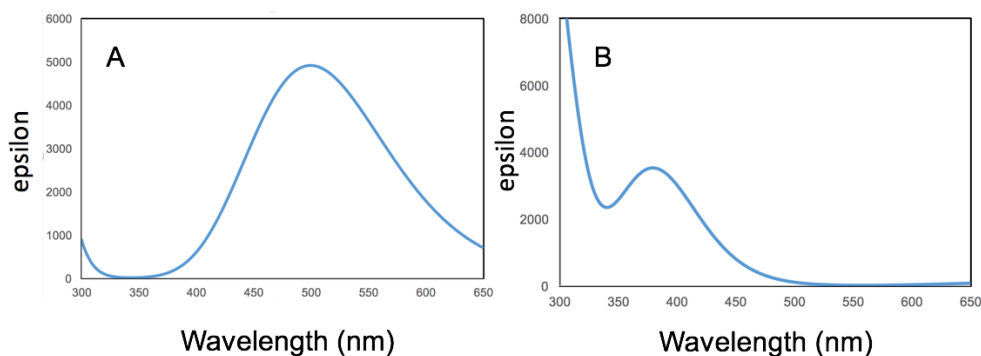


Figure 3.7 Shown are the computed electronic spectra of (A) the closed-shell singlet 4-acetylphenyloxenium ion $^1\mathbf{2}$ and (B) the n,π^* triplet excited state $^3\mathbf{2}$ using TD-(U)B3LYP/6-311+G(d,p).

In comparison to the theoretical prediction of the UV-vis spectrum of the closed-shell singlet 4-acetylphenyloxenium ion $^1\mathbf{2}$ shown in Figure 3.7.A, the absence of the 500 nm peak in the experimental data strongly indicates that the corresponding phenyloxenium ion produced is not the singlet state one. Instead, the computed electronic spectra of the n,π^* triplet excited state $^3\mathbf{2}$, featuring absorbance maximum at around 380 nm, has reasonable agreement with the LFP study.

Photochemical Product Studies of 1. Photoproduct studies provide further confirmation of the current proposed reaction channel. Spiking experiments were conducted to confirm the assignments of the generated photoproducts. To elaborate, in the photolyzed sample, authentic compounds are added. If the existing peaks in NMR spectra grow, it then indicates the same species are already present in the sample solution and are generated from the photolysis. In contrast, the appearance of new peaks demonstrates incorrect product characterization which needs further interpretation.

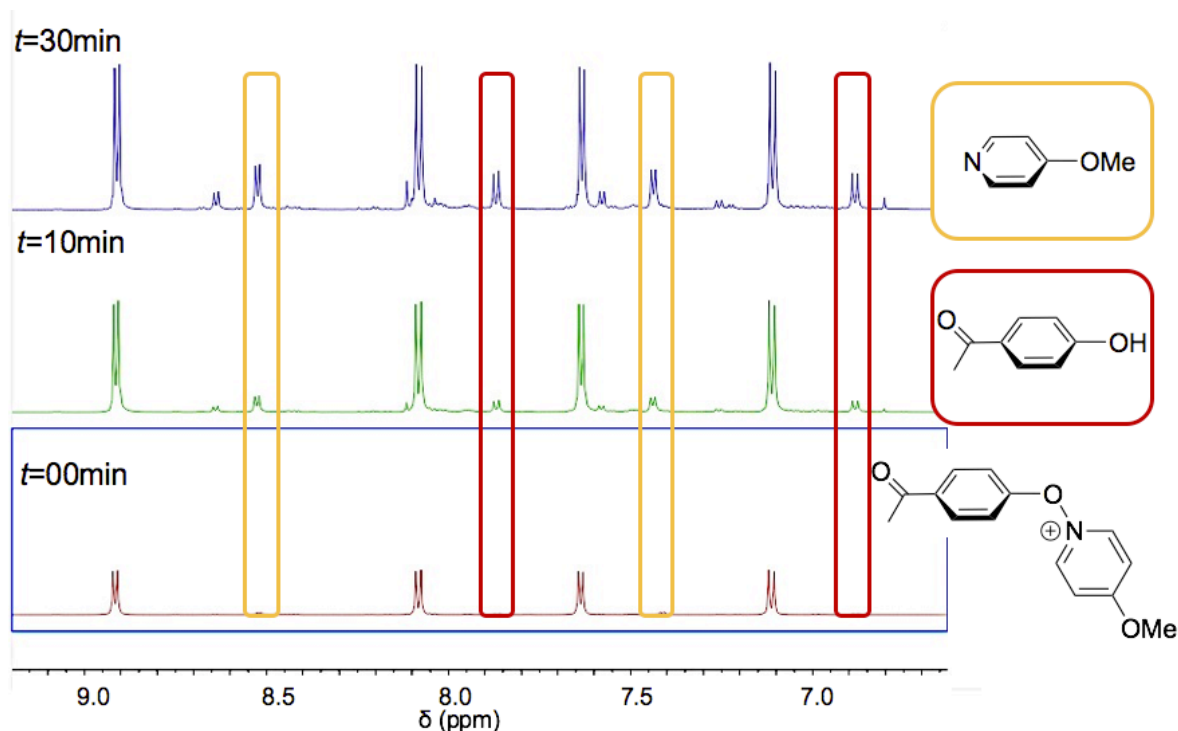


Figure 3.8 ^1H NMR spectrum of **1** photolyzed for 30 min in a mixture acetonitrile of and water (95:5) and the assignment of peaks.

Figure 3.8 shows the photo product ^1H NMR spectra of the aromatic regions within 30 minutes. Initially, the four doublets in the aromatic region represent the 4 sets of hydrogens on the pyridine core and benzene ring, respectively. Over the course of photolysis, several new peaks emerge, 4 of which are growing with the identical integration number. They are characterized as the leaving group, 4-methoxypyridine, and the reduced hydroxyacetophenone by comparing to the ^1H NMR spectra of authentic compounds. The assignment of these two products is further verified by spiking experiments shown in Figure 3.9. After 30 minutes of photolysis, the ^1H NMR spectra is taken, followed by the addition of hydroxyacetophenone, and then ^1H NMR information is collected. The direct comparison clearly shows that the hydroxyacetophenone peaks grow at the exact locations of the existing peaks, indicating the

attribution of the photo product is correct. Meanwhile, spiking experiments are also carried out to affirm the production of the leaving group in Figure 3.9.

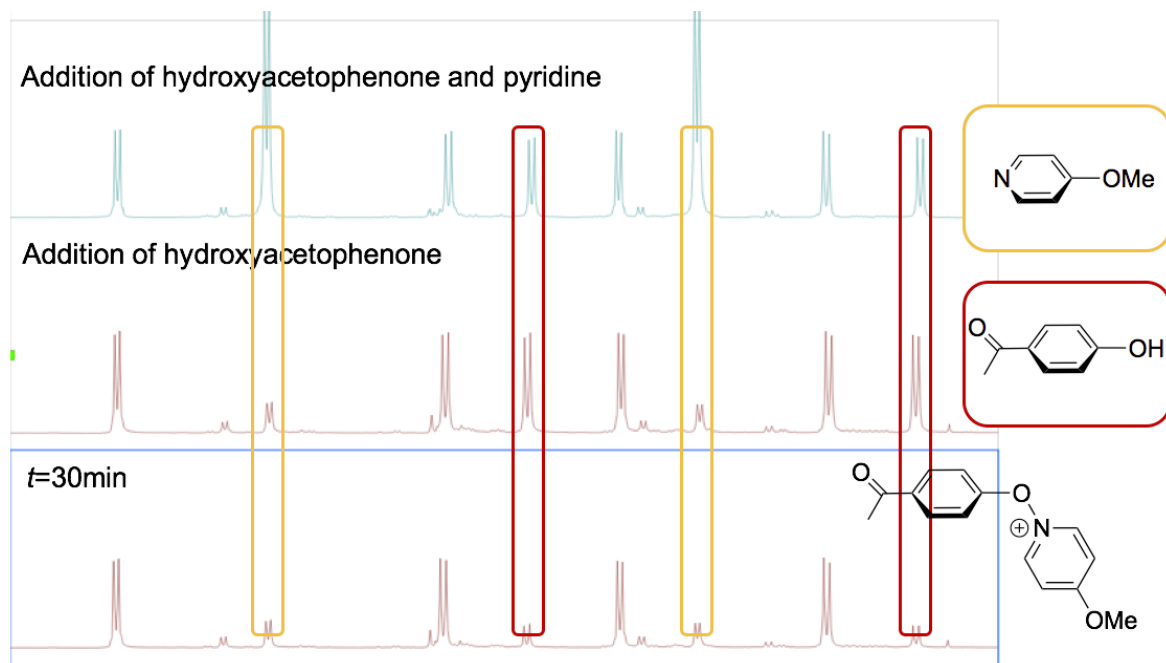


Figure 3.9. Confirmation of the assignments of the generated photoproducts by spiking experiments.

The two major products suggest that the generated n,π^* triplet excited state $^3\mathbf{2}$ does not operate nucleophilic addition, but it behaves as a typical diradical species as expected. Through two reduction processes by hydrogen atom abstractions (HATs), hydroxyacetophenone is one of the ultimate stable compounds.

3.5 Conclusions

In conclusion, by looking into the preliminary time resolved pump pulse laser spectroscopies and the photo product studies, this chapter has been able to map out essentially

the photo physic and photochemistry pathway of **1**. This photoprecursor is initially excited to singlet excited states and decays back to its first singlet excited state S_1 via fast internal conversion. Because of the stabilized $T_2 \pi, \pi^*$ state, fast intersystem crossing occurs, which is suggested by El-Sayed's rule. ISC finishes before the bond cleavage, resulting in a $T_1 n, \pi^*$ triplet precursor after another step of internal conversion. Then bond dissociation happens simultaneously to produce the $T_1 n, \pi^*$ triplet excited state phenyloxenium ion, which performs two sequential hydrogen atom abstractions to yield a reduced product, hydroxyacetophenone.

This study has also allowed to investigate the reactivity of an excited triplet oxenium ion, given that triplet oxenium ion has only been detected and studied at its ground state. [2] Distinct from the singlet state oxenium ions, which react as electrophiles in a nucleophilic addition fashion, the n, π^* triplet excited state oxenium ion behaves just like π, π^* ground state triplet oxenium ion, preferring hydrogen atom abstractions, which is very much similar to triplet carbenes and triplet nitrenium ions.

3.6 References

- [1] Hanway, P. J.; Xue, J.; Bhattacharjee, U.; Milot, M. J.; Ruixue, Z.; Phillips, D. L.; Winter, A. H. *J. Am. Chem. Soc.* **2013**, *135* (24), 9078.
- [2] Li, M. D.; Albright, T. R.; Hanway, P. J.; Liu, M.; Lan, X.; Li, S.; Peterson, J.; Winter, A. H.; Phillips, D. L. *J. Am. Chem. Soc.* **2015**, *137* (32), 10391.
- [3] Winter, A. H.; Falvey, D. E.; Cramer, C. J. *J. Am. Chem. Soc.* **2004**, *126* (31), 9661.
- [4] Du, L.; Qiu, Y.; Lan, X.; Zhu, R.; Phillips, D. L.; Li, M.-D.; Dutton, A. S.; Winter, A. H. *J. Am. Chem. Soc.* **2017**, *139* (42), 15054.
- [5] El-Sayed, M. A. *J. Chem. Phys.* **1963**, *38*, 2834.

- [6] Gwaiz, A. A.; El-Sayed, M. A. *Chem. Phys. Lett.* **1973**, *19*, 11.
- [7] Kasha, M. *Discussions of the Faraday Society*, **1950**, *9*, 14.
- [8] Du, L.; Zhang, X.; Xue, J.; Tang, W.; Li, M.-D.; Lan, X.; Zhu, J.; Zhu, R.; Weng, Y.; Li, Y.; Phillips, D. L. *J. Phys. Chem. B* **2016**, *120*, 11132.
- [9] Frisch, M. J.; Trucks, G. W.; Schlegel, H. B.; Scuseria, G. E.; Robb, M. A.; Cheeseman, J. R.; Scalmani, G.; Barone, V.; Mennucci, B.; Petersson, G. A.; Nakatsuji, H.; Caricato, M.; Li, X.; Hratchian, H. P.; Izmaylov, A. F.; Bloino, J.; Zheng, G.; Sonnenberg, J. L.; Hada, M.; Ehara, M.; Toyota, K.; Fukuda, R.; Hasegawa, J.; Ishida, M.; Nakajima, T.; Honda, Y.; Kitao, O.; Nakai, H.; Vreven, T.; Montgomery, J. A., Jr.; Peralta, J. E.; Ogliaro, F.; Bearpark, M. J.; Heyd, J.; Brothers, E. N.; Kudin, K. N.; Staroverov, V. N.; Kobayashi, R.; Normand, J.; Raghavachari, K.; Rendell, A. P.; Burant, J. C.; Iyengar, S. S.; Tomasi, J.; Cossi, M.; Rega, N.; Millam, N. J.; Klene, M.; Knox, J. E.; Cross, J. B.; Bakken, V.; Adamo, C.; Jaramillo, J.; Gomperts, R.; Stratmann, R. E.; Yazyev, O.; Austin, A. J.; Cammi, R.; Pomelli, C.; Ochterski, J. W.; Martin, R. L.; Morokuma, K.; Zakrzewski, V. G.; Voth, G. A.; Salvador, P.; Dannenberg, J. J.; Dapprich, S.; Daniels, A. D.; Farkas, Ö.; Foresman, J. B.; Ortiz, J. V.; Cioslowski, J.; Fox, D. J. *Gaussian 09*, Gaussian, Inc.: Wallingford, CT, 2009.
- [10] Gritsan, N. P.; Likhovorik, I.; Zhu, Z.; Platz, M. S. *J. Phys. Chem. A* **2001**, *105*, 3039.
- [11] Delamere, C.; Jakins, C.; Lewars, E. *J. Mol. Struct.* **2002**, *593*, 79.
- [12] Xue, J.; Luk, H. L.; Eswaran, S. V.; Hadad, C. M.; Platz, M. S. *J. Phys. Chem. A* **2012**, *116*, 5325.
- [13] Baptista, J. L.; Burrows, H. D. *J. Chem. Soc., Faraday Trans. 1* **1974**, *70*, 2066.
- [14] Tripathi, G. N. R.; Schuler, R. H. *J. Chem. Phys.* **1984**, *81*, 113.
- [15] Land, E. J.; Porter, G.; Strachan, E. *Trans. Faraday Soc.* **1961**, *57*, 1885.

CHAPTER 4. ARYL OXENIUM IONS WITH UNUSUAL HIGH-SPIN π, π^* GROUND STATES: EXPLOITING (ANTI)AROMATICITY

Modified and reprinted from *J. Org. Chem.* **2017**, *82*, 13550

Copyright © 2017, American Chemical Society

Yunfan Qiu, Logan J. Fischer, Andrew S. Dutton and Arthur H. Winter

4.1 Abstract

Oxenium ions are important reactive intermediates in synthetic and biological processes, and their ground electronic configurations are of great interest due to having distinct reactivities and properties. In general, the closed-shell singlet state of these intermediates usually react as electrophiles, while reactions of the triplet states of these ions react like typical diradicals such as hydrogen atom abstractions. Non-substituted phenyloxenium ions (Ph-O^+) have closed-shell singlet ground states with large singlet-triplet gaps resulting from a strong break in the degeneracy of the p orbitals on the formal oxenium center. Remarkably, we find computationally (CBS-QB3 and G4MP2) that azulenyl oxenium ions can have triplet ground states depending upon the attachment position on the azulene core. For instance, CBS-QB3 predicts 1-azulenyl oxenium ion is a singlet ground state species with considerable singlet-triplet gaps of -45 kcal/mol to the lowest-energy triplet state. In contrast, 6-azulenyl oxenium ion has triplet ground state with a singlet-triplet gap of +10 kcal/mol. Moreover, the triplet states are π, π^* states, rather than the typical n, π^* states seen for the first triplet excited states of many aryl oxenium ions. This dramatic switch in favored electronic states can be ascribed to changes in ring aromaticity/antiaromaticity, with the switch from ground-state singlet ions to triplet-favored ions resulting from both a destabilized singlet state (Hückel antiaromatic) and a stabilized triplet

(Baird aromatic) state. Density functional theory (UB3LYP/6-31+G(d,p)) was used to determine substituent effects on the singlet-triplet energy gap for azulenyl oxenium ions, and the unusual ground triplet states can be further tuned by employing electron-donating or -withdrawing groups on the azulene ring. This chapter demonstrates that azulenyl oxenium ions can have triplet π, π^* ground states, and provides a simple recipe for making ionic intermediates with distinct electronic configurations and consequent prediction of unique reactivity and magnetic properties from these species.

4.2 Introduction

Oxenium ions are important cationic reactive intermediates featuring a hypovalent oxygen atom ($R-O^+$).^[1] This species is of great biological significance regarding their roles in carcinogenesis and other biological processes.^[2-4] In the field of synthetic chemistry, it also has been proposed as intermediates in a number of important reactions.^[5,6] Oxenium ions possess a lone pair of electrons that can be distributed in two orbitals, resulting in multiple energetically accessible electronic configurations (Figure 4.1).

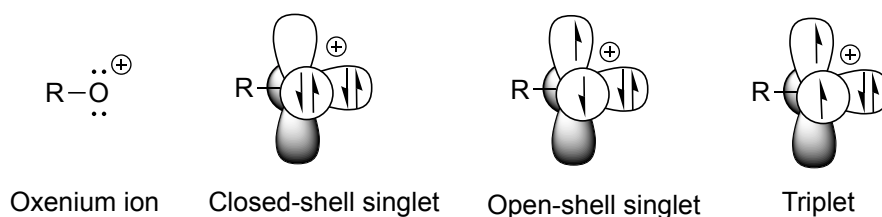


Figure 4.1 Commonly considered electronic configurations of oxenium ions. R stands for substituents.

The possibility of these species adopting triplet ground states is particularly intriguing, if appropriately stabilized, such species have application in materials with interesting magnetic and electronic properties. [7] The singlet-triplet energy gap (ΔG_{ST}) is an important factor for determining the spin state of the ground state. Notably, the parent oxenium ion, OH^+ , favors the triplet ground state by 54 kcal/mol. [8,9] The preference of the triplet state of this simple reactive intermediate results from a degeneracy in the p orbitals for OH^+ , which leads to the lowest-energy spin unpaired electronic configuration complying with a molecular orbital (MO) extension of Hund's rule. The ground states of aryl oxenium ions, however, are difficult to be predicted from simple models due to the broken degeneracy of the p orbitals. Indeed, both experimental and theoretical studies reveal that the parent phenyl oxenium ions have closed-shell singlet ground states,[10,11] because the filled p orbitals on the benzene ring mix with the out-of-plane p orbital on the centered atom (oxygen atom), raising its energy, and both stabilizing the singlet state and destabilizing the triplet state.[12] Yet some aryl oxenium ions, such as heteroaryl and substituted aromatic, may adopt triplet ground states.[13] These triplet aryl oxenium ions switch the reactivity behavior from reacting as electrophilic species to reacting as diradicals. Thus, manipulating the ground state provides direct control over the reactivity of the intermediates.

Recently, it has been reported that aryl non-alternant hydrocarbon carbenium ions can have low-energy or ground triplet states, and can be explained by aromaticity/antiaromaticity arguments. [14] Here, this chapter demonstrate that this effect applies to azulenyl oxenium ions as well. Certain azulenyl oxenium ions also exhibit triplet ground states, which can be further tuned by substitution of electron-donating/withdrawing groups around the azulene core. Here, a detailed computational study of azulenyl oxenium ions is provided, including substitution pattern

investigation, nucleus independent chemical shift (NICS) calculations, harmonic oscillator model of aromaticity (HOMA) values, linear free-energy relationships (LFERs), and orbital analysis. These results suggest that depending on the substitution location, either the singlet state or the triplet state can be favored. Furthermore, unlike typical aryl oxenium ions that have n, π^* triplet states as the lowest-energy, the lowest energy triplet states of these azulenyl oxenium ions are π, π^* triplet states in nature.

4.3 Experimental Section

Computational details. To investigate the ground electronic states of the azulenyl oxenium ions in this work, the singlet-triplet energy gap (ΔG_{ST}) was calculated by subtracting the lowest triplet energy from the lowest singlet energy, eq. 1.

$$\Delta G_{ST} = G_{\text{singlet}} - G_{\text{triplet}} \quad (1)$$

Both CBS-QB3 and G4MP2 methods were performed to compute the singlet-triplet energy gap (ΔG_{ST}) of the azulenyl oxenium ions. The overall results produced by these two methods are nearly the same with CBS-QB3 slightly overestimating the ΔG_{ST} values of triplet state favored azulenyl oxenium ions in comparison with G4MP2. [15] To evaluate the effect of the attachment point of the cationic center atom (oxygen atom), the complete basis set method (CBS-QB3) was utilized to calculate the absolute energies of singlet and triplet states. NICS calculations were done at HF/6-31+g(d,p)//G4MP2 level with the Gauge-Independent Atomic Orbital (GIAO) method. Harmonic oscillator model of aromaticity (HOMA) value calculations used the optimized geometries from the G4MP2 calculations. To plot the linear free-energy relationships (LFERs), an unrestricted broken-symmetry method is used for B3LYP calculations, which was benchmarked previously. [14] Unfortunately, this approach using density functional

theory (DFT) suffers from spin contamination when there are low-energy triplet states ($\langle S^2 \rangle$ values greater than zero). In all cases where broken-symmetry DFT calculations were performed, eq. 2 was used to titrate out contamination from a low-energy triplet state and determine a spin-purified energy of the singlet state:

$$E_{\text{singlet}} = \frac{2E_{\langle S_z \rangle=0} - \langle S^2 \rangle E_{\langle S_z \rangle=1}}{2 - \langle S^2 \rangle} \quad (2)$$

where E_{singlet} is the corrected singlet energy, $E_{\langle S_z \rangle=0}$ is the broken-symmetry energy, $\langle S^2 \rangle$ is the expectation value of the total-spin operator for the broken-symmetry, and $E_{\langle S_z \rangle=1}$ is the energy of the triplet state at the singlet geometry. [16]

Regarding the absolute quantitative accuracy, CBS-QB3 [17] has been shown to agree with experimental singlet-triplet gaps within 3 kcal/mol. [14] While slightly less accurate, B3LYP is sufficiently accurate (error < 5 kcal/mol) but much more computationally economical to predict the trends upon analyzing LFERs. [14] All calculations were performed using the Gaussian 09 software suite. [18] DFT computations were performed employing the B3LYP functional, along with the 6-31+G(d,p) basis set. When more than one rotamer was possible, the lowest energy conformation from each spin state was used to calculate the ΔG_{ST} value. All calculations were performed in the gas phase at the default temperature (298.15 K). All optimized geometries were found to have zero imaginary frequencies.

4.4 Results and Discussion

Azulenyl oxenium ions can have π, π^* triplet ground states. The azulene ring has eight hydrogen atoms to be replaced, but, due to symmetry, only five unique azulenyl oxenium ions

are available possible by substituting the azulene ring at the 1, 2, 4, 5 and 6 positions, the detailed nomenclature used in this chapter is displayed in Figure 4.2.

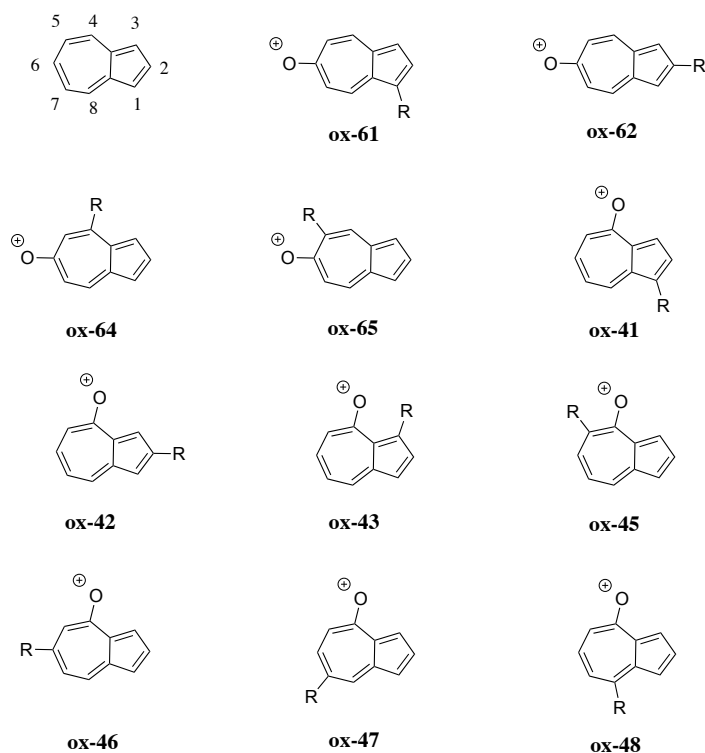


Figure 4.2 Nomenclature of substituted azulenyl oxenium ions.

Figure 4.3 shows that a dramatic change in the ΔG_{ST} depending on the attachment position of the oxygen atoms on the azulene ring. For azulenyl oxenium ions, the ΔG_{ST} varies from -45.0 kcal/mol for connection at the 1-position of azulene (**ox-1**) (a negative value indicates a singlet ground state), to +10.4 kcal/mol for connection at the 6-position (**ox-6**). The positive value of ΔG_{ST} in **ox-6** strongly indicate an unusual and intriguing triplet ground states. Additionally, for oxenium ions, connection at the 4-position (**ox-4**) yields ions with nearly degenerate singlet and triplet states.

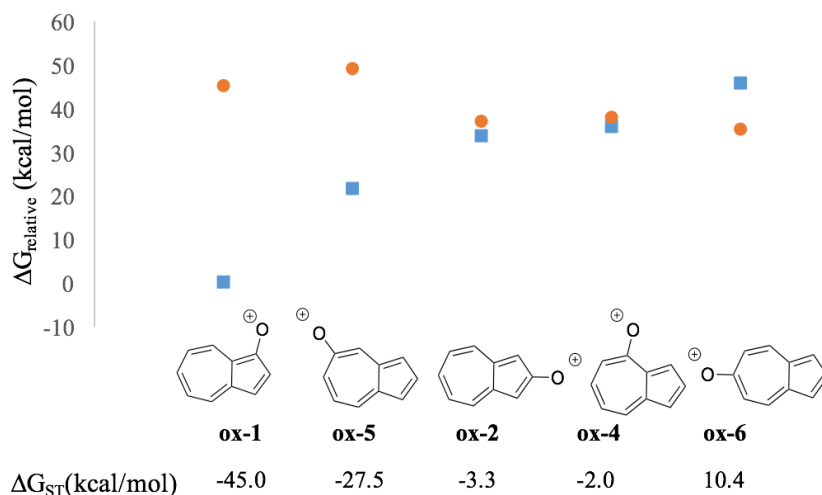


Figure 4.3 Singlet and triplet energies azulenyloxy ions with different substitution patterns. CBS-QB3 energies in kcal/mol. (■ Singlet, ● Triplet). Structures are ordered by ΔG_{ST} values.

As stated earlier, non-substituted aryl hydrocarbon oxenium ions are frequently thought to have singlet ground states, while triplet ground states are rare. [11] To reveal the origin of the unexpected triplet ground states of azulenyloxy ions, relative absolute energies, obtained using the CBS-QB3 level of theory method, are displayed in Figure 4.3 to compare the stabilities of the singlet and triplet states. These species are isomers allowing for the direct comparison of their absolute energies. In Figure 4.3, **ox-1** has the most favorable singlet ground state with the ΔG_{ST} value of -45.0 kcal/mol, while **ox-6** has a positive ΔG_{ST} value of 10.4 kcal/mol, suggesting a triplet ground state correspondingly. The remarkable swing of >50 kcal/mol in the ΔG_{ST} values of **ox-1** and **ox-6** can be rationalized by both a destabilization of the singlet state and a stabilization of the triplet state for **ox-6** compared to **ox-1** on the basis of the higher singlet energy and lower triplet energy in **ox-6**. Note that ions **ox-2**, **ox-4**, and **ox-6** have nearly identical stabilized triplet energies compared to **ox-1** and **ox-5**, but only **ox-6** is computed to have triplet ground state due to more destabilized singlet state. In general, along with the increasing ΔG_{ST}

values, triplet energies drop off and singlet energies increase drastically. On the other hand, **ox-2** and **ox-4** are calculated to have singlet ground states with narrow singlet-triplet energy gap ($\Delta G_{ST} = -3.3$ kcal/mol for **ox-2** and $\Delta G_{ST} = -2.0$ kcal/mol for **ox-4**, respectively). Overall, **ox-6** can be considered to be triplet ground state species due to the large singlet-triplet energy gap.

Aryl oxenium ions are normally considered to have typical n, π^* states as their lowest triplet energy states. [11] To investigate the electronic configurations of **ox-6** with its stunning triplet ground states, the SOMOs of **ox-1** and **ox-6**, the most singlet or triplet favored structures respectively, are visualized in Figure 4.4. When analyzing the displayed orbitals, no matter which type of ground state (singlet or triplet) these ions retain (singlet or triplet), the two SOMOs of the lowest triplet states are both distributed throughout the whole azulene plane core, clearly indicating the π electron character of each SOMO. The orbital presentation in Figure 4.4 shows a solid evidence that not only can azulenyl oxenium ions may adopt triplet ground states, but, more importantly, adopt an unusual π, π^* electronic configuration rather than the traditional n, π^* triplet states.

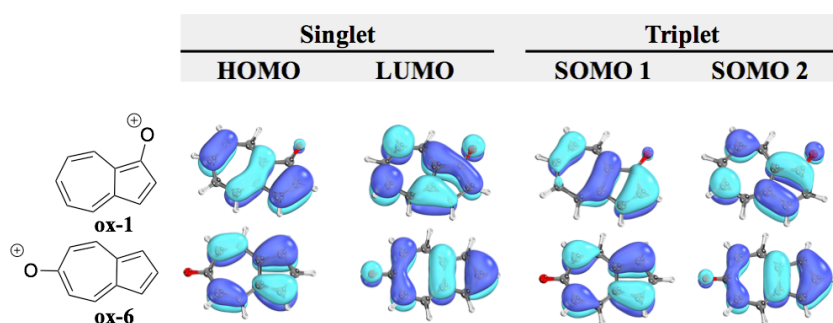


Figure 4.4 Orbital representatives of the HOMO, LUMO, SOMO1 and SOMO2 of structures **ox-1** and **ox-6**.

Triplet stabilization and singlet destabilization can be explained by aromaticity/triplet aromaticity arguments, but not exchange energies. Inspection of Figure 4.3 implies that the favored triplet ground state of **ox-6** is driven by two forces: triplet stabilization and singlet destabilization. One possible explanation of greater triplet stabilization in the 2, 4 and 6-position substituted azulenyl oxenium ions, may arise from greater amount of triplet-favoring electron exchange. Borden, et. al., classified the unpaired electrons of a diradical into two categories: disjoint or non-disjoint. [19] If the orbital amplitudes of the SOMOs are located at the same atoms, the orbitals are described as non-disjoint, and the unpaired electrons will enjoy large exchange integrals energies favoring a triplet configuration. This preference of the electrons to be in a spin unpaired state can be attributed to the reduction of electron-electron repulsion gained by the unpaired spins. If the orbital amplitudes of the SOMOs occupy different atoms, the orbitals are considered as disjoint. Since the electrons placed in disjoint orbitals do not overlap the same physical space, little exchange energy will be gained by adopting a triplet versus singlet configuration. Figure 4.4 shows that the SOMOs of **ox-1** and **ox-6**, the most singlet or triplet favored structures, can be classified as non-disjoint because the SOMO amplitudes are distributed on the same carbons. Given that **ox-1** is the most favored singlet ground states, **ox-1** is expected to have less shared SOMO amplitudes than **ox-6**, which conflicts with the realistic orbital representations exhibition in Figure 4.4. Thus, the facile explanation of differences in electron exchange energies cannot account for the relative stabilization of the triplet states.

The next possibility was changes in aromaticity/antiaromaticity between the different reactive intermediates. Aromaticity was first proposed by Hückel to explain the special stability of cyclic, unsaturated structures via a quantum mechanical basis., [20] which later formalized into the $4n+2$ equation widely used today. Later, Breslow introduced the antiaromaticity concept

to analyze the destabilized cyclic conjugated systems with $4n$ electrons. [21] Then Baird further extended aromaticity ideas to describe the stabilized structures with triplet configurations. [22] Hückel aromaticity is traditionally applied to stable structures with singlet states, while Baird aromaticity can be well applied to interpret stabilized triplet structures. In a recent work, an aromaticity/antiaromaticity theory argument can remarkably explain the singlet or triplet ground states of carbenium ions by employing Hückel's $4n+2$ equation for singlet state aromaticity and Baird's $4n$ equation for triplet state aromaticity. [14] To verify whether the aromaticity/antiaromaticity theory arguments can also elucidate the triplet ground states of azulenyl oxenium ions, the resonance structures of **ox-1** and **ox-6** are illustrated and analyzed in Figure 4.5.

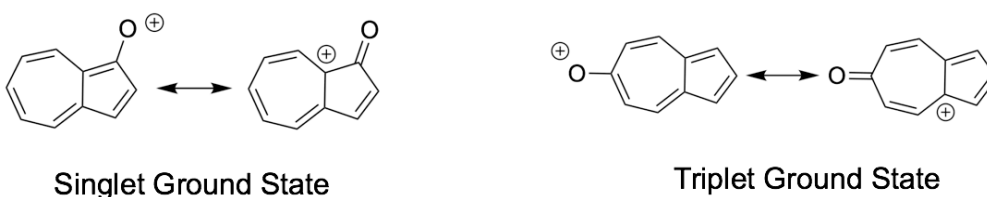


Figure 4.5 Resonance structures of **ox-1** (left), having tropylium cation character and resonance structures of **ox-6** (right), having cyclopentadienyl cation character.

For **ox-1**, its 7-membered ring features the Hückel singlet state tropylium cation character and both cyclic rings fulfill the Hückel's $4n+2$ aromaticity equation, resulting in stabilized singlet structures. On the contrary, the two rings of **ox-6** have $4n$ delocalized π electrons following Baird aromaticity rules. Moreover, the 5-membered ring of **ox-6** resembles the cyclopentadienyl cation, which is famous for having a ground triplet state. [23] By using facile resonance structures, the aromaticity/antiaromaticity argument appears to be able to

qualitatively explain the singlet/triplet stabilization/destabilization of the most singlet or triplet favored azulenyl oxenium ions. Quantitatively, the general aromaticity/antiaromaticity concept can be expressed by a variety of indices (NICS values, HOMA values, etc). However, much debate still surrounds each method and its ability to describe aromaticity/antiaromaticity. [24] In this section, several multiple measurements indices were computed to evaluate the aromaticity/antiaromaticity of the azulenyl oxenium ions.

Nucleus independence independent chemical shift (NICS) values are thought to be a crucial criterion of the existence of aromaticity. [25-27] A negative NICS value indicates the cyclic structure has aromaticity, while a positive value suggests antiaromaticity in the cyclic system. In most cases, aromaticity leads to stabilized structures and antiaromaticity tends to destabilized the system. Fortunately, NICS methodology calculations can also justify Baird aromaticity decently. For instance, the cyclopentadienyl cation, with a triplet ground state, has a negative NICS value when computed on the triplet surface. [28] There is no particular criteria regarding the distance of the dummy atom to the ring plane and this chapter selectively utilizes a procedure proposed by Schleyer, NICS(1) values, which are acquired by placing the dummy atom 1 Å away above the ring. [29] This distance above the ring attempts to isolate the π current from the σ current. The NICS(1) values of the 5-membered and 7-membered rings of azulenyl oxenium ions are plotted against ΔG_{ST} in Figure 4.6. For oxenium ions, the two cyclic rings were evaluated separately as individual aromatic/antiaromatic systems. The NICS(1) values of the singlet and triplet surfaces of the same structure are illustrated together for direct comparisons.

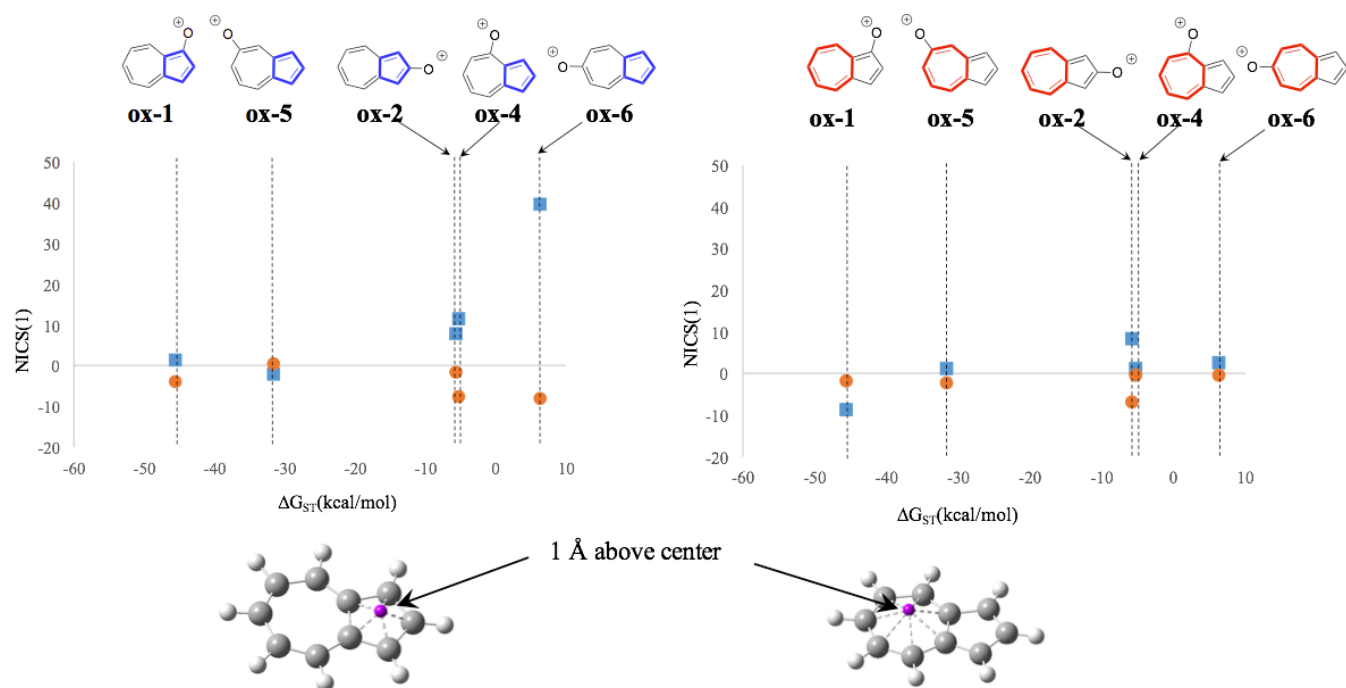


Figure 4.6 NICS(1) values against ΔG_{ST} of the 5-membered (blue) and 7-membered (red) rings for azulenylium oxenium ions on the singlet and triplet surfaces. (■ Singlet, ● Triplet). GIAO-HF/6-31+G(d,p)//G4MP2.

Generally speaking, The NICS(1) values mostly match the previous prediction that aromaticity/antiaromaticity is influencing the preferred ground state. For example, the 5-membered ring of **ox-6**, which can be thought of a cyclopentadienyl cation from the resonance structures in Figure 4.5, does have a negative NICS(1) value on the triplet surface, suggesting Baird aromaticity. When ΔG_{ST} increases, the NICS(1) values of the singlet states gradually increase in the beginning from negative (aromatic) and dramatically become very positive (antiaromatic) in **ox-4** and **ox-6**. In contrast, NICS(1) values of the triplet states generally behave in an opposite trend, starting close to zero and becoming and turn to be fairly negative in **ox-4**

and **ox-6**. Therefore, the 5-membered rings of **ox-4** and **ox-6** have display antiaromaticity on the singlet surface but aromaticity on the triplet triplet. This agrees with what we discussed earlier in Figure 4.3: **ox-4** and **ox-6** are ground state triplets due to singlet destabilization and triplet stabilization. In contrast to the 5-membered ring, the NICS(1) values of the 7-membered rings have less fluctuation than the 5-membered rings on both the singlet and triplet surfaces under the same magnitude. This suggests that the 7-membered ring has weaker influence on determining the ground states and the triplet favoring singlet-triplet energy gap of **ox-4** and **ox-6** is primarily induced by the aromaticity changes of the 5-membered ring in the bicyclic azulene system. In addition, **ox-1** has the most negative NICS(1) values in the 7-membered rings, which supports the fact that **ox-1** has the most stabilized singlet states displayed in Figure 4.3. Moreover, NICS(1) values provide us a straightforward insight as to what type of aromaticity (Hückel/Baird) dominates each individual ring in the azulene structure.

Apart from NICS model, there are plenty of other measurements to evaluate aromaticity, and harmonic oscillator model of aromaticity (HOMA) index, introduced by Kruszewski and Krygowski, has been used as one of the most effective indices for aromaticity. [30-32] To calculate the HOMA values, equation (3) is used:

$$\text{HOMA} = 1 - \frac{257.7}{n} \sum_i^n (d_{opt} - d_i)^2 \quad (3)$$

where 257.7 is the normalization value, n is the number of carbon-carbon bonds in the cyclic hydrocarbon, and d is the bond length (d_{opt} is optimized (1.388 Å), and d_i is the experimental or computational bond length). As an example, if all of the carbon-carbon bonds in one a given conjugated, cyclic system are the “optimal” length of 1.388 Å, then the HOMA value is supposed to equal to 1 and this system is assumed to have full aromatic character.

Presumably, the closer to 1 HOMA value is, the more aromatic character the structure has. To the best of our knowledge, it is reasonable to consider HOMA, to some certain degree, is a bond length alternation measurement.

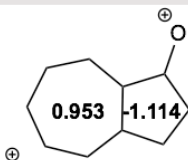
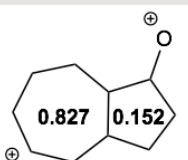
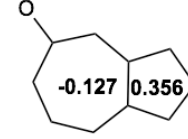
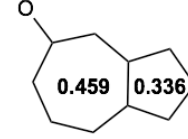
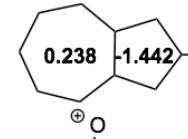
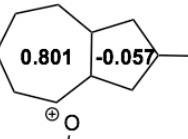
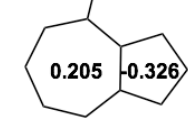
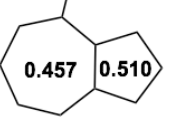
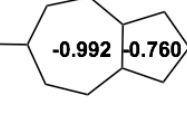
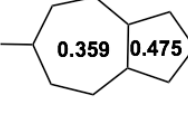
Compound	ΔG_{ST} (kcal/mol)	Singlet	Triplet
ox-1	-45.6		
ox-5	-31.6		
ox-2	-5.7		
ox-4	-5.2		
ox-6	6.4		

Figure 4.7 HOMA values against ΔG_{ST} (G4MP2) of the 5-membered and 7-membered rings for azulenyl oxenium ions on the singlet and triplet surfaces. Geometries optimized at G4MP2 level of theory

Figure 4.7 shows the HOMA values of the 5-membered and 7-membered rings for azulenyl oxenium ions on their singlet and triplet surfaces. Overall, the HOMA values have a satisfactory agreement with the results of NICS(1) values. For example, the 7-membered ring of **ox-1** has nearly a HOMA value close to 1 on the singlet surface, indicating strong aromaticity,

which is consistent with the large negative NICS(1) value seen in Figure 4.6. Particularly, the intriguing ion with triplet ground state, **ox-6**, has negative HOMA values for either 5-membered or 7-membered rings on the singlet surface and positive values (much closer to 1) on the triplet surface. This can be interpreted as singlet **ox-6** is nonaromatic but triplet **ox-6** gains aromaticity, consistent with the NICS(1) conclusions, and triplet states are consequently preferred. Though the HOMA value is highly effective in certain circumstances, it has its own flaws since it can only define a system as aromatic or nonaromatic by comparing to 1. Comparing HOMA values one between structures may not allow us to tell which structure contains more/less aromaticity. Despite the defects of each method individually, by combining the NICS(1) and HOMA values, a more comprehensive argument can be made. From aromaticity analysis, the triplet stabilization and singlet destabilization in azulenyl oxenium ions (**ox-6** particularly) can be adequately explained by Hückel aromaticity for singlet states and Baird aromaticity for triplet states.

Substitution effects and linear free energy relationships. It is always significant to study and understand the substituent effects on the electronic configurations of reactive intermediates and the subsequent change of the reactivity and properties. Ion **ox-6** itself is fundamentally interesting as a purely triplet ground state ion with large singlet-triplet energy splitting. In addition to this, we wondered if the singlet-triplet gap could be modulated by substituting additional electron-donating/-withdrawing functional groups around the system? To answer this question, linear free energy relationships (LFERs) were determined by plotting the ΔG_{ST} vs. the σ_{para}^+ Hammett-like substituent parameter (Figure 4.8). [33] As broken-symmetry DFT calculations were performed to produce the LFERs, spin contamination can give erroneous energy values for structures with low-energy triplet states. Both uncorrected and corrected ΔG_{ST} values are presented in Figure 4.8.

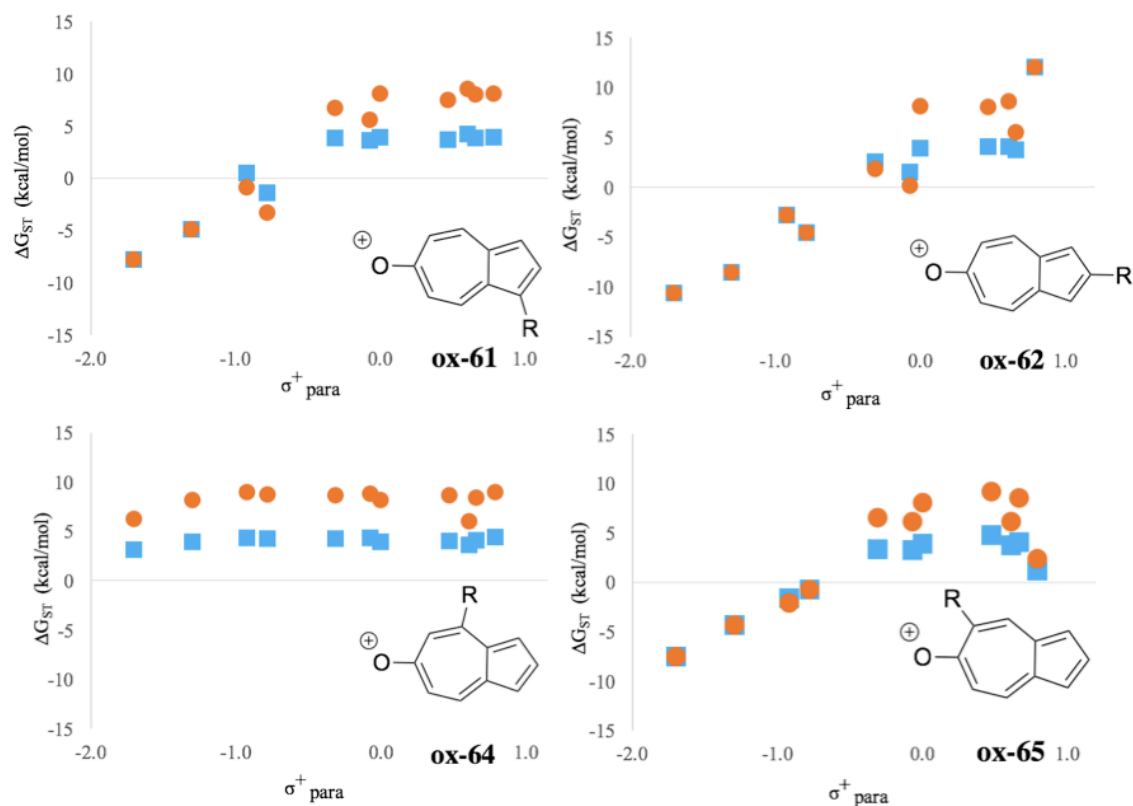


Figure 4.8 Linear free-energy relationships (LEFRs) of azulenyl oxenium ions with different substitution patterns. Substituents are ordered by σ^+_{para} values: NMe₂, NH₂, OH, OMe, Me, F, H, CHO, CF₃, CN, NO₂. ΔG_{ST} energies in kcal/mol. (■ Uncorrected, ● Corrected). Ions with large differences between the corrected and uncorrected energies are indicative of the singlet state possessing diradical character

In principle, any time an electron donating group is installed in a way that can directly stabilize the ion through resonance, the singlet state should be stabilized by raising the energy of the out-of-plane p orbital on the centered atom, increasing the cost of adopting a triplet state involving promotion of an electron into this orbital. With the exception (**ox-64**), this assumption

is illustrated in the LFER plots (Figure 4.8): the more negative σ_{para}^+ value (electron donating groups) leads to lower singlet state energies. An inversion of the singlet-triplet gap can even occur with a sufficiently strong donors compared to the unsubstituted azulenyl oxenium ions. However, strong withdrawing groups do not carry this trend to further push the ΔG_{ST} in favor of the triplet. The trendlines flatten when σ_{para}^+ values turn become positive (electron withdrawing). Here, large differences between the corrected and uncorrected singlet-triplet gap energies are typically indicative of the singlet state having diradical character. The flattening of the trendlines can be attributed to the substituent equally influencing a diradical singlet and a diradical triplet state, with the flattening point marking the switch as a change in the nature of the singlet state from a closed-shell singlet ion to an open-shell singlet ion. Additionally, substituent effects are negligible when the substituent is not directly conjugated to the cation center. In the case of ion **ox-64**, the slope of the plot is nearly flat and the ΔG_{ST} values stay positive (triplet ground state). Note that structure **ox-4** has an approximately degenerate singlet-triplet gap (~ -2.0 kcal/mol at the CBS-QB3 level). LFER plot of this structure was also carried out (see APPENDIX C) and shows similar properties that both singlet and triplet states can be further favored by differing the substituents on the core azulene rings. In summary, not only it is predicated that the triplet ground state aryl oxenium ions can be obtained, and substituent effects lead to ions with tunable energy gap.

4.5 Conclusions

In conclusion, this computational investigation has demonstrated that certain azulenyl oxenium ions are computed to have triplet ground states, and the nature of the ion depends strongly on the point of attachment and any additional ring substituents. By substituting electron-

donating or electron-withdrawing groups, the singlet-triplet energy gap of oxenium ions can be further altered or even inverted. This appealing discovery of the ground states of reactive intermediates can be interpreted by employing Hückel's $4n+2$ equation for singlet state aromaticity and Baird's $4n$ for triplet state aromaticity. Overall, this work makes specific predictions: 6-azulenyl oxenium ion is predicted to have triplet ground states, which should be observable both in reactivity trends, as well as magnetic properties (e.g. observable EPR spectra for matrix-isolated ions). In contrast, the 1-azulenyl oxenium ions should behave like typical closed-shell electrophilic singlet species. This chapter extends our perspective on making reactive intermediates with specific triplet ground states and we are looking forward to future experimental studies to generate these species and understand their reactivity.

4.6 Acknowledgments

We thank the National Science Foundation (CHE-1464956), the Department of Energy (DESC0014038), and the ACS PRF (PRF55820-ND4) for support of this work. This work used the Extreme Science and Engineering Discovery Environment (XSEDE), which is supported by National Science Foundation grant number ACI-1053575, as well as the HPC@ISU equipment at Iowa State University, some of which has been purchased through funding provided by NSF under MRI grant number CBS 1229081 and CRI grant number 1205413.

4.7 References

- [1] Moss, R. A.; Platz, M. S.; Jones, M., Jr. *Reactive Intermediate Chemistry*; Wiley: Hoboken, NJ, 2004.
- [2] Osborne, R. L.; Coggins, M. K.; Raner, G. M.; Walla, M.; Dawson, J. H., *Biochemistry* **2009**, *48* (20), 4231

- [3] Kennedy, S. A.; Novak, M.; Kolb, B. A., *J. Am. Chem. Soc.* **1997**, *119* (33), 7654-7664.
- [4] Chan, P. Y.; Kwok, W. M.; Lam, S. K.; Chiu, P.; Phillips, D. L., *J. Am. Chem. Soc.* **2005**, *127* (23), 8246.
- [5] Wardrop, D. J.; Basak, A., *Org. Lett.* **2001**, *3* (7), 1053.
- [6] Guerard, K. C.; Chapelle, C.; Giroux, M. A.; Sabot, C.; Beaulieu, M. A.; Achache, N.; Canesi, S., *Org. Lett.* **2009**, *11* (20), 4756.
- [7] Rajca, A., *Chem. Rev.* **1994**, *94* (4), 871.
- [8] Qiu, Y.; Winter, A. H., *Org. Biomol. Chem* **2017**, *15* (13), 2666.
- [9] Katsumata, S.; Lloyd, D. R., *Chem. Phys. Lett.* **1977**, *45* (3), 519.
- [10] Hanway, P. J.; Xue, J. D.; Bhattacharjee, U.; Milot, M. J.; Zhu, R.; Phillips, D. L.; Winter, A. H. *J. Am. Chem. Soc.* **2013**, *135*, 9078.
- [11] Hanway, P. J.; Winter, A. H. *J. Am. Chem. Soc.* **2011**, *133*, 5086.
- [12] Cramer, C. J.; Dulles, F. J.; Falvey, D. E., *J. Am. Chem. Soc.* **1994**, *116* (21), 9787.
- [13] Li, M. D.; Albright, T. R.; Hanway, P. J.; Liu, M.; Lan, X.; Li, S.; Peterson, J.; Winter, A. H.; Phillips, D. L. *J. Am. Chem. Soc.* **2015**, *137* (32), 10391.
- [14] Fischer, L. J.; Dutton, A. S.; Winter, A. H., *Chem. Sci.* **2017**, *8*, 4231.
- [15] Simmie, J. M.; Somers, K. P., *J. Phys. Chem. A* **2015**, *119* (28), 7235.
- [16] Yamaguchi, K.; Jensen, F.; Dorigo, A.; Houk, K. N., *Chem. Phys. Lett.* **1988**, *149* (5-6), 537.

- [17] Montgomery, J. A.; Frisch, M. J.; Ochterski, J. W.; Petersson, G. A., *J. Chem. Phys.* **1999**, *110* (6), 2822.
- [18] Frisch, M. J.; Trucks, G. W.; Schlegel, H. B.; Scuseria, G. E.; Robb, M. A.; Cheeseman, J. R.; Scalmani, G.; Barone, V.; Mennucci, B.; Petersson, G. A.; Nakatsuji, H.; Caricato, M.; Li, X.; Hratchian, H. P.; Izmaylov, A. F.; Bloino, J.; Zheng, G.; Sonnenberg, J. L.; Hada, M.; Ehara, M.; Toyota, K.; Fukuda, R.; Hasegawa, J.; Ishida, M.; Nakajima, T.; Honda, Y.; Kitao, O.; Nakai, H.; Vreven, T.; Montgomery, J. A., Jr.; Peralta, J. E.; Ogliaro, F.; Bearpark, M. J.; Heyd, J.; Brothers, E. N.; Kudin, K. N.; Staroverov, V. N.; Kobayashi, R.; Normand, J.; Raghavachari, K.; Rendell, A. P.; Burant, J. C.; Iyengar, S. S.; Tomasi, J.; Cossi, M.; Rega, N.; Millam, N. J.; Klene, M.; Knox, J. E.; Cross, J. B.; Bakken, V.; Adamo, C.; Jaramillo, J.; Gomperts, R.; Stratmann, R. E.; Yazyev, O.; Austin, A. J.; Cammi, R.; Pomelli, C.; Ochterski, J. W.; Martin, R. L.; Morokuma, K.; Zakrzewski, V. G.; Voth, G. A.; Salvador, P.; Dannenberg, J. J.; Dapprich, S.; Daniels, A. D.; Farkas, Ö.; Foresman, J. B.; Ortiz, J. V.; Cioslowski, J.; Fox, D. J. *Gaussian 09*, Gaussian, Inc.: Wallingford, CT, 2009.
- [19] Borden, W. T.; Davidson, E. R., *J. Am. Chem. Soc.* **1977**, *99* (14), 4587.
- [20] Hückel, E., *Z. Phys.* **1931**, *70*, 204.
- [21] Breslow, R., *Acc. Chem. Res.* **1973**, *6* (12), 393.
- [22] Baird, N. C., *J. Am. Chem. Soc.* **1972**, *94* (14), 4941.
- [23] Saunders, M.; Berger, R.; Jaffe, A.; McBride, J. M.; O'Neill, J.; Breslow, R.; Hoffmann, J. M.; Perchonock, C.; Wasserman, E. *J. Am. Chem. Soc.* **1973**, *95* (9), 3017.
- [24] Feixas, F.; Matito, E.; Poater, J.; Sola, M., *J. Comput. Chem.* **2008**, *29* (10), 1543.
- [25] Schleyer, P. v. R.; Maerker, C.; Dransfeld, A.; Jiao, H.; van Eikema Hommes, N. J. R., *J. Am. Chem. Soc.* **1996**, *118* (26), 6317.
- [26] Gershoni-Poranne, R.; Stanger, A., *Chem. Soc. Rev.* **2015**, *44* (18), 6597.
- [27] Chen, Z.; Wannere, C. S.; Corminboeuf, C.; Puchta, R.; Schleyer, P., *Chem. Rev.* **2005**, *105* (10), 3842.

- [28] Stanger, A., *J. Org. Chem.* **2006**, 71 (3), 883.
- [29] Subramanian, G.; Schleyer, P. V.; Jiao, H. J., *Organometallics* **1997**, 16 (11), 2362.
- [30] Feixas, F.; Matito, E.; Poater, J.; Sola, M., *J. Comput. Chem.* **2008**, 29 (10), 1543.
- [31] Schleyer, P. v. R., *Chem. Rev.* **2001**, 101 (5), 1115.
- [32] Kruszewski, J.; Krygowski, T. M., *Tetrahedron Lett.* **1972**, 13, 3839.
- [33] Hammett, L. P., *J. Am. Chem. Soc.* **1937**, 59 (1), 96.

CHAPTER 5. ANOMALOUS ELECTRONIC PROPERTIES OF IODOUS MATERIALS: APPLICATION TO HIGH-SPIN PHENYLOXENIUM IONS

Modified and reprinted from *J. Org. Chem.* **2020**, *85*, 4145

Copyright © 2020, American Chemical Society

Yunfan Qiu and Arthur H. Winter

5.1 Abstract

Manipulating frontier orbital energies of aromatic molecules with substituents is key to a variety of chemical and material applications. This chapter presents a simple strategy for achieving high-energy in-plane orbitals for aromatics simply by positioning iodine atoms next to each other. The lone pair orbitals on the iodines mix to give a high-energy in-plane σ -antibonding orbital as the HOMO. It shows that this effect can be used to manipulate orbital gaps, the symmetry of the highest occupied orbital, and the adopted electronic state for reactive intermediates. For example, ubiquitous cationic reactive intermediates such as aryl oxenium ions adopt n, π^* triplet ground states when buttressed iodine atoms are appended on the aromatic ring. Thus, while the parent phenyl oxenium ion has a large singlet-triplet gap in favor of the singlet state, iodinated derivatives are computed to have n, π^* triplet ground states. Similar effects are observed for other benzylic cationic reactive intermediates, such as phenylnitrenium ions. When replacing iodine for other halogens, the observed effects are either drastically attenuated or disappear entirely, suggesting that this electronic effect is unique to iodine. This iodine buttressing approach for generating high-energy in-plane HOMOs is anticipated to be highly general. This electronic effect is not limited to reactive intermediates, this iodine buttressing strategy should also be able to achieve small HOMO-LUMO gaps in organic electronic materials. While the unusual properties of fluorous

materials are well established, at the other extreme on the periodic table, novel properties of iodous materials may await discovery.

5.2 Introduction

The ability to manipulate frontier orbitals [1] is critical to numerous chemical phenomena, including controlling the ground state spin configurations of reactive intermediates [2-4] and organometallics complexes, [5] tuning the optical properties of molecules and polymers, and altering photochemical pathways and photophysical processes. It is also fundamentally important to the design of magnetic and electronic materials, as well as conducting and semiconducting conjugated polymers. [6-9]

Here, this chapter demonstrates that adjacent iodines appended to aromatic rings results in the generation of a very high-energy occupied orbital that result from the antibonding mixing of the in-plane iodine lone pair orbitals, and this electronic effect can be used to drastically alter the properties of reactive intermediates containing multiple iodines. We show that this property is unique to iodine, as related bromo or other halo-substituted derivatives do not show this electronic effect. This novel property for iodous materials invites experimental exploration.

Unusual properties of iodine-containing molecules have previously been suggested. For example, the σ orbital mixing pattern of iodine lone pair orbitals (shown in Figure 5.1) has previously been used [10-12] to develop a system that may feature σ -aromaticity, the term first used by Dewar [13] for describing the bond properties in cyclopropane. As shown in Figure 5.2, the 5p orbitals of the iodines produce an in-plane σ -antibonding HOMO for the neutral hexaiodobenzene C_6I_6 . After two-electron oxidation, the cyclic I_6 portion of its dication meets the Hückel ($4n+2$) criteria. As a result, the σ - π double aromaticity, suggested by Schleyer,

[14,15] is argued to exist in the C_6I_6 dication. Iodine can also engage in halogen bonding and features strong dispersion interactions as a result of its high polarizability. [16-18]

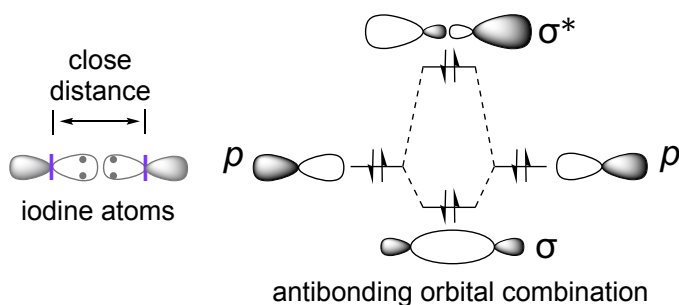


Figure 5.1 LCAO diagram for the orbital mixing of two nonbonding orbitals on two adjacent iodine atoms.

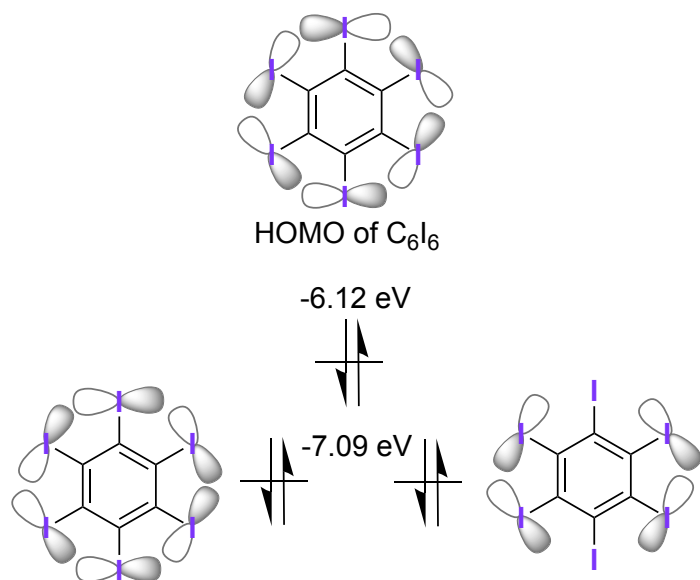


Figure 5.2 Three cyclic in-plane σ -delocalized MOs of neutral C_6I_6 . Neutral form has a σ -antibonding HOMO and its dication $C_6I_6^{2+}$ contains the bottom two σ -delocalized MOs after two-electron oxidation.

Beyond such studies, however, relatively little work has been performed on iodine-containing materials, as they are synthetically more challenging to make than bromo or chloro compounds, and have many more electrons than the other halogens, making them more computationally expensive to model. Indeed, basis sets for iodine are not even included in popular computational programs such as Gaussian. Thus, there has been relatively little exploration of the properties of iodous materials, either by experimental or computational means, and so unique properties may have been overlooked by the common assumption that iodine behaves similarly to other halogens.

Nevertheless, elements at the extremes on the periodic table often feature unique properties. In this chapter, computationally, iodine buttressing can achieve unprecedented spin states for phenyloxenium ions. Among the high-spin manifolds, benzylic cationic reactive intermediates, especially phenyloxenium ions [19-23], have drawn broad attention because of their critical role in many important industrially and synthetically useful reactions, as well as in biological processes. [24, 25] Benzylic cationic reactive intermediates, including phenyloxenium ions, exhibit contrasting reactivities and accordingly produce distinct reaction products depending on their electronic configurations. In general, oxenium ions adopting closed-shell singlet ground states react as typical electrophiles and thus undergo nucleophilic addition reactions, while those with high-spin triplet ground states react like diradicals (e.g., hydrogen atom abstraction or radical additions). [2,26,27] Switching the ground states of phenyloxenium ions can consequently switch the reactivity patterns of these intermediates between electrophilic and diradical reactions. Furthermore, triplet ions, if appropriately stabilized, may find use as building blocks for magnetic organic materials. [28,29]

Both experimental and theoretical studies have shown that the parent phenyloxenium ion (Ph-O^+) has closed-shell singlet ground states. [30] Conceptually, it is energetically unfavorable to populate an electron into the empty p orbital on the heteroatom to achieve a triplet state because the p orbital energy is elevated by the antibonding conjugation with the benzene ring. Thus, the singlet state is favored, with large singlet-triplet energy gaps for these species. As a result, almost all aryl oxenium ions are ground state singlet species, [31,32] with a few exceptions. [33]

However, substituting the parent phenyloxenium ion can alter the energies of the frontier orbitals and lead to triplet ground states being adopted. [34] Here, this chapter shows that iodine atoms substituted on the aromatic rings lower the singlet-triplet gaps of phenyloxenium ion, in some cases making the triplet state the computed ground state. It shows that this unusual effect arises from the lone pair orbitals on the adjacent iodine atoms mixing to construct a high-energy in-plane σ -antibonding orbital via a filled—filled molecular orbital combination. (see Figure 5.1). This σ -delocalized antibonding orbital acts as an energy-raised HOMO and substantially lowers the HOMO-LUMO gap, which encourages the phenyloxenium ion to adopt the triplet state as a result of the favorable exchange energy enjoyed by electrons with identical spins. This study also implies that this iodine buttressing strategy is applicable to other chemical processes where small HOMO-LUMO gap are desirable, such as optical and electronic materials. While in general iodination reactions are less well developed than other halogenations, recent developments in organo-iodine synthesis [35-38] may allow the synthesis of such new iodinated materials featuring novel properties.

5.3 Experimental Section

Density functional theory calculation were performed using the Gaussian 09, Revision E.01, software suite [39] applying the B3LYP functional that includes Becke's three-parameter gradient-corrected exchange functional [40] and the LYP correlation functional [41] of Lee, Yang, and Parr along with the 6-311G(d,p) polarized triple- ζ basis set. Heavy atoms, like iodine, exceed the boundary of the employed split-valence basis set and the equivalent valence basis set (see Table D1 in the APPENDIX D), which was initially constructed by Radom and others [42] for carrying out Gaussian-2(G2) theoretical calculations on iodine-containing molecules, is obtained from the basis set exchange database. [43,44] A reason for selecting this level of theory is that it has been benchmarked extensively for singlet-triplet gaps for these reactive intermediates. A recent benchmarking study gave an RMSD error of 2.3 kcal/mol for computing the singlet-triplet gaps for hypovalent reactive intermediates including carbenium ions, oxenium ions, and carbenes, for a test set compared to experimentally determined values. [45] Though iodine-containing moieties were not discussed in that benchmarking study, various substituents were investigated, which makes us believe the computational method in this work is adequate to evaluate the singlet-triplet gaps for iodous phenyloxenium ions. To determine the ground electronic states of the benzylic cationic reactive intermediates in this work, the singlet-triplet energy gap (ΔE_{ST}) was calculated by subtracting the lowest triplet energy from the lowest singlet energy, eq. 1.

$$\Delta E_{ST} = E_{\text{singlet}} - E_{\text{triplet}} \quad (1)$$

In all cases where broken-symmetry DFT calculations were performed, eq. 2 was used to titrate out contamination from a low-energy triplet state and achieve a spin-purified energy of the singlet state: [46,47]

$$E_{\text{singlet}} = \frac{2E_{\langle S_z \rangle=0} - \langle S^2 \rangle E_{\langle S_z \rangle=1}}{2 - \langle S^2 \rangle} \quad (2)$$

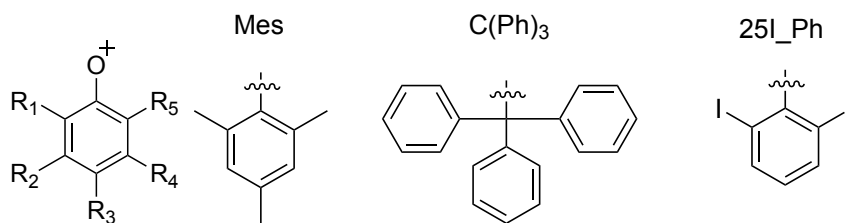
where E_{singlet} is the corrected singlet energy, $E_{\langle S_z \rangle=0}$ is the broken-symmetry energy, $\langle S^2 \rangle$ is the expectation value of the total-spin operator for the broken-symmetry, and $E_{\langle S_z \rangle=1}$ is the energy of the triplet state at the singlet geometry.

All optimized geometries were found to have zero imaginary frequencies. Selected Kohn-Sham molecular orbitals are visualized utilizing IBOview software with the iso surface threshold value as 80.00. [47,48]

5.4 Results and Discussion

Iodine buttressing lowers HOMO-LUMO energy gaps for hypovalent reactive intermediates and leads to predicted triplet ground state phenyloxenium ions. Table 5.1 shows the computed singlet-triplet gaps along with the HOMO-LUMO gaps of the lowest energy singlet state for some aryl oxenium ions. As is well known from both experiment and theory, the parent phenyloxenium ion (Ph-O^+ , **1**), has closed-shell singlet ground states with large singlet-triplet energy gaps, which are also reflected by large HOMO-LUMO gaps. [20-22] Thus, these ions react like typical closed-shell electrophiles by undergoing nucleophilic additions. It is also worth noting that phenyloxenium ions have n, π^* triplets as their lowest triplet energy states. These triplet states can be arrived at conceptually by starting with the singlet state and transferring one electron from the in-plane lone pair to the out-of-plane empty p orbital on the heteroatom, with an accompanying change in the electron spin.

Table 5.1 Singlet-triplet state energy gaps (ΔE_{ST} in kcal/mol) and the HOMO-LUMO gaps ($E_{HOMO-LUMO}$ in eV) of the singlet state for phenyloxenium ions (B3LYP/6-311G(d,p)). A negative ΔE_{ST} indicates a singlet ground state.



Structure	R ₁	R ₂	R ₃	R ₄	R ₅	ΔE_{ST} (kcal/mol)	$E_{HOMO-LUMO}$ (eV)
1	H	H	H	H	H	-13.2	2.7
2	I	I	I	I	I	-1.3	1.2
3	Mes	I	I	I	Mes	+3.9	1.2
4	H	Mes	I	I	Mes	+2.9	1.0
5	C(Ph) ₃	I	I	I	C(Ph) ₃	+6.5	
6	I	I	C(Ph) ₃	I	I	+1.9	
7	H	I	Mes	I	H	+0.4	
8	Mes	I	H	I	Mes	+1.3	
9	H	25I_Ph	25I_Ph	25I_Ph	H	+0.4	

However, a large change is observed when iodines are substituted on the phenyl rings. For the phenyloxenium ion, **1**, when all five hydrogen atoms on the benzene ring of **1** are replaced with iodine atoms (pentaiodo phenyloxenium ion, **2**), the singlet-triplet gap changes from -13.2 kcal/mol to -1.3 kcal/mol (a negative value indicates a singlet ground state), making the computed singlet and triplet states nearly degenerate. To understand the basis behind the lowered singlet-triplet gap, visualized Kohn-Sham orbitals of the HOMO and LUMO for the closed-shell singlet ground states are shown in Figure 4.3. As expected, the LUMO of **1** is derived from the orbital mixing involving the filled p orbitals on the benzene ring and the out-of-plane empty p orbital, while the majority of the HOMO consists of the nonbonding orbital on the

oxygen atom. For ion **2**, however, the planar delocalized molecular orbital shape of the nature of the LUMO is largely unperturbed, while the HOMO switches from an oxygen centered orbital to a through-space iodine-centered σ antibonding orbital. The absolute energy values of the frontier orbitals in Figure 5.3 also indicate that, despite both absolute energies of HOMO and LUMO being elevated, the high energetic nature of an antibonding orbital still results in a much lower HOMO-LUMO gap for ion **2**.

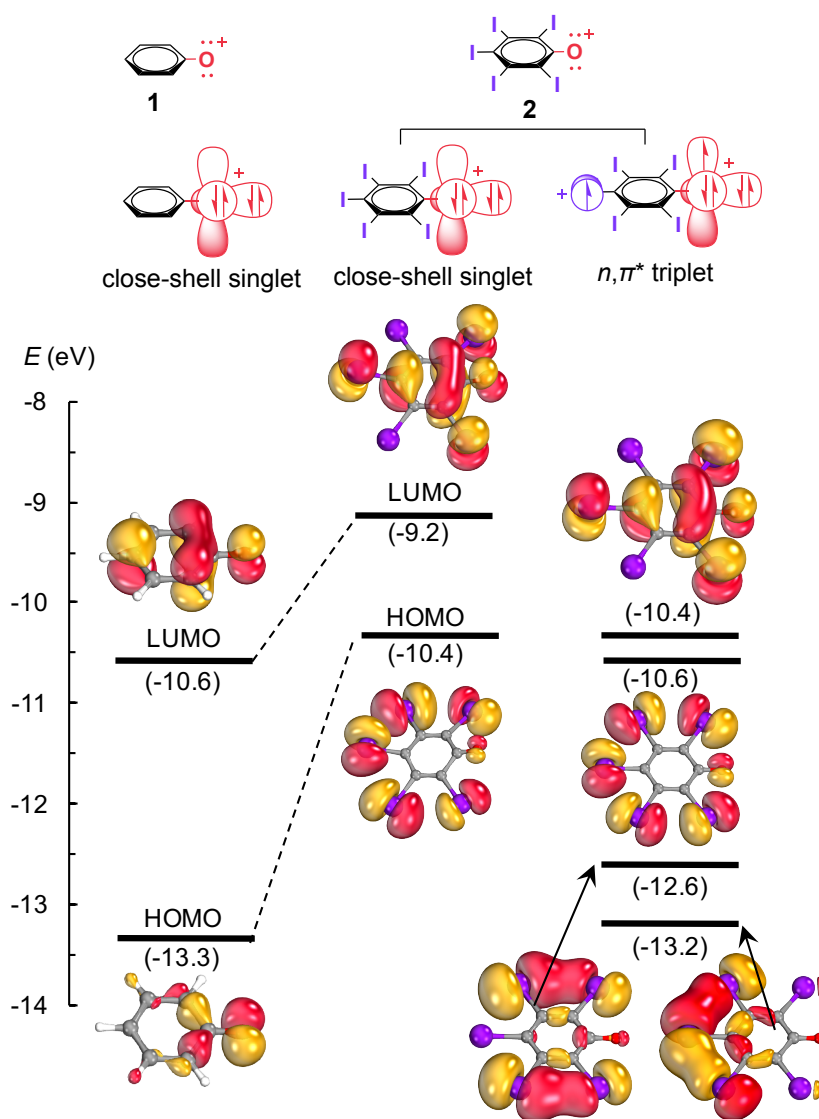


Figure 5.3 Kohn-Sham molecular orbitals are depicted along with the absolute energies (eV, values in the parentheses) of the HOMO, LUMO and selected orbitals for **1** and **2**.

Specifically, the HOMO-LUMO gap of **1** is computed to be 2.7 eV, while the other of **2** is lowered to 1.2 eV. Furthermore, the two SOMOs of **2** for its lowest triplet energy state are presented in Figure 5.3 as well, suggesting an n, π^* triplet state where one electron initially from the lone pair of an iodine atom is populated into the delocalized π orbital. The comparison between the molecular orbitals of **1** and **2** shows that the through-space antibonding orbital induced by iodine buttressing can alter the predicted ground state from closed-shell singlet to triplet. In addition, two through-space bonding orbitals of **2** are also pictured in Figure 5.3 as further confirmation of the spatial interaction between the nonbonding orbitals of iodine atoms.

We then anticipated that other groups, like mesityl groups (Mes), can also be incorporated to further increase the energy of the σ -delocalized antibonding iodine-centered HOMOs. Mes was selected because it adopts a geometry orthogonal to the core aromatic ring, potentially allowing the filled π orbitals on the mesityl group to overlap with the iodine lone pair orbitals, which can further amplify the antibonding orbital mixing. Iodinated phenyloxenium ion derivatives were examined with mesityl groups substituted. A striking feature from the intermediates substituted with both iodine and mesityl groups is that, for **3** and **4**, the positive values for their singlet-triplet energy gaps in Table 5.1 indicate that these ions are predicted to adopt triplet ground states. The two SOMOs for the lowest triplet states of **3** and **4**, visualized in Figure 5.4, strongly indicate that the frontier orbitals of **3** and **4** are involved in the same fashion as those in the purely iodinated oxenium ion **2**, but also show that the filled p orbitals of the Mes group are engaged in the σ -antibonding combination. The two SOMO orbitals also suggest **3** and **4** adopt n, π^* triplet spin configuration for these iodinated phenyloxenium ions. Thus, a combination of iodination and ring substitution can lead to substituted phenyloxenium ions with high-spin ground states predicted.

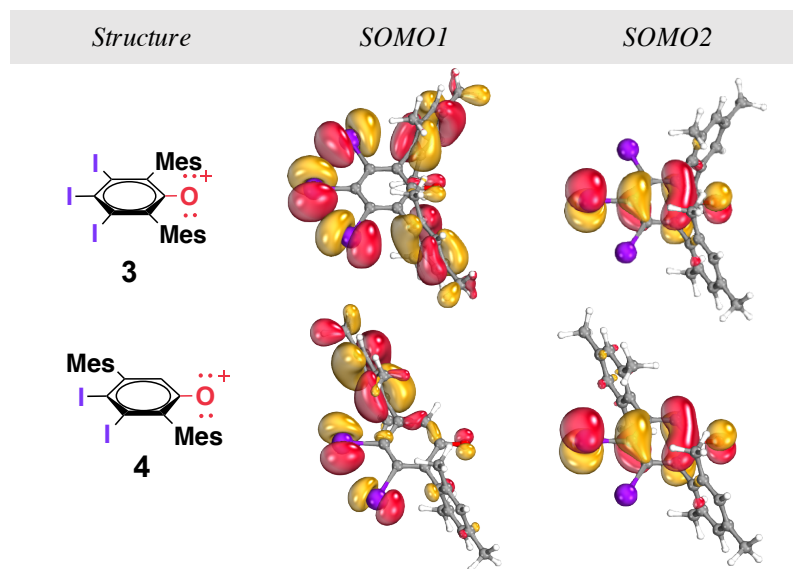


Figure 5.4 Orbital representation for the two SOMOs of their lowest triplet states of **3** and **4**.

Importantly, this iodine—iodine orbital interaction effect is restricted to iodine, as other halogens, such as bromines, do not show the same capability of changing the nature of the HOMO. (see APPENDIX D). The antibonding formation is attenuated and not observed when replacing iodine with bromine. More importantly, the singlet-triplet energy gap of pentabromo phenyloxenium ion is computed to be -11.4 kcal/mol while the parent version, **1**, has -13.2 kcal/mol energy difference. The comparison between these two energy values also demonstrates that bromine substituents have very limited potential to construct a high energy molecular orbital via antibonding formation.

5.5 Conclusions

In summary, adjacent iodine atoms can participate in through-space orbital mixing and lead to high energy in-plane σ -antibonding HOMOs. When this iodine buttressing strategy is used to the phenyloxenium ion, the generated through-space antibonding orbital acts as the HOMO and

the high energy of the antibonding orbital lowers the HOMO-LUMO energy gap. By narrowing the HOMO-LUMO gap, phenyloxenium ions are predicted to adopt n, π^* triplet ground states, which should feature distinct magnetic properties and unique reactivity. This electronic effect of iodine-containing materials is anticipated to be highly general. For example, this iodine buttressing strategy can also be applied to other reactive intermediate such as nitrenium ions and other aromatic systems like organic electronic materials.

Iodo-organics have seen use as substrates and reagents for cross-couplings, or as oxidants with hypervalent iodine reagents, but they have largely been ignored as potential end target materials with novel properties. Thus, one impact of these computational predictions is that they could spur the development of new methods for iodination to probe the unusual properties of iodous materials, much as we have recently seen developments in the ability to fluorinate organics to make fluorous materials. Such fluorous materials were once difficult to prepare, but new synthetic methodologies have enabled the use of polyfluorinated organics in a variety of applications, from separations science to pharmaceuticals to ultrahydrophobic surfaces and materials. Extremes on the periodic table often lead to unique properties. These computational predictions invite experimental evaluation, and suggest that unique properties of iodous materials may await discovery.

5.6 Acknowledgments

We thank the National Science Foundation (NSF CHE-1464956) and the Bailey Research Award for support of this work. This work used the HPC@ISU equipment at Iowa State University, some of which has been purchased through funding provided by NSF.

5.7 References

- [1] Fukui, K.; Yonezawa, T.; Shingu, H. *J. Chem. Phys.* **1952**, *20* (4), 722.
- [2] Moss, R. A.; Platz, M. S.; Jones, M., Jr. *Reactive Intermediate Chemistry*. Wiley: Hoboken, NJ, **2004**.
- [3] Abe, M. Diradicals. *Chem. Rev.* **2013**, *113* (9), 7011.
- [4] Rajca, A. *Chem. Rev.* **1994**, *94* (4), 871.
- [5] Wedler, H. B.; Wendelboe, P.; Power, P. P. *Organometallics* **2018**, *37* (18), 2929.
- [6] Kim, B.-G.; Ma, X.; Chen, C.; Je, Y.; Coir, E. W.; Hashemi, H.; Aso, Y.; Green, P. F.; Kieffer, J.; Kim, J. *Adv. Funct. Mater.* **2013**, *23* (4), 439.
- [7] Aihara, J.-i. *J. Phys. Chem. A* **1999**, *103* (37), 7487.
- [8] Heinze, J. r.; Frontana-Uribe, B. A.; Ludwigs, S. *Chem. Rev.* **2010**, *110* (8), 4724.
- [9] Meng, H.; Wudl, F. *Macromolecules* **2001**, *34* (6), 1810.
- [10] Sagl, D. J.; Martin, J. C. *J. Am. Chem. Soc.* **1988**, *110* (17), 5827.
- [11] Ciofini, I.; Lainé, P. P.; Adamo, C. *Chem. Phys. Lett.* **2007**, *435* (4-6), 171.
- [12] Havenith, R. W. A.; Fowler, P. W.; Fias, S.; Bultinck, P. *Tetrahedron Lett.* **2008**, *49* (8), 1421.
- [13] Dewar, M. J. S. *J. Am. Chem. Soc.* **1984**, *106* (3), 669.
- [14] Chandrasekhar, J.; Jemmis, E. D.; Schleyer, P. v. R. *Tetrahedron Lett.* **1979**, *20* (39), 3707.

- [15] Schleyer, P. v. R.; Jiao, H.; Glukhovtsev, M. N.; Chandrasekhar, J.; Kraka, E. *J. Am. Chem. Soc.* **1994**, *116* (22), 10129.
- [16] Riley, K. E.; Hobza, P. *J. Chem. Theory Comput.* **2008**, *4* (2), 232.
- [17] Riley, K. E.; Hobza, P. *Phys. Chem. Chem. Phys.* **2013**, *15* (41), 17742.
- [18] Politzer, P.; Lane, P.; Concha, M. C.; Ma, Y.; Murray, J. S. *J. Mol. Model.* **2006**, *13* (2), 305.
- [19] Abramovitch, R. A.; Alvernhe, G.; Inbasekaran, M. N. *Tetrahedron Lett.* **1977**, *13*, 1113.
- [20] Wang, Y. T.; Wang, J.; Platz, M. S.; Novak, M. *J. Am. Chem. Soc.* **2007**, *129* (47), 14566.
- [21] Hanway, P. J.; Xue, J.; Bhattacharjee, U.; Milot, M. J.; Ruixue, Z.; Phillips, D. L.; Winter, A. H. *J. Am. Chem. Soc.* **2013**, *135* (24), 9078.
- [22] Qiu, Y.; Winter, A. H. *Org. Biomol. Chem.* **2017**, *15* (13), 2666.
- [23] Du, L.; Qiu, Y.; Lan, X.; Zhu, R.; Phillips, D. L.; Li, M.-D.; Dutton, A. S.; Winter, A. H. *J. Am. Chem. Soc.* **2017**, *139* (42), 15054.
- [24] Chan, P. Y.; Kwok, W. M.; Lam, S. K.; Chiu, P.; Phillips, D. L. *J. Am. Chem. Soc.* **2005**, *127* (23), 8246.
- [25] Osborne, R. L.; Coggins, M. K.; Raner, G. M.; Walla, M.; Dawson, J. H. *Biochemistry* **2009**, *48* (20), 4231.
- [26] Falvey, D. E. *J. Phys. Org. Chem.* **1999**, *12* (8), 589.
- [27] Zhang, Y.; Burdzinski, G.; Kubicki, J.; Platz, M. S. *J. Am. Chem. Soc.* **2008**, *130* (48), 16134.

- [28] Iwamura, H.; Murata, S. *Mol. Cryst. Liq. Cryst. Inc. Nonlinear Opt.* **1989**, *176* (1), 33.
- [29] Prigodin, V. N.; Bergeson, J. D.; Lincoln, D. M.; Epstein, A. J. *Synth. Met.* **2006**, *156* (9-10), 757.
- [30] Hanway, P. J.; Winter, A. H. *J. Am. Chem. Soc.* **2011**, *133* (13), 5086.
- [31] Novak, M.; Poturalski, M. J.; Johnson, W. L.; Jones, M. P.; Wang, Y.; Glover, S. A. *J. Org. Chem.* **2006**, *71* (10), 3778.
- [32] Abramovitch, R. A.; Alvernhe, G.; Bartnik, R.; Dassanayake, N. L.; Inbasekaran, M. N.; Kato, S. *J. Am. Chem. Soc.* **1981**, *103* (15), 4558.
- [33] Li, M. D.; Albright, T. R.; Hanway, P. J.; Liu, M.; Lan, X.; Li, S.; Peterson, J.; Winter, A. H.; Phillips, D. L. *J. Am. Chem. Soc.* **2015**, *137* (32), 10391.
- [34] Winter, A. H.; Falvey, D. E.; Cramer, C. J.; Gherman, B. F. *J. Am. Chem. Soc.* **2007**, *129* (33), 10113.
- [35] Barluenga, J.; González, J. M.; García-Martín, M. A.; Campos, P. J. *Tetrahedron Lett.* **1993**, *34* (24), 3893.
- [36] Kitamura, T.; Rahman, M.; Shito, F. *Synthesis* **2009**, *2010* (01), 27.
- [37] Rodríguez-Lojo, D.; Cobas, A.; Peña, D.; Pérez, D.; Guitián, E. *Org. Lett.* **2012**, *14* (6), 1363.
- [38] Mattern, D. L. Direct Aromatic Periodination. *J. Org. Chem.* **1984**, *49* (17), 3051.
- [39] Frisch, M. J.; Trucks, G. W.; Schlegel, H. B.; Scuseria, G. E.; Robb, M. A.; Cheeseman, J. R.; Scalmani, G.; Barone, V.; Mennucci, B.; Petersson, G. A.; Nakatsuji, H.; Caricato, M.; Li, X.; Hratchian, H. P.; Izmaylov, A. F.; Bloino, J.; Zheng, G.; Sonnenberg, J. L.; Hada, M.; Ehara, M.; Toyota, K.; Fukuda, R.; Hasegawa, J.; Ishida, M.; Nakajima, T.; Honda, Y.; Kitao, O.; Nakai, H.; Vreven, T.; Montgomery, J. A., Jr.; Peralta, J. E.; Ogliaro, F.; Bearpark, M.; Heyd, J. J.; Brothers, E.; Kudin, K. N.; Staroverov, V. N.;

- Kobayashi, R.; Normand, J.; Raghavachari, K.; Rendell, A. P.; Burant, J. C.; Iyengar, S. S.; Tomasi, J.; Cossi, M.; Rega, N.; Millam, N. J.; Klene, M.; Knox, J. E.; Cross, J. B.; Bakken, V.; Adamo, C.; Jaramillo, J.; Gomperts, R.; Stratmann, R. E.; Yazyev, O.; Austin, A. J.; Cammi, R.; Pomelli, C.; Ochterski, J. W.; Martin, R. L.; Morokuma, K.; Zakrzewski, V. G.; Voth, G. A.; Salvador, P.; Dannenberg, J. J.; Dapprich, S.; Daniels, A. D.; Farkas, O.; Foresman, J. B.; Ortiz, J. V.; Cioslowski, J.; Fox, D. J. *Gaussian 09*, Gaussian, Inc.: Wallingford, CT, 2013.
- [40] Becke, A. D. *J. Chem. Phys.* **1993**, *98* (7), 5648.
- [41] Lee, C.; Yang, W.; Parr, R. G. *Phys. Rev. B* **1988**, *37* (2), 785.
- [42] Glukhovtsev, M. N.; Pross, A.; McGrath, M. P.; Radom, L. *J. Chem. Phys.* **1995**, *103* (5), 1878.
- [43] Feller, D. *J. Comput. Chem.* **1996**, *17* (13), 1571.
- [44] Schuchardt, K. L.; Didier, B. T.; Elsethagen, T.; Sun, L. S.; Gurumoorthi, V.; Chase, J.; Li, J.; Windus, T. L. *J. Chem. Inf. Model.* **2007**, *47* (3), 1045.
- [45] Fischer, L. J.; Dutton, A. S.; Winter, A. H. *Chem. Sci.* **2017**, *8*, 4231.
- [46] Yamaguchi, K.; Jensen, F.; Dorigo, A.; Houk, K. N. *Chem. Phys. Lett.* **1988**, *149* (5-6), 537.
- [47] Lim, M. H.; Worthington, S. E.; Dulles, F. J.; Cramer, C. J. *ACS Symp. Ser.* **1996**, *629*, 402.
- [47] Knizia, G. *J. Chem. Theory Comput.* **2013**, *9* (11), 4834.
- [48] Knizia, G.; Klein, J. E. *Angew. Chem. Int. Ed.* **2015**, *54* (18), 5518.

CHAPTER 6. GENERAL CONCLUSIONS

This dissertation has centered on exploring phenyloxenium ions with intriguing electronic configurations, corresponding reactivities and spectroscopic properties. Apart from the known cases of closed-shell singlet ground state phenyloxenium ion and π,π^* ground triplet state phenyloxenium ion, two more alternative electronic configurations of oxenium ions have been investigated and discussed. With the help of laser flash photolysis and advanced modern computations, detection and characterization of several phenyloxenium ions have been successfully accomplished.

By using the 4-methoxy pyridine as the photo cleavage group, the parent phenyloxenium ions is surprisingly generated in its open-shell singlet diradical configuration (1A_2), permitting an unexpected look at the reactivity of an atom-centered open-shell singlet diradical. Remarkably, despite possessing singly occupied molecular orbitals and no empty valence orbitals, this open-shell singlet phenyloxenium ion behaves as an even more powerful electrophile than the closed-shell singlet phenyloxenium ion, undergoing solvent trapping by weakly nucleophilic solvents such as water and acetonitrile or externally added nucleophiles rather than engaging in typical diradical chemistry. Moreover, the usage of pyridine as a novel leaving group for photo generating oxenium ion shows much cleaner ion generation, which prompts the discoveries of oxenium ion to certain extent.

By taking advantages of El-Sayed' rule, a n,π^* triplet excited oxenium ion has been achieved, permitting the insight into the reactivity of a triplet oxenium ion with two spins in two distinct symmetry types, which also supplements some parts of the research vacancy for phenyloxenium ions. This n,π^* triplet phenyloxenium ion has a much shorter lifetime than the previously observed π,π^* triplet ground state phenyloxenium ion due to its excited state nature.

This n,π^* triplet phenyloxenium ion behaves no difference compared to other triplet reactive intermediates (e.g. carbenes, nitrenes.), reacting in a typical diradical fashion.

In addition to the experimental studies, theoretical investigations have also been highlighted in this dissertation in searching for triplet ground state oxenium ions. In general, non-substituted aryl oxenium ions have closed-shell singlet ground states with large singlet-triplet gaps resulting from a strong break in the degeneracy of the p orbitals on the formal oxenium center. Remarkably, this dissertation presents that computationally (CBS-QB3 and G4MP2) that azulenyl oxenium ions can have triplet ground states depending upon the attachment position on the azulene core, which can be rationalized by employing Hückel aromaticity for singlet states and Baird aromaticity for triplet states.

Just like aromaticity, as one of the most fundamental theories in chemistry, constructing molecular orbital can also yield to triplet ground state oxenium ions. By positioning iodine atoms next to each other, the lone pair orbitals on the iodines mix to give a high-energy in-plane σ -antibonding orbital as the HOMO. It shows that this effect can be used to manipulate orbital gaps and can even invert the ground state from singlet to triplet for phenyloxenium ions.

As far as I am concerned, the remaining challenge of studying oxenium ion is still the lack of suitable photoprecursors, more specifically, appropriate photo leaving groups. I look forward to seeing oxenium ions to be used as synthetic building blocks in solving modern practical synthesis problems.

APPENDIX A. SUPPLEMENTAL INFORMATION ACCOMPANYING CHAPTER 2

Synthesis of 4-methoxyphenoxyppyridinium tetrafluoroborate 1

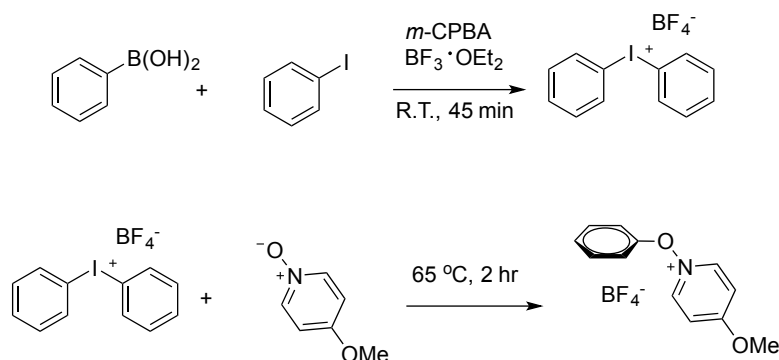


Figure A1. Synthesis route of 4-methoxyphenoxyppyridinium tetrafluoroborate salt.

Synthesis of diphenyliodonium tetrafluoroborate. *m*-chloroperoxybenzoic acid (81% active oxidant, 640 mg, 3.0 mmol) was dissolved in 10 mL CH_2Cl_2 . To the solution was added iodobenzene (310 μL , 2.7 mmol) followed by slow addition of $\text{BF}_3 \cdot \text{OEt}_2$ (850 μL , 6.8 mmol) at room temperature. The resulting yellow solution was stirred at r.t. for 30 min and then cooled to 0°C , and phenylboronic acid (370 mg, 3.0 mmol) was added. After 15 min of stirring at r.t., the crude reaction mixture was applied on a silica plug (6.0 g) and eluted with CH_2Cl_2 (60 mL) followed by $\text{CH}_2\text{Cl}_2/\text{MeOH}$ (120 mL, 20:1). The latter solution was concentrated, and diethyl ether (10 mL) was added to the residue to induce a precipitation. The solution was allowed to stir for 15 min, and then the ether phase was decanted. The solid was washed twice more with diethyl ether (2×10 mL) and then dried in vacuo to give diphenyliodonium tetrafluoroborate salt (825 mg, 83%). The solid was used without further purification.

Synthesis of 4-methoxyphenoxyppyridinium tetrafluoroborate 1. 4-methoxy-1-oxidepyridine (230 mg, 1.84 mmol) was dissolved in 5 mL dry acetonitrile and then freshly prepared

diphenyliodonium tetrafluoroborate salt (670 mg, 1.82 mmol) was added in small portions to the solution. The solution was heated at 65 °C for 2 hours under Argon. Evaporation of the acetonitrile gave a light brown solid and recrystallization from MeOH gave colorless prisms. The solid was then dried under reduced pressure to yield the colorless desired crystallized salt (313 mg, 60%). It was reasonably stable stored in a freezer in the dark under inert atmosphere.

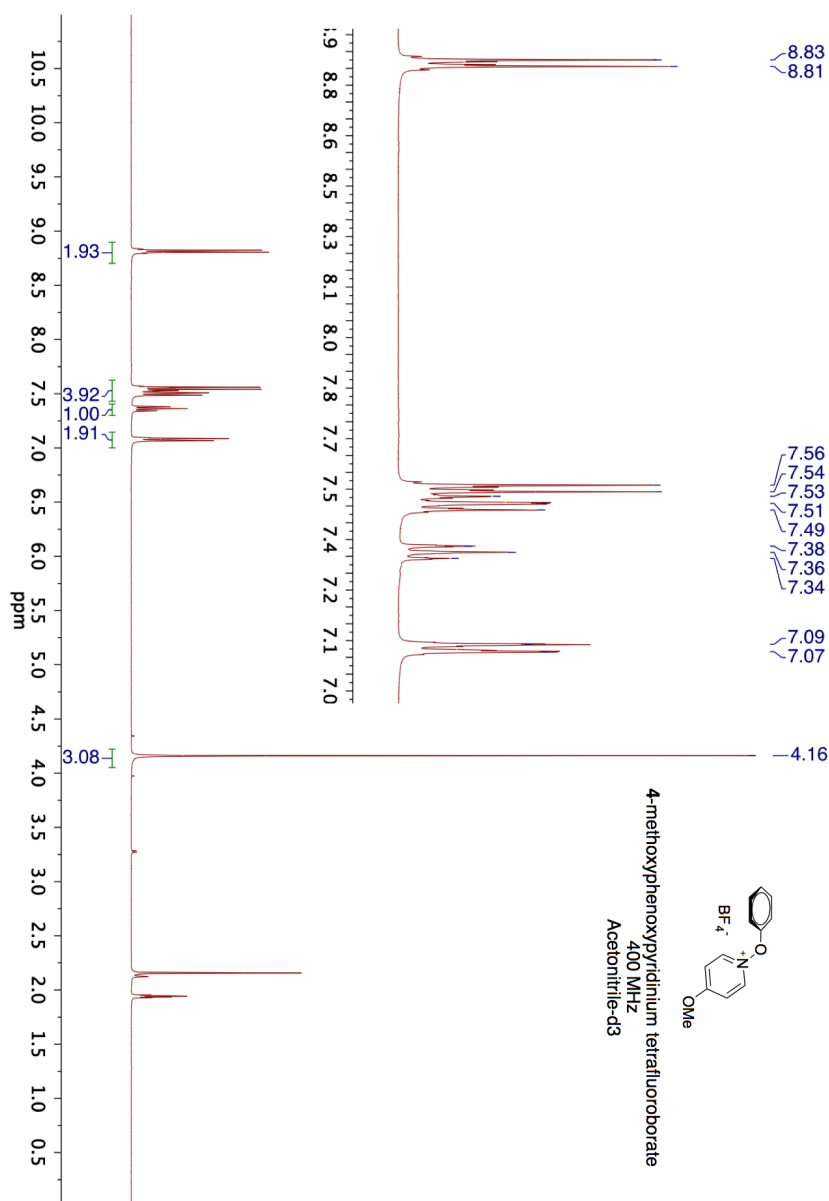


Figure A2. ^1H NMR of 4-methoxyphenoxy-pyridinium tetrafluoroborate **1**.

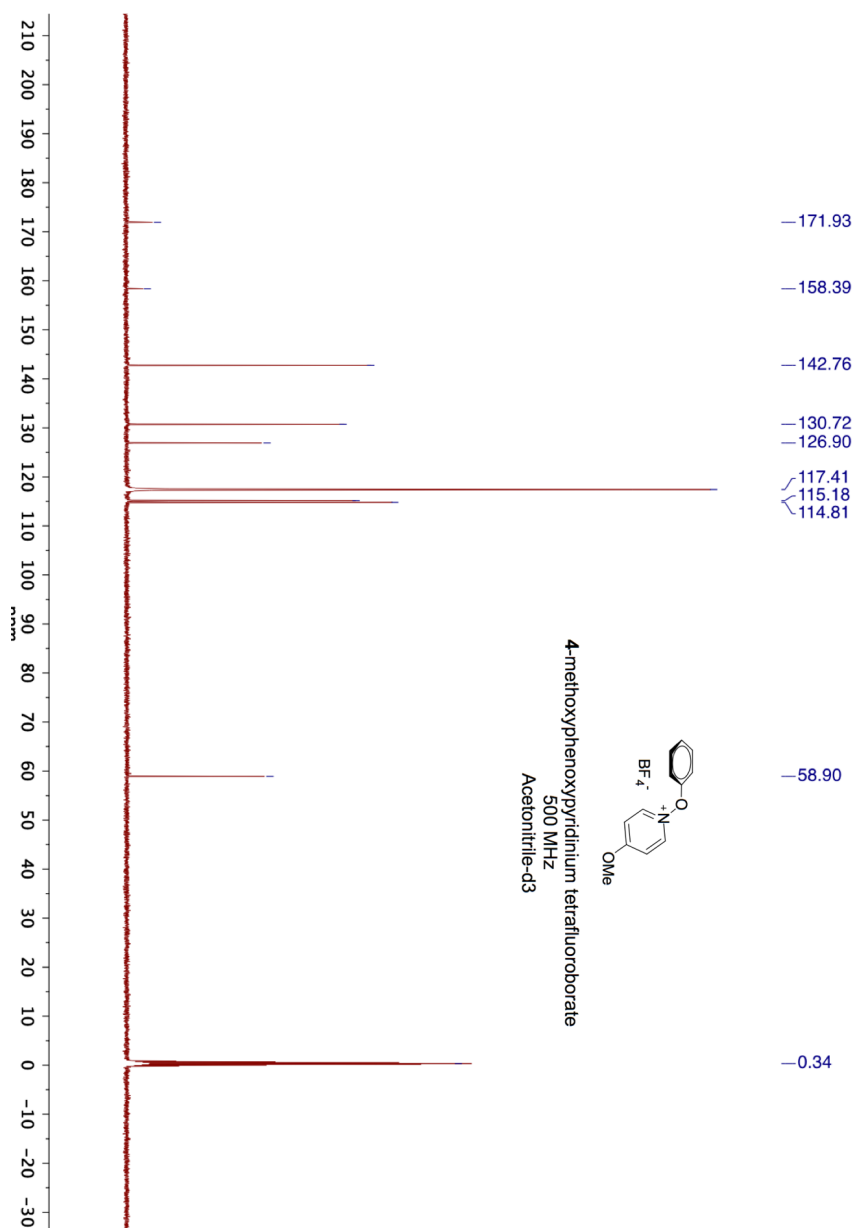


Figure A3. Full ^{13}C NMR of 4-methoxyphenoxypyridinium tetrafluoroborate **1**. Spectrum was obtained in deuterated acetonitrile.

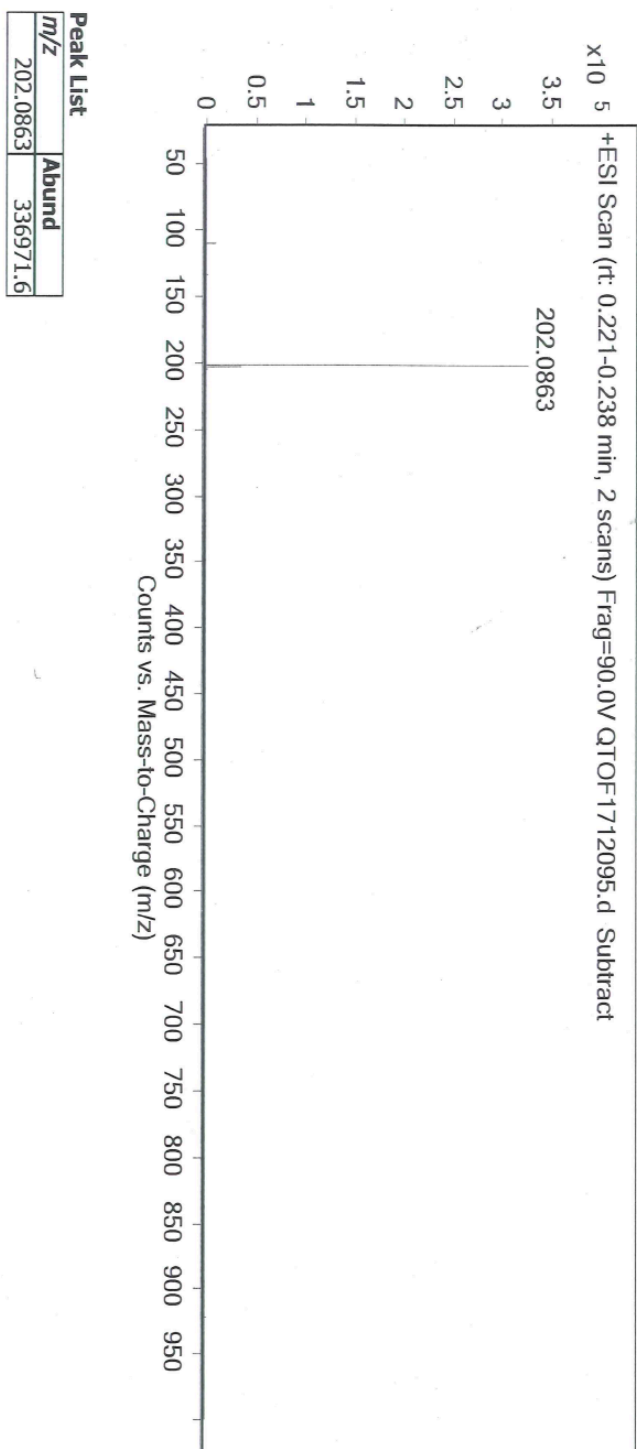


Figure A4. High resolution mass spectrum of 4-methoxyphenoxyridinium tetrafluoroborate **1** ($m/z=202.0863$).

Quantitative Product studies by ^1H NMR General procedure.

Photolysis product studies in deuterated solvents were performed with 2.5 mg of precursor 4-methoxyphenoxy pyridinium tetrafluoroborate **1** dissolved in 1 ml of acetonitrile- d_3 and 1 mL internal standard (decane) or deuterium oxide. Remaining solids were filtered and an initial ^1H NMR was taken with a 90-degree angle and a relaxation delay of 60 seconds in a quartz NMR tube. The sample was then irradiated with 254 nm UV light from a mercury vapor lamp for different desired time durations in a Rayonet photoreactor. Spectra were taken with the previous parameters. Radiation for shorter times leads to similar product ratios but has starting material present, suggesting that the products are not formed from secondary photolysis. After the photolysis and ^1H NMR characterization were completed, the sample was submitted to LC-MS for further product confirmation. Comparison between the ^1H NMR spectra of the sample and the standard chemicals also clarified the peak assignment and the products generated. Other product studies with additional methanol or sodium azide were performed in the same manner.

Photolysis product studies in non-deuterated solvents were performed by a similar method. 2.5 mg precursor was dissolved in 1 ml of regular acetonitrile or water and the sample was transferred in a quartz cuvette. The solution was photolyzed for 30 min (40 min for aqueous solution) in a Rayonet photoreactor fitted with 254 nm bulbs. After the photolysis was completed, the solvent was removed under reduced pressure and the residue was dissolved in acetonitrile- d_3 or deuterium oxide for ^1H NMR.

Photolysis product studies in non-deuterated acetonitrile.

The solution was irradiated with 254 nm UV light for 30 min and the color changed from colorless to brownish. Before removing the solvent under reduced pressure, methanol was added immediately to the brown solution to verify the existence of the adduct **5**. The oil like residue

was then re-dissolved by acetonitrile-d₃ for ¹H NMR and LC-MS. Several new methyl peaks located around 2 ppm region were only observed in regular acetonitrile but not in acetonitrile-d₃, which indicated the formation of Ritter intermediate adduct **3** between open-shell singlet phenyloxenium ion and the solvent acetonitrile. An additional adduct generated from methanol addition to **5** was also detected by ¹H NMR and LC-MS (166 m/z), which agreed with recent work by van Dijk et al that pyridine-stabilized nitrilium ions can react with nucleophiles.

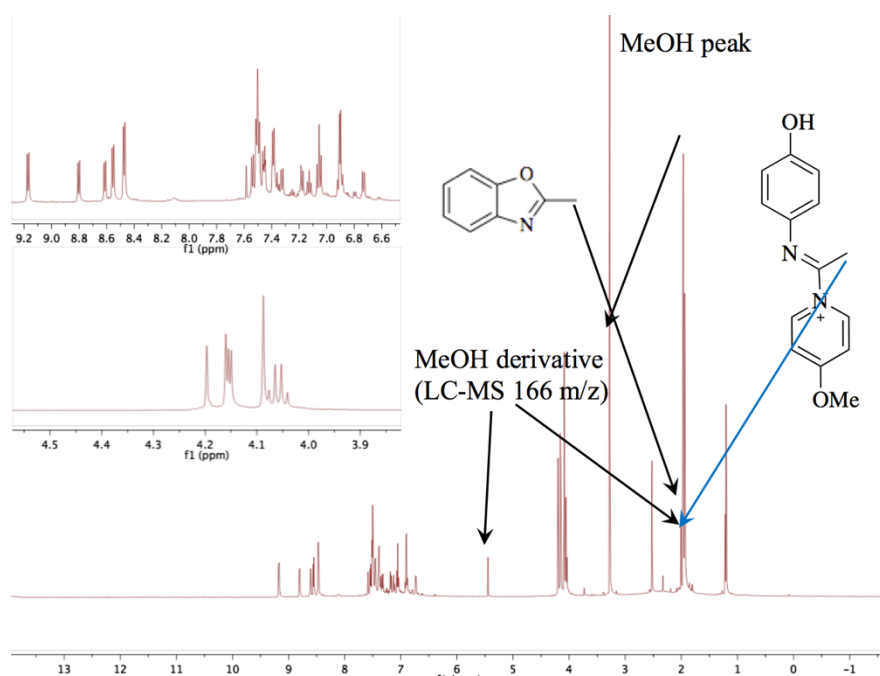


Figure A5. ¹H NMR spectrum of **1** photolyzed for 30 min in regular acetonitrile and the assignment of peaks. Full ¹H NMR spectrum.

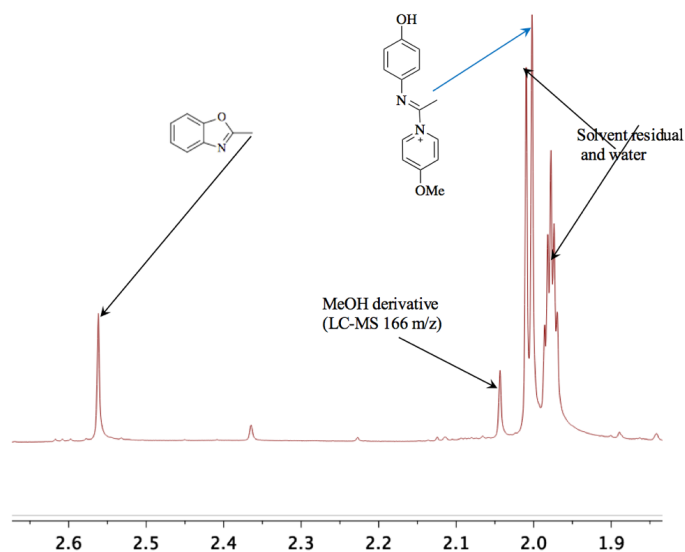


Figure A6. ^1H NMR spectrum of **1** photolyzed for 30 min in regular acetonitrile and the assignment of peaks. ~2 ppm region of the ^1H NMR spectrum.

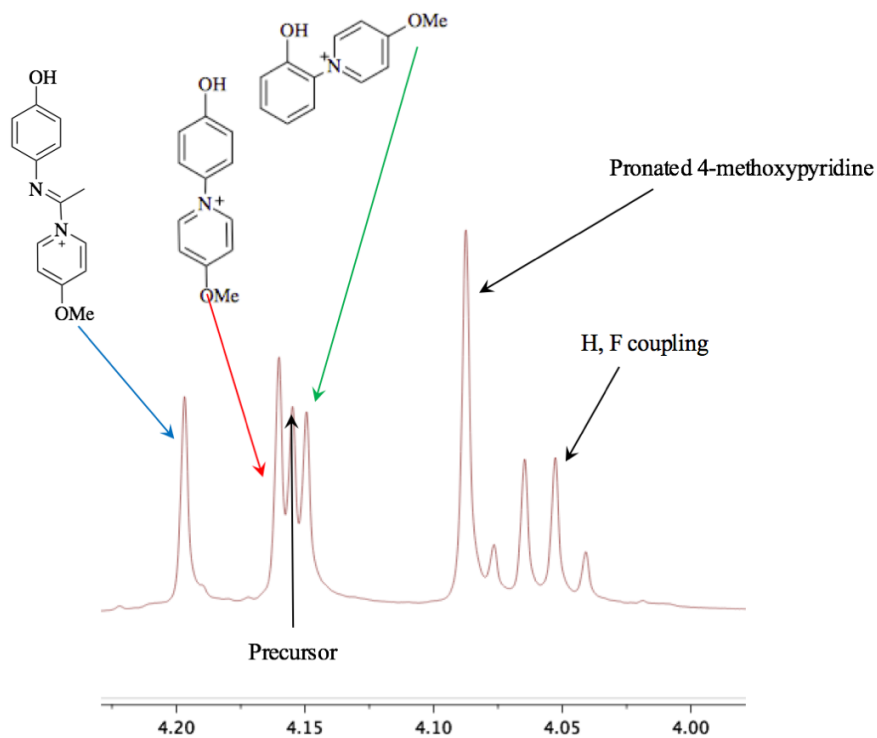


Figure A7. ^1H NMR spectrum of **1** photolyzed for 30 min in regular acetonitrile and the assignment of peaks. ~4 ppm region of the ^1H NMR spectrum.

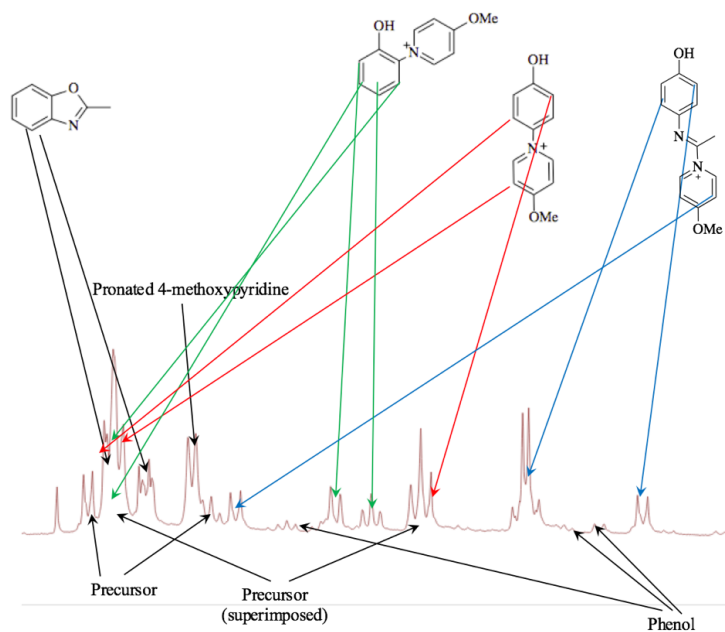


Figure A8. ^1H NMR spectrum of **1** photolyzed for 30 min in regular acetonitrile and the assignment of peaks. ~7 ppm region of the ^1H NMR spectrum.

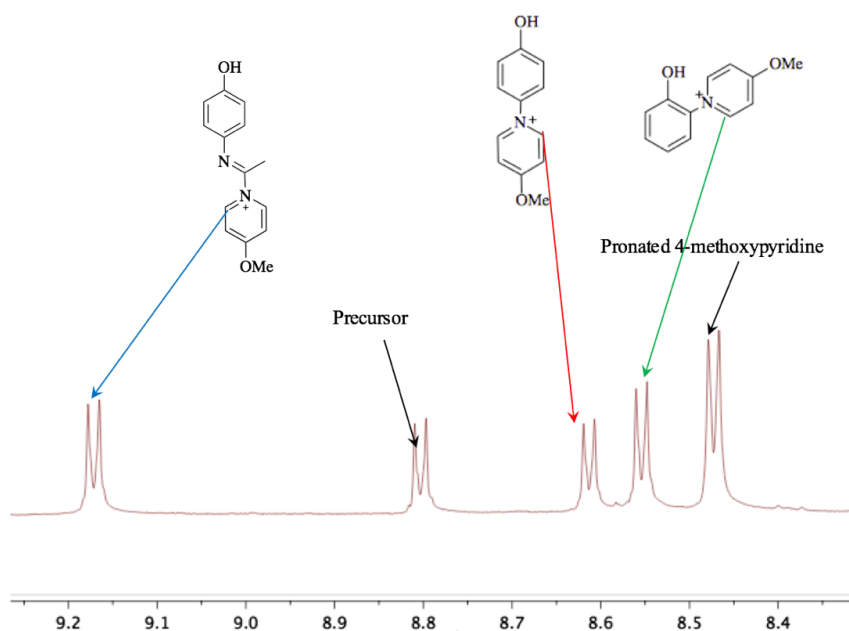


Figure A9. ^1H NMR spectrum of **1** photolyzed for 30 min in regular acetonitrile and the assignment of peaks. ~9 ppm region of the ^1H NMR spectrum.

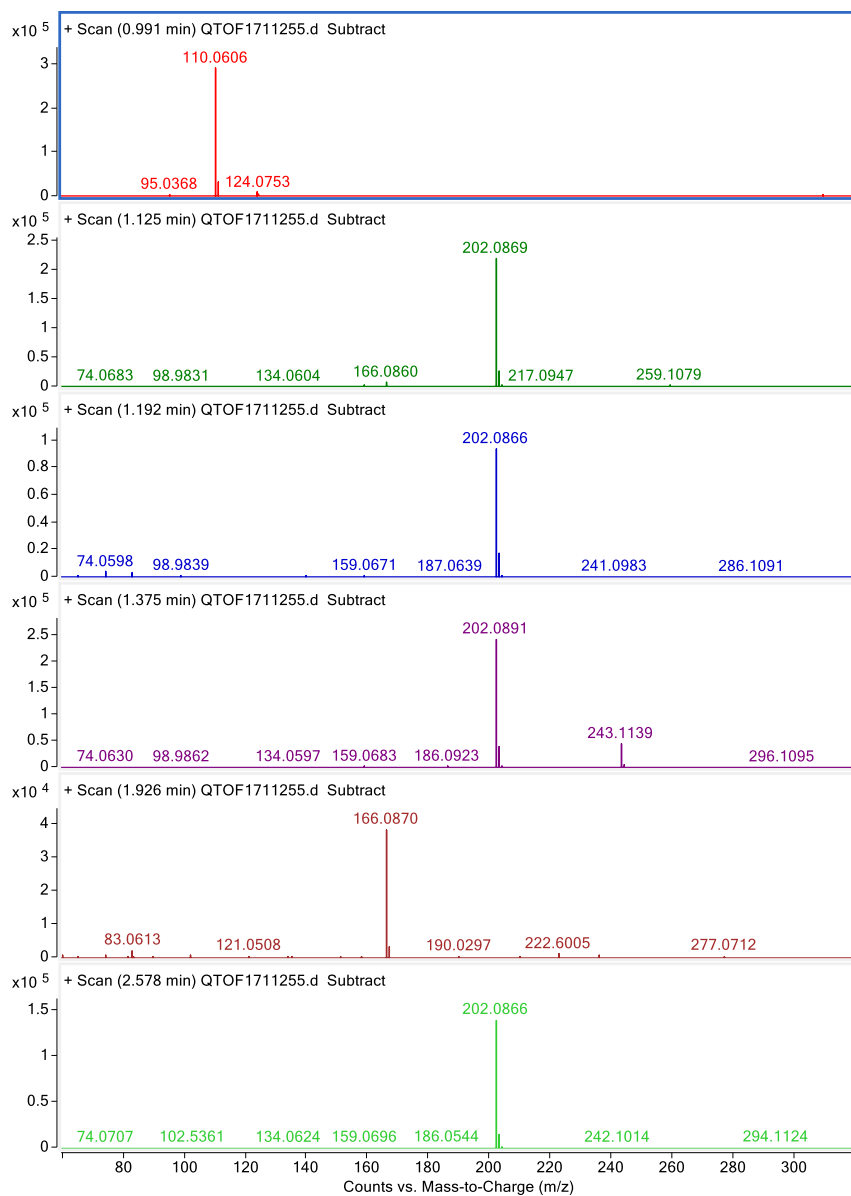


Figure A10. LC-MS of 4-methoxyphenoxypyridinium tetrafluoroborate **1** photolyzed for 30 min in regular acetonitrile.

Photolysis product studies in acetonitrile-d₃.

The solution with decane as internal standard was radiated by 254 nm UV light. Radiation for shorter times leads to similar product ratios but has starting material present, suggesting that the products are not formed from secondary photolysis. The ¹H NMR spectrum collected at 30 min was used to calculate the relative ratio of all the photolysis products based on the ¹H NMR integration.

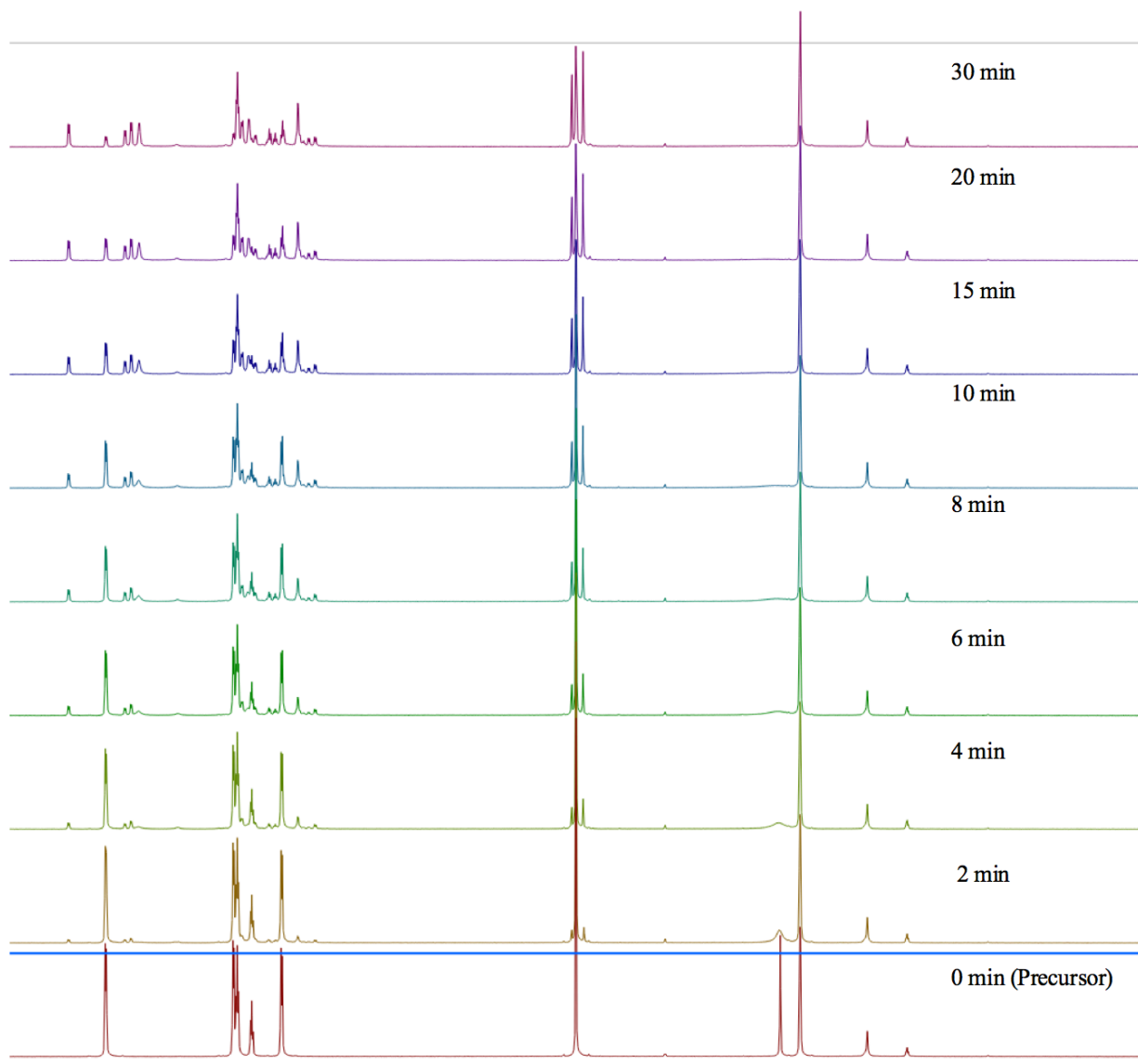


Figure A11. ¹H NMR spectrum of **1** photolyzed in acetonitrile-d₃ for different time durations.

Photolysis product studies in regular water and deuterium oxide.

The solution was irradiated with 254 nm UV light (Rayonet) for 40 min and the color changed from colorless to light brown. The solvent was removed under reduced pressure and the oil like residual was then re-dissolved into deuterium oxide for ^1H NMR and LC-MS. ^1H NMR spectra of standard chemicals and LC-MS results were combined to identify the photolysis products. Notably, phenol, one of the photolysis products, was not detected on the ^1H NMR spectrum since it was also removed under the reduced pressure. In this case, the relative ratio of all the photolysis products are determined by ^1H NMR integration of the photolysis in deuterated oxide. Photolysis with excess sodium azide showed reaction between azide ion and oxenium ion.

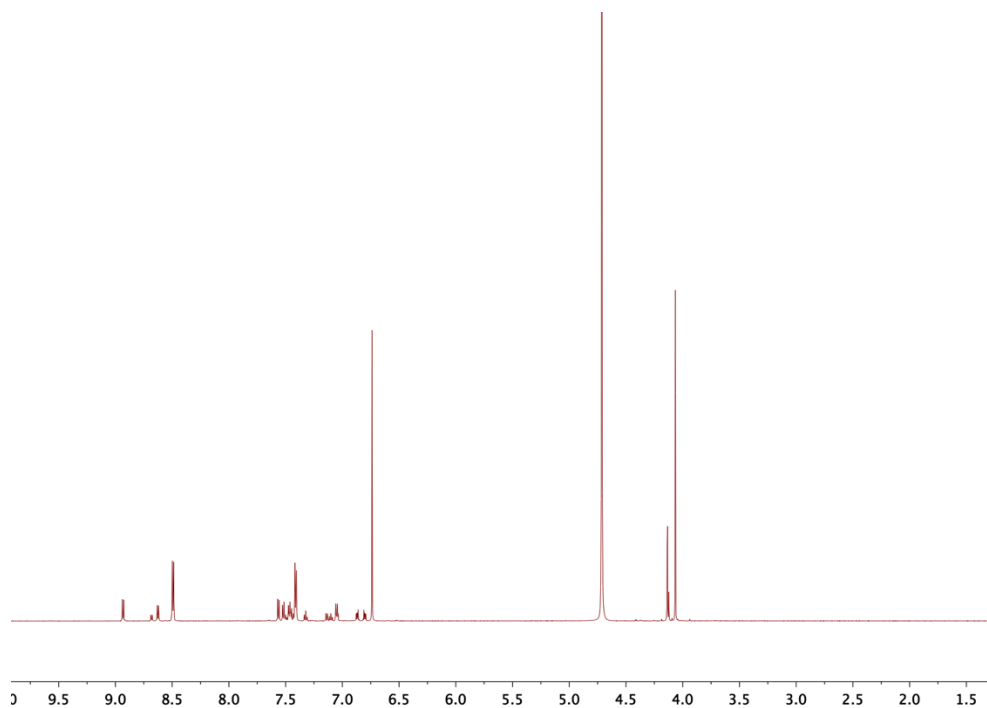


Figure A12. ^1H NMR spectrum of **1** photolyzed for 40 min in water and the assignment of peaks. Full ^1H NMR spectrum.

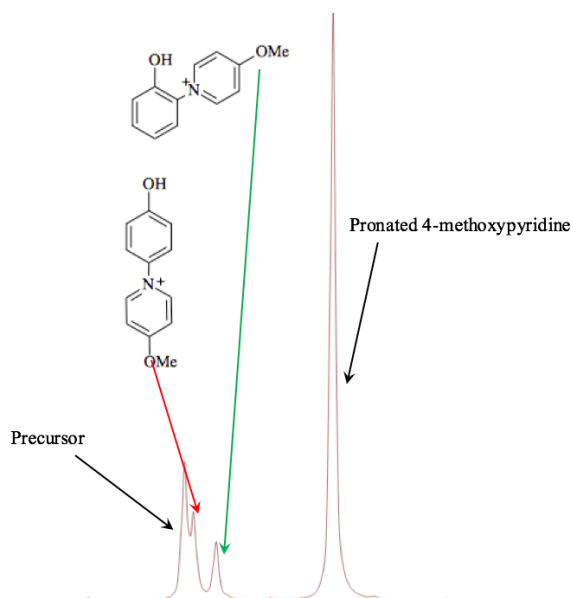


Figure A13. ^1H NMR spectrum of **1** photolyzed for 40 min in water and the assignment of peaks. ~ 4 ppm region of the ^1H NMR spectrum.

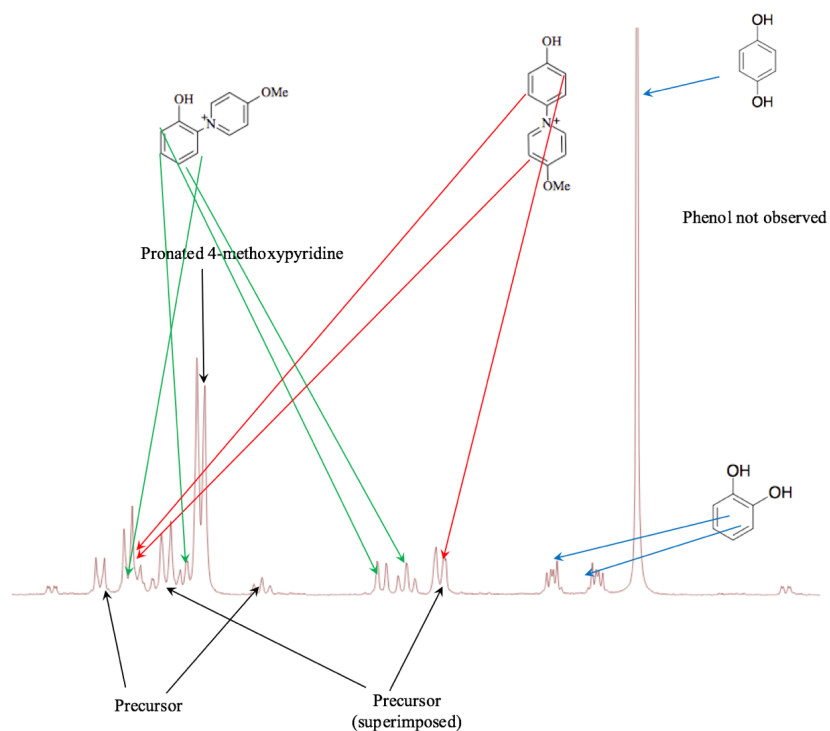


Figure A14. ^1H NMR spectrum of **1** photolyzed for 40 min in water and the assignment of peaks. ~ 7 ppm region of the ^1H NMR spectrum.

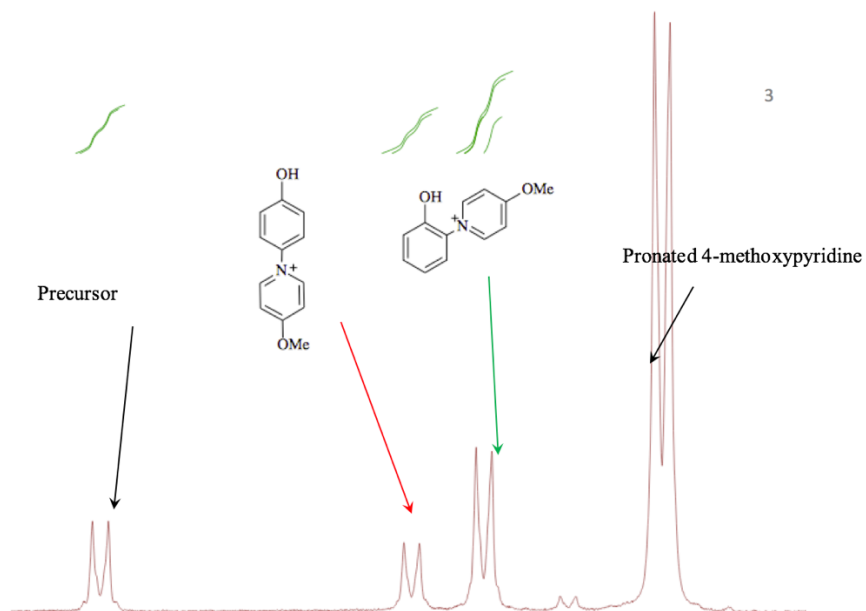


Figure A15. ^1H NMR spectrum of **1** photolyzed for 40 min in water and the assignment of peaks. ~ 9 ppm region of the ^1H NMR spectrum.

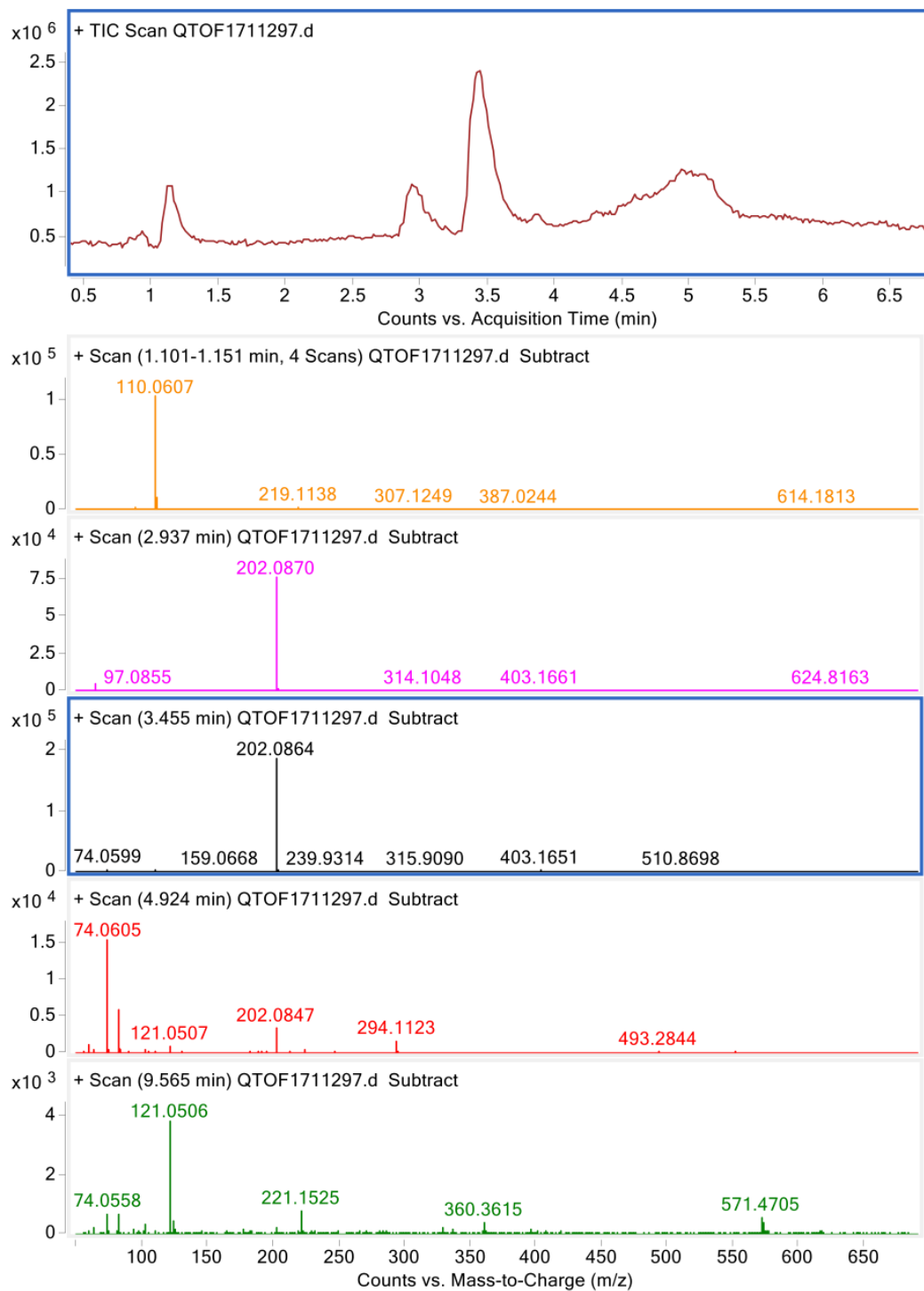


Figure A16. LC-MS of 4-methoxyphenoxy pyridinium tetrafluoroborate **1** photolyzed for 40 min in water.

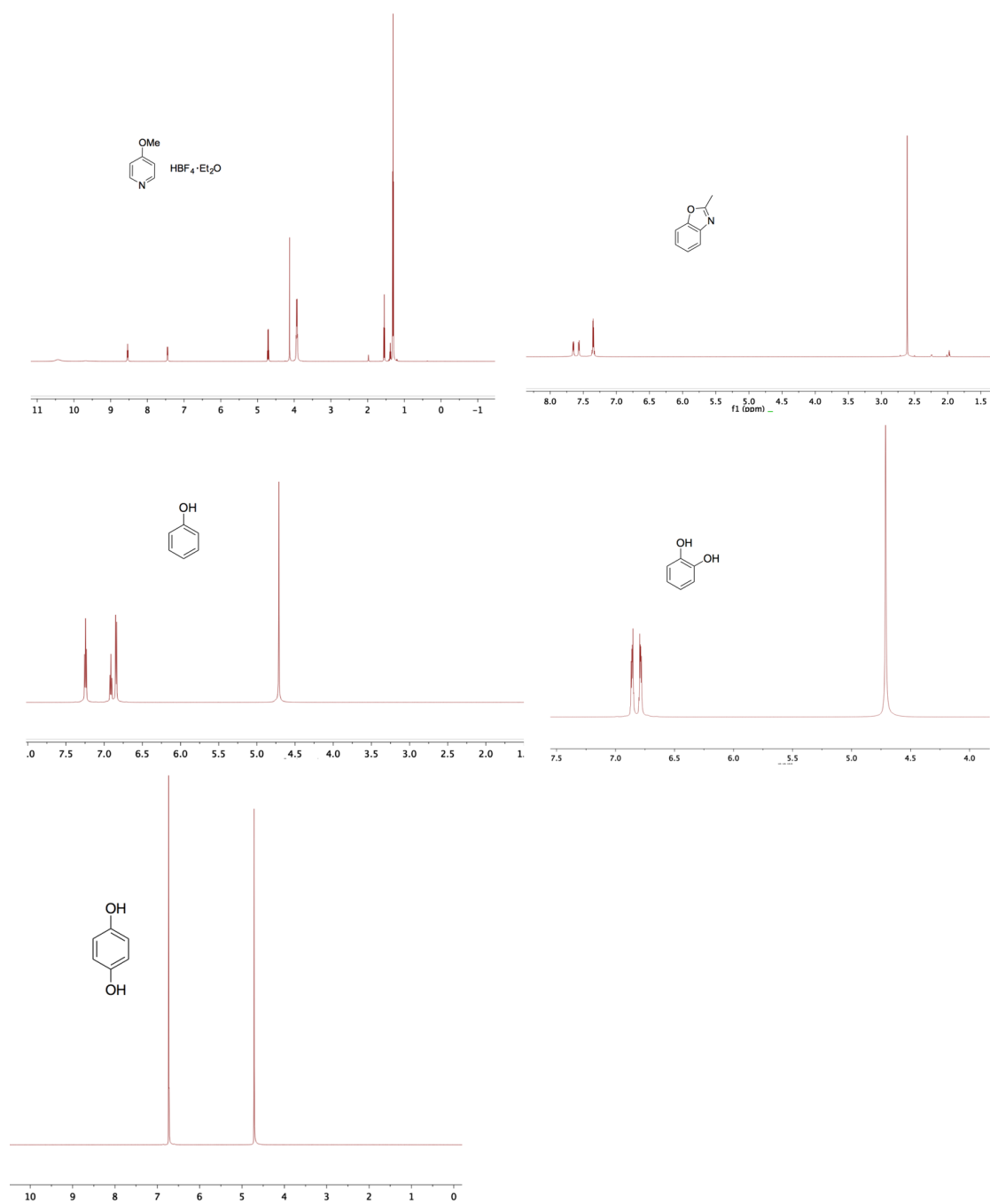


Figure A17. ^1H NMR spectrum of authentic chemicals, which were used to identify and attribute the photo products from the photolysis.

APPENDIX B. SUPPLEMENTAL INFORMATION ACCOMPANYING CHAPTER 3

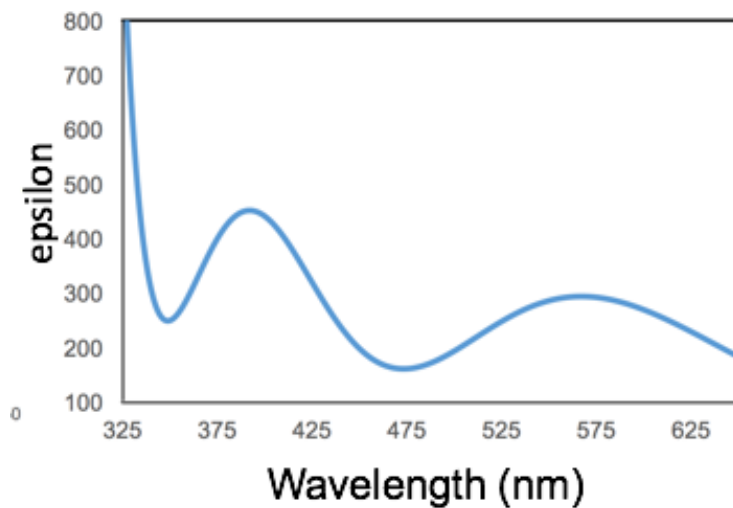
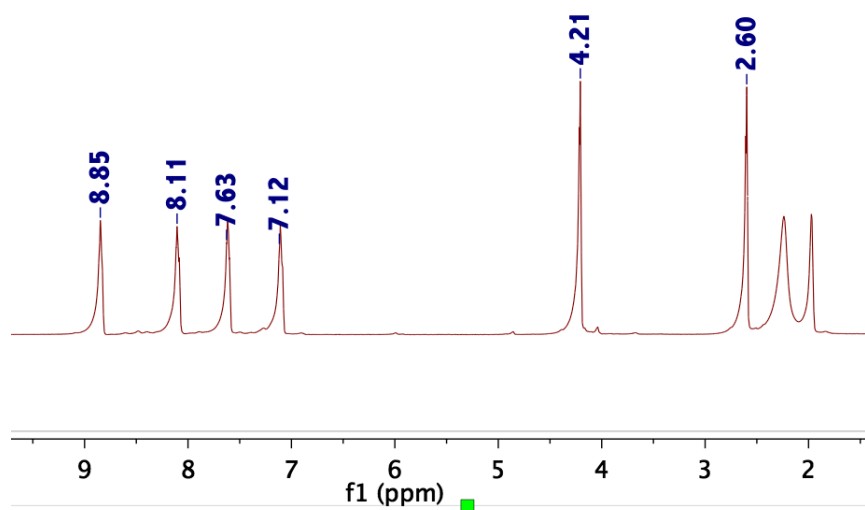


Figure B1. Shown is the computed electronic spectrum of the 4- acetylphenoxy radical, featuring two absorption maximums located at ~ 390 nm and ~ 580 nm.

(a)



(b)

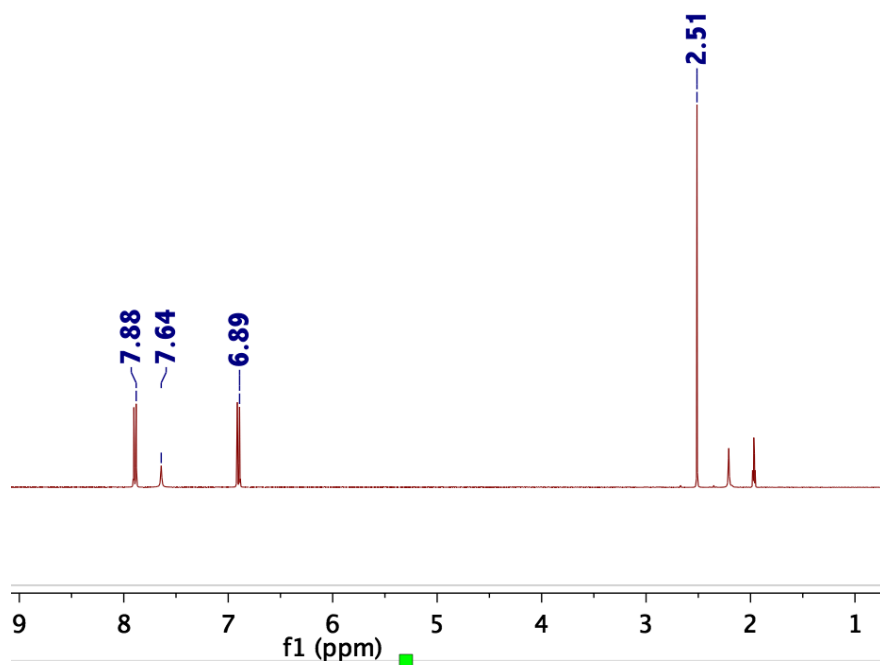


Figure B2. (a) ¹H NMR spectrum of the photoprecursor **1**. (b) ¹H NMR spectrum of 4-hydroxyacetophenone.

APPENDIX C. SUPPLEMENTAL INFORMATION ACCOMPANYING CHAPTER 4

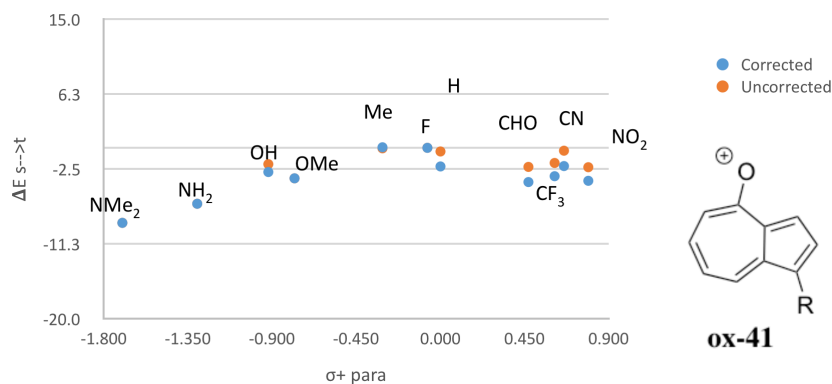


Figure C1. Linear free-energy relationships (LEFRs) of azulenyloxonium ion **ox-41**. Energies in kcal/mol. (● Uncorrected, ● Corrected) UB3LYP/6-31+G(d,p).

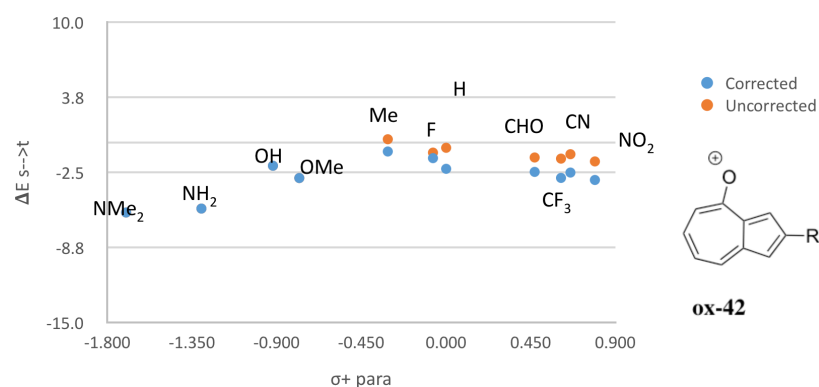


Figure C2. Linear free-energy relationships (LEFRs) of azulenyloxonium ion **ox-42**. Energies in kcal/mol. (● Uncorrected, ● Corrected) UB3LYP/6-31+G(d,p).

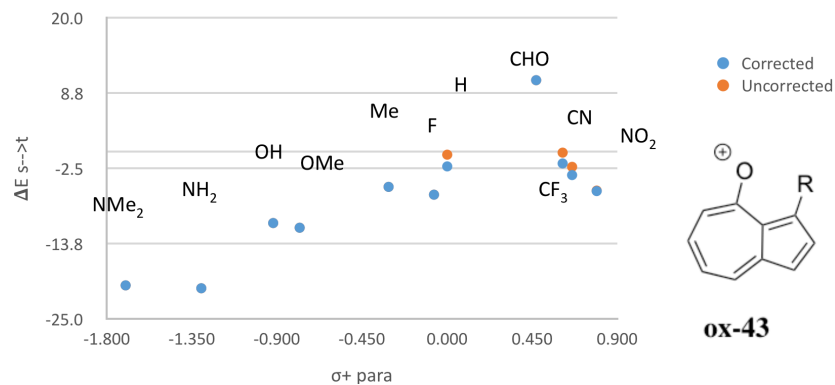


Figure C3. Linear free-energy relationships (LEFRs) of azulenyli oxenium ion **ox-43**. Energies in kcal/mol. (● Uncorrected, ● Corrected) UB3LYP/6-31+G(d,p).

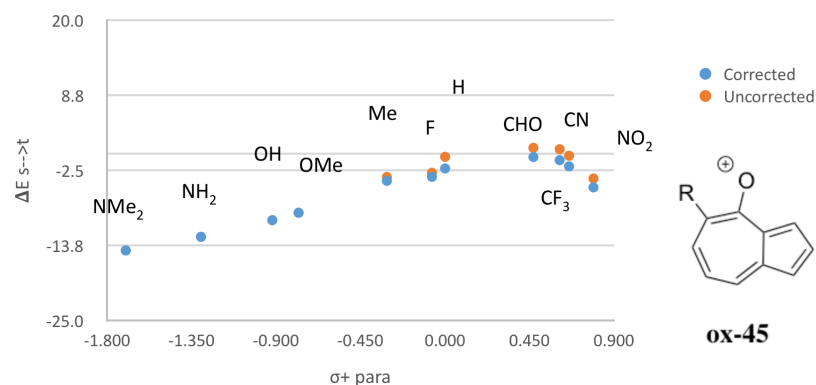


Figure C4. Linear free-energy relationships (LEFRs) of azulenyli oxenium ion **ox-45**. Energies in kcal/mol. (● Uncorrected, ● Corrected) UB3LYP/6-31+G(d,p).

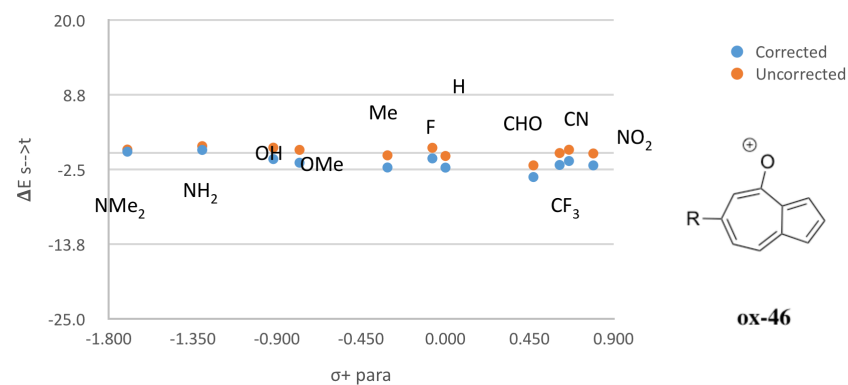


Figure C5. Linear free-energy relationships (LEFRs) of azulenyli oxenium ion **ox-46**. Energies in kcal/mol. (● Uncorrected, ● Corrected) UB3LYP/6-31+G(d,p).

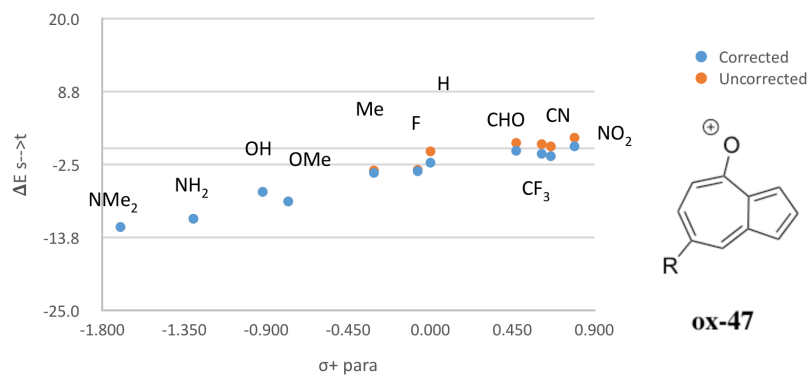


Figure C6. Linear free-energy relationships (LEFRs) of azulenyloxenium ion **ox-47**. Energies in kcal/mol. (● Uncorrected, ● Corrected) UB3LYP/6-31+G(d,p).

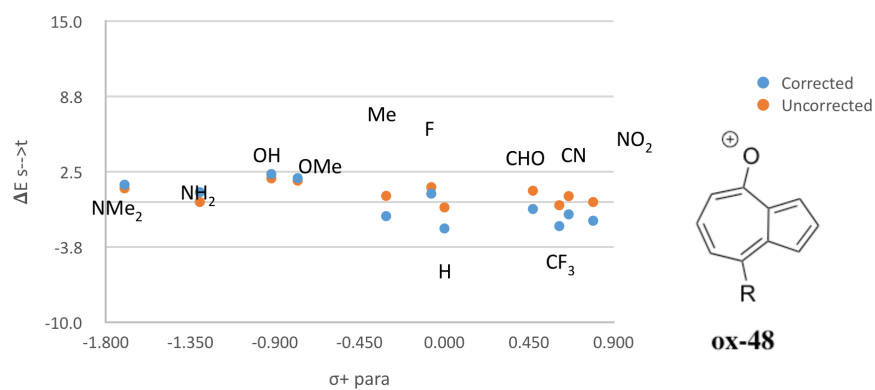


Figure C7. Linear free-energy relationships (LEFRs) of azulenyloxenium ion **ox-48**. Energies in kcal/mol. (● Uncorrected, ● Corrected) UB3LYP/6-31+G(d,p).

APPENDIX D. SUPPLEMENTAL INFORMATION ACCOMPANYING CHAPTER 5

Table D1. Iodine 6-311G (and supplementary function) Gaussian exponents (α_i), and contraction coefficients (c_i). (*J. Chem. Phys.* **1995**, *103* (5), 1878.)

	α_i	c_i
1s'	444 750	0.000 89
	66 127	0.006 94
	14 815	0.036 09
	4 144.9	0.135 68
	1 361.2	0.338 78
1s''	508.44	0.436 59
	209.59	0.183 75
2s'	81.959	1
2s''	36.805	1
3s'	13.495	1
3s''	6.885 9	1
4s'	2.552 0	1
4s''	1.208 8	1
5s'	0.273 4	1
5s''	0.100 9	1
2p'	2 953.6	0.012 21
	712.61	0.085 87
	236.71	0.294 93
	92.631	0.478 49
2p''	39.732	1
3p'	17.273	1
3p''	7.957 0	1
4p'	3.152 9	1
4p''	1.332 8	1
5p'	0.494 7	1
5p''	0.216 0	1
5p'''	0.082 93	1
3d'	261.95	0.031 44
	76.734	0.190 28
	27.551	0.472 47
3d''	10.606	1
4d'	3.421 7	1
4d''	1.137 0	1
Supplementary functions		
s ^{diff}	0.046 8	1
p ^{diff}	0.028 6	1
d	0.302	1
f	0.38	1

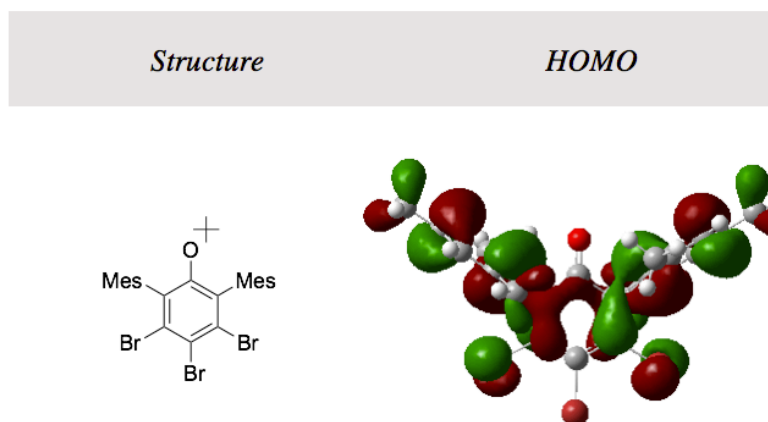


Figure D1. HOMOs of other halogenated reactive intermediates demonstrate the antibonding formation is attenuated (not observed).